THE UNIVERSITY of ADELAIDE

HILLGROVE RESOURCES

Crustal evolution and exploration potential of Delamerian south-eastern South Australia

Thesis submitted in accordance with the requirements of the University of Adelaide for an Honours Degree in Geology/ Geophysics

Braden Morgan

November 2019

CRUSTAL EVOLUTION AND EXPLORATION POTENTIAL OF DELAMERIAN SOUTH-EASTERN SOUTH AUSTRALIA

EXPLORATION POTENTIAL IN SOUTH-EAST SOUTH AUSTRALIA

ABSTRACT

The Delamerian Orogeny compressional tectonic system commenced at 514 ± 3 Ma and for approximately 24 Mys, provided the necessary mechanisms for the generation of hydrothermal intrusives and mineralisation events throughout much of south-eastern South Australia. The Hillgrove Resources Kanmantoo Cu-Au mine located 50 km south-east of Adelaide, hosts Delamerian age mineralisation formed by hydrothermal activity related to a pluton at depth. Many additional Delamerian aged intrusives have been identified distal to the Kanmantoo deposit and are hypothesised to provide temporal and spatial constraints of additional, and potentially mineralising, Delamerian events. Using monazite, titanite and zircon U-Pb geochronology, this investigation has identified the date and locations of two magmatic stages and one minor stage within sampled Delamerian intrusive rocks of south-east South Australia. Pre-Delamerian Magmatism (~520 Ma) consisting of the previously documented Truro Volcanics suite, occurs throughout pre-Delamerian passive margin. Syn-Delamerian Magmatism (~490 – 480 Ma) has been identified at two locations (55 km north-east and 224 km south-east of Kanmantoo) and is interpreted to have been emplaced during late peak metamorphism, D3. Post-Delamerian Magmatism (~471 Ma) is represented by one sample location and is interpreted to represent a magmatic stage occurring during the final minor stages of the Delamerian Orogeny, during post D3 extensional reactivation conditions. Pyrite and pyrrhotite mineralisation is present throughout the entire sample suite particularly within sampled intrusions representing Syn-Delamerian Magmatism at the Kanappa drilling project (approximately 60 km north-east of the Kanmantoo deposit) and 224 km south-east of Kanmantoo. The samples from these two locations were formed during relatively late Delamerian D3 post peak metamorphism, indicating two regions of enhanced prospectivity.

KEYWORDS

Delamerian Orogeny, Kanmantoo, mineralisation, intrusions, U-Pb geochronology, prospectivity.

WORD COUNT

7921 words

TABLE OF CONTENTS

List of Figures

List of Tables

1. INTRODUCTION

Located 52 Km south-east of Adelaide, South Australia, Hillgrove Resources Kanmantoo Cu-Au mine represents a highly prospective style of base metal mineralisation. Recent studies have partly characterised the style, type and timing of economic mineralisation throughout the deposit and its association with intrusive magmatism related to the Delamerian Orogeny (514 ± 3 million years ago (Ma) to 490 ± 3 Ma) (Foden, Elburg, Dougherty-Page & Burtt, 2006; Kimpton, 2018). The exploration-related implications to these findings are yet to be extrapolated through the other Delamerian affected terrains of South Australia to potentially identify other syn-orogenic hydrothermal mineralising systems. Using geochronology of felsic veins and monazite mineral chemistry from samples collected within the Kanmantoo Mine, Kimpton (2018) concluded that mineralisation was resultant of hydrothermal fluids related to an intrusive pluton at depth. These findings support the continued prospectivity of Delamerian orogeny affected regions throughout south-east South Australia, where intrusive igneous units and their associated hydrothermal systems are present. While it is unlikely the exact style of mineralisation present at the Kanmantoo Cu-Au deposit is repeated, other similar syn-orogenic base metal deposits may be present throughout the greater region. Much of the Australian mainland and western Tasmania includes Cambrian age rock which exhibit deformation and mineralisation related to the Delamerian Orogeny (Berry & Crawford, 1988; Crawford & Berry, 1991) and it is hypothesised that ore deposits analogous to Kanmantoo, may be present, concealed by cover sequences and regolith throughout much of the Murray Darling Basin of South Australia.

This study will extend the investigation of Kimpton (2018), and step-away from the mine surroundings to date intrusive rocks from locations throughout south-eastern Southern Australia, to investigate the potential for the presence of ore forming hydrothermal systems within Delamerian affected strata under the Murray Darling Basin cover sequences. This investigation will analyse existing rock samples provided by Hillgrove Resources, field samples and samples collected from open file drillholes. It is hypothesised that by dating intrusive units throughout the greater region it may be possible to identify whether potentially fertile hydrothermal systems were present, and has direct implications for future exploration throughout south-east South Australia. In order to understand these possible relationships, the following research questions will be addressed:

- Are Delamerian-age intrusions present in the sample suite?
- Do the sampled rocks have temporal links with Kanmantoo-style syn-orogenic mineralisation?
- Is there a temporal association between the sampled intrusive materials and known hydrothermally mineralised rocks throughout areas affected by the Delamerian Orogeny?

2. GEOLOGICAL BACKGROUND

2.1. Delamerian Orogeny

The Delamerian Orogeny, a period of compressional tectonics along the palaeo-pacific margin of Gondwanaland, has significantly affected much of south-eastern South Australia (Belperio et al., 1998; Foden et al., 2006; Schiller, 2000). The orogeny represents a fold-thrust belt with associated inverted extensional fault thrust zones

(Burtt, 2003). Delamerian affected regions include Precambrian and Cambrian sequences in Tasmania, the Wonaminta Block in western New South Wales, the Glenelg Complex in western Victoria and the Adelaide Rift Complex (Adelaide Fold Belt) in South Australia (Coney, Edwards, Hine, Morrison & Windrim, 1990). The contractional deformation persisted for approximately 24 Ma commencing at 514 ± 3 Ma and lasted until 490 ± 3 Ma (Foden et al., 2006). Oliver, Dipple, Cartwright & Schiller (1998) states the formation of crenulation and growth of porphyroblasts in early rock fabrics are proof that the Delamerian deformation has multiple stages and has been widely recognised that the polyphase deformation of the Delamerian Orogeny (Wilson, 2009) has three main phases referred to D1, D2 and D3 (Oliver et al. 1998; Schiller, 2000; Wilson, 2009).

- **D1:** Development of schistosity parallel with bedding, cleavage and upright to inclined folding.
- **D2:** Peak metamorphism, D1 overprinted by crenulation fabric, north-south strain zones exhibit the formation of tight folds.
- **D3:** Regional scale development of weak crenulation, open folds and major faults. Significance and existence of D3 is debated with many regions including that of the Kanmantoo Cu-Au mine, which does not preserve evidence of the D3 deformation (Rolley & Wright, 2017). However, Oliver at al. (1998) and Lyons (2012) have expressed that this regional deformation may provide structural controls for concurrent ore transport and localisation.

2.2. The Kanmantoo Cu-Au deposit

Hillgrove Resources Kanmantoo Cu-Au mine is located within the southern region of the Adelaide Rift Complex, part of a larger orogenic belt stretching east as far as West Victoria (Schiller, 2000). All economic mineralisation within the Kanmantoo mine is hosted within the Kanmantoo Group, a rapidly deposited series of deep water turbidites believed to represent a change in depositional environment from a passive to active setting (Belperio et al., 1998; Foden et al., 2002; Jago, Gum, Haines & Burtt, 2003) and exhibiting syn- and post-Delamerian Orogeny deformation between 514 ± 4 Ma to 478 ± 2 Ma (Foden et al., 2006). The Kanmantoo Group is a 7-8km thick early Cambrian clastic metasedimentary sequence and is the youngest group within the Adelaide Rift Complex (Jago et al., 2003; Seccombe, Spry, Both, Jones & Schiller, 1985). Mineralisation within the Kanmantoo Cu-Au deposit is present as veins and disseminations of sulphides including pyrrhotite, chalcopyrite, sphalerite and pyrite in a series of north-south trending podiform lenses (Parker, 1986; Schiller, 2000). Igneous intrusive units studied by Kimpton (2018) occupied variable chemistry of felsic and mafic compositions of which moved to an A-type magmatism toward the cessation of the orogeny (Foden et al., 2006).

Monazite grains within 10 individual samples throughout intrusive rock of the Kanmantoo mine allowed Kimpton (2018) to state that two generations of felsic veining were present with absolute and relative ages further supporting Oliver et al. (1998) whom concluded that mineralisation at Kanmantoo is representative of peak and post-peak metamorphism. Kimpton also identified that the age range for all samples includes first generation felsic veining at 503.44 ± 3.32 Ma and a second generation of felsic

veining at 483.43 ± 2.52 Ma, interpreted to represent Delamerian D2 through D3 deformational events.

2.3. Ore genesis

The Kanmantoo Group metasediments also host a number of other small deposits, including Wheal Ellen and Angus, which have been worked historically for Pb, Zn and Ag. Two models of ore genesis are most commonly favoured: syngenetic (Belperio et al., 1998; Seccombe et al., 1985; Spry, 1976) and epigenetic (Kimpton, 2018; Oliver et al., 1998; Parker, 1986; Schiller, 2000). The Pb, Zn and Ag deposits have historically been interpreted to be related to a syngenetic hydrothermal exhalative origin, which have subsequently been modified during orogenesis (Toteff, 1999; Tott et al., 2019), whereas the origin of then Cu-Au deposits such as the Kanmantoo deposit remains contentious (Tott et al., 2019). Supporters of a syngenetic genesis theorise the Kanmantoo Cu-Au deposit was once a sub-seafloor hydrothermal exhalative feeder zone (Belperio et al., 1998; Seccombe et al., 1985; Spry, 1976). However, in recent years, the epigenetic model originally proposed by Oliver et al. (1998) and supported by Parker (1986), Schiller (2000) and Kimpton (2018), is more commonly supported. The epigenetic model requires that mineralisation took place during peak to post-peak metamorphic conditions as a result of the interaction between metamorphic and syn-orogenic hydrothermal fluids related to magmatic intrusive units. Further support of this theory is provided by Belperio et al. (1998), whom states that the western margin structure of the Kanmantoo Trough represents a location of compressional orogenesis where listric faults were inverted providing an environment for major thrusting and

shearing; which are considered as key structures for localising basin dewatering and hydrothermal fluids prior to mineral formation (Belperio et al., 1998).

3. METHODS

3.1. Field work and sample collection

A total of 40 samples have been collected from various locations in south-east South Australia (Figure 1) with the aim of identifying minerals suitable for geochronology. Four samples were provided by Hillgrove Resources and eight samples of intrusive rocks were collected on April 2nd from diamond drill core held at the South Australian Drill Core Reference Library, Tonsley South Australia. A further three samples were gathered on April 15th from field locations within Hillgrove Resources exploration tenements adjacent to the Kanmantoo Cu-Au mine.

An additional data set was made available for this project by Prof. John Foden which contained whole-rock and trace element geochemical data for 720 intrusive rock samples collected from a period of over 20 years (Foden et al., 2019). A second additional data set was made available for this project by Hillgrove Resources containing geochemical sample information from the Kanappa Drilling Project located 55km north-east of the Kanmantoo Cu-Au mine. Detailed sample information is listed in Appendix A.

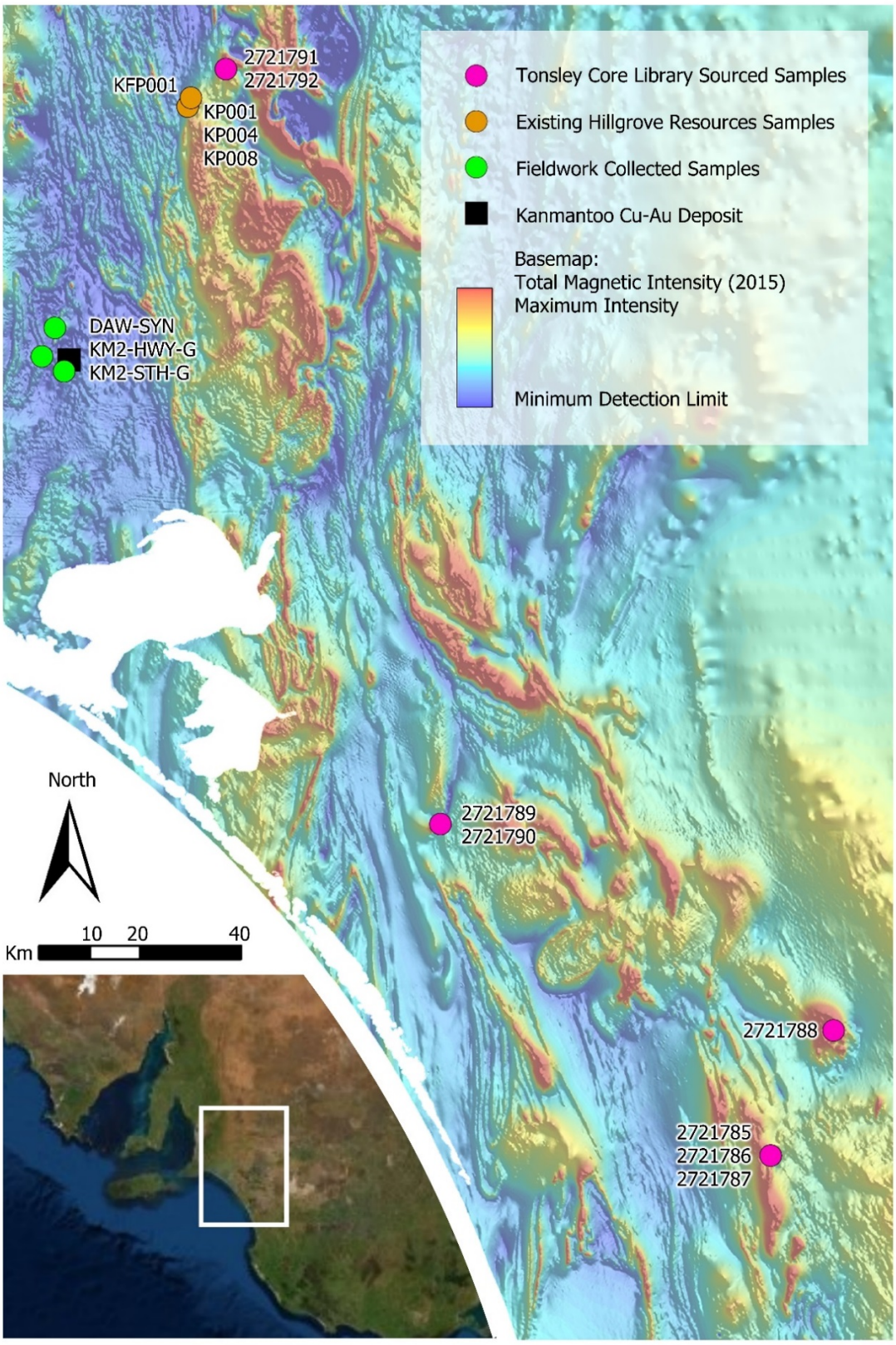

Figure 1: Geographic location of all 15 samples utilised within this investigation with total magnetic intensity basemap sourced from the Department of Primary industries and Resources, South Australia.

3.2. Microscopy

3.2.1. PETROGRAPHY

A total of 15 (30µm) polished thin sections were manufactured by Adelaide Petrographic Laboratories, South Australia, from drill core and field samples. All petrographic analysis was conducted at the University of Adelaide using an Olympus BX51 polarizing microscope to observe host rock, alteration and to identify the presence of minerals suitable for geochronology. Petrographic descriptions and images of the samples are located in Appendix B.

3.2.2. SEM-MLA

Mineral liberation analysis (MLA) and electron backscatter (EBS) image analysis was completed using a tungsten filament FEI Quanta600 scanning electron microscope (SEM) with dual 30mm2 Bruker SDD detectors at the University of Adelaide, Adelaide Microscopy. All 15 thin sections were analysed to identify and map distribution of monazite, zircon and titanite for subsequent LA-ICP-MS analysis. All image parameters used are listed within Appendix C.

3.3. LA-ICP-MS

3.3.1. GEOCHRONOLOGY

Eight samples were analysed with methods of laser ablation inductively coupled plasma mass spectrometry (LA-ICP-MS) at the University of Adelaide, Adelaide Microscopy using an Agilent 7900x with RESOlution LR 193nm excimer laser system. Laser ablation for U-Pb was conducted on in situ monazite, zircon and titanite with fluences of 2 J/cm^3, 2 J/cm^3 and 3.5 J/cm^3. Data processing, reduction and bracketing (a process

of reducing both ends the received signal in order to capture the strongest section of the signal) was completed using Iolite software (Paton, Hellstrom, Paul, Woodhead & Hergt, 2011). Further data reduction of common lead affected samples completed using Microsoft Excel. Detailed methods and equipment parameters are located in Appendix D.

3.3.2. TRACE ELEMENT ANALYSIS

Utilising an Agilent 7900x with RESOlution LR 193nm excimer laser system at the University of Adelaide, Adelaide Microscopy, grains of monazite were analysed for trace elements simultaneously with U-Pb within sample KP001. Data reduction and processing was completed using Iolite data reduction and processing software at Adelaide Microscopy.

Utilising an Agilent 7900x with a NWR213 (213nm) laser system at the University of Adelaide, Adelaide Microscopy, grains of pyrite were analysed for trace elements with two methods, quantitative spot analysis and semi-quantitative geochemical maps. Data reduction and processing was completed using Iolite data reduction and processing software at Adelaide Microscopy. Detailed methods and equipment parameters are located in Appendix E.

4. RESULTS

4.1. Microscopy

The 15 polished thin sections were petrographically studied to assist with rock classification and mineral abundances. The samples were also subject to SEM-MLA imaging to identify the presence and abundance of minerals suitable for geochronology

including titanite, zircon and monazite. Apatite was also identified, however, dating inconsistencies in previous studies with relatively large uncertainties (e.g. Kimpton, 2018) resulted in apatite geochronology not being considered suitable for this project. Sample specific petrographic analysis and imagery is located within Appendix B and C.

4.1.1. ALTERED GRANITE

Petrology defined six samples as granites with all containing retrograde chlorite or sericite alteration at variable abundances (Figure 2). Sample KP001 exhibits crystalline grain supported structure with abundant unaltered, irregular shaped quartz grains. Biotite and muscovite (both sericite altered) are present with titanite as euhedral crystals and irregular rounded grains. MLA imaging identified zircon with very small sub 20 μm inclusions of quartz and biotite within sample KP001.

Sample 2721788 exhibits two intrusions, a 2-3 cm vein (biotite absent) positioned within the main sample composition containing 10% biotite. Both intrusions are otherwise compositionally comprised of quartz, plagioclase (both altered and non-altered) and chlorite alteration groundmass. Pyrrhotite (Fe_xS) grains (up to 600 μm in diameter) are present within both intrusions and are commonly surrounded with chlorite alteration halos. MLA imagery identified zircon and titanite within the intrusive composition containing biotite and not within the biotite absent vein.

Samples 2721791 and 2721792 from drill-hole S11 were sampled due to the presence of visible Au and known Au anomalism. Both samples are compositionally very similar comprising of fine-grained sericite altered groundmass, chlorite, quartz with minor plagioclase and pyrite. Quartz grains exhibit euhedral crystal structure with euhedral pyrite reaching 150 μm. S11 drill-hole samples contain the highest abundance of pyrite

of all altered granite classified samples (visual estimate of 8%). MLA mapping of these samples displayed very low abundances of zircon, monazite and titanite.

Kanmantoo Cu-Au mine proximal samples KM2-STH-G (2.4 km from Kanmantoo) and KM2-HWY-G (5.4 km from Kanmantoo) represent the highest alteration abundances of all altered granite classified samples. KM2-STH-G is heavily altered that the rock no longer exhibits crystalline texture within hand specimen. Within thin section, groundmass alteration (visual estimation of 71% abundance) is a very fine grained, blue birefringent, undulatory extincting complex, hypothesised to be berlin blue chlorite alteration of quartz. Remaining mineralogy includes fine grain biotite (500 μm grain length) and altered muscovite (500 μm grain length).

KM2-HWY-G contains 60% dense sericite alteration of which the original mineral is unidentifiable; however, a large abundance of muscovite is visible in hand sample with only a small abundance being visible in thin section, denoting the sericite altered mineral is likely muscovite. Minor sericite altered chlorite, potassium feldspar and tourmaline are also present with tourmaline crystals being visible in hand sample reaching 2 cm in length. Both Kanmantoo proximal altered granite samples contain very low to zero abundance of dating minerals zircon, monazite and titanite.

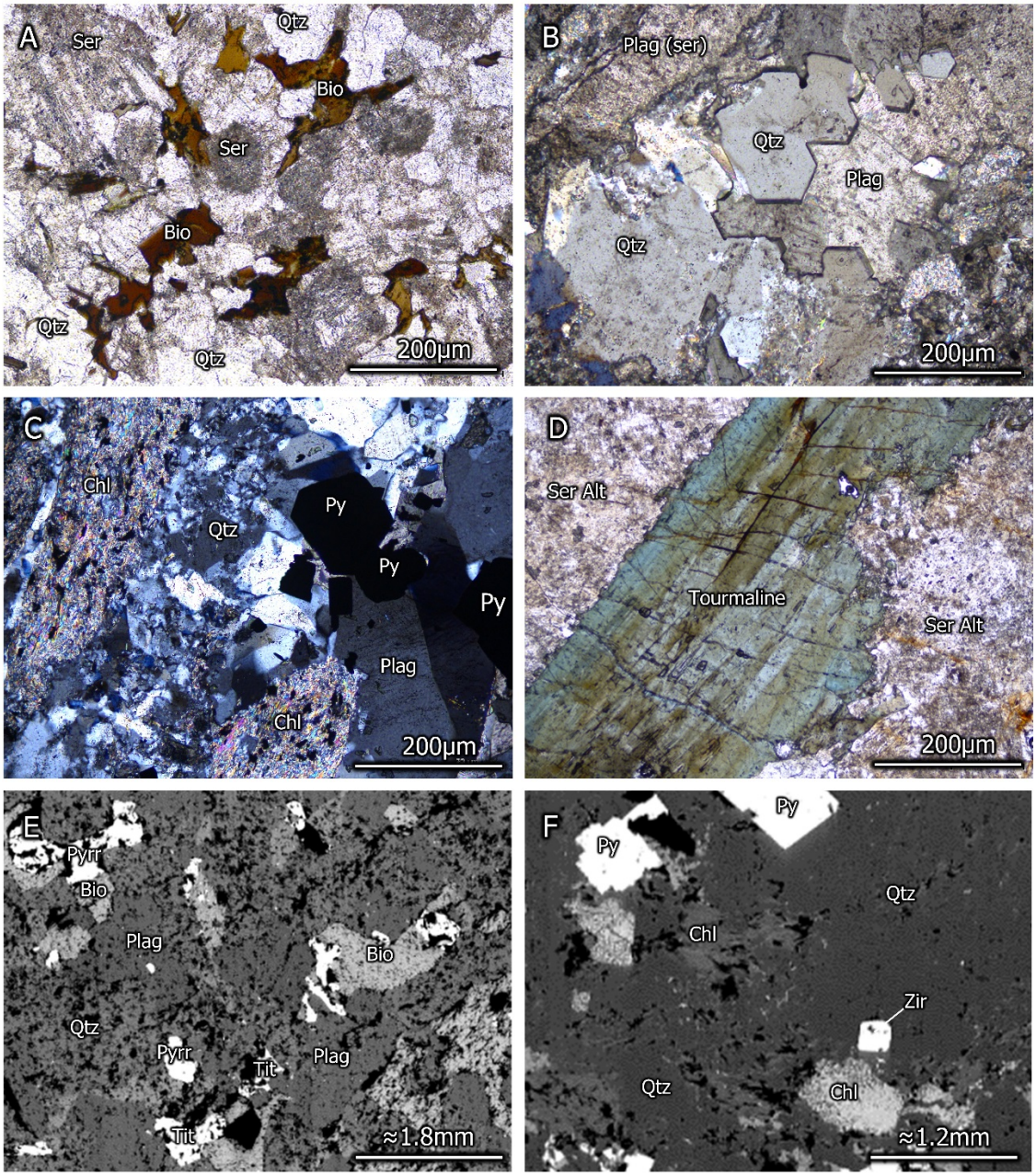

Figure 2: Representation of the variable alteration, structure and mineralogy within the altered granite samples. A - KP001: infill biotite, irregular quartz, sericite alteration with relic mineral dominantly muscovite and minor irregular chlorite. B - 2721791: euhedral quartz crystals surrounded with strong sericite altered plagioclase feldspar and chlorite. C - 2721792: euhedral pyrite grains as inclusions of quartz and chlorite. D - KM2-HWY-G: 2cm long tourmaline crystal surrounded with strong sericite alteration of which relic minerals are undistinguishable. E – 2721788 BSE Image: irregular titanite grains located within chlorite altered groundmass with relic minerals of quartz and plagioclase. F – 2721792 BSE Image: zircon present as an inclusion within sericite altered quartz.

4.1.2. SYENITE

Sample DAW-SYN, 7 km north-west from the Kanmantoo mine, has a minor mineral alignment fabric throughout the fine grained rock visible within hand sample and outcrop. Sericite altered muscovite present with major minerals of orthoclase, hornblende and magnetite with minor plagioclase (Figure 3). Euhedral tabular grains of hornblende reach 1 mm in length and include irregular rounded magnetite inclusions. MLA imagery displayed zircon, monazite and titanite, however utilising the SEM these grains are <20 µm of which are too small to generate accurate geochronological data.

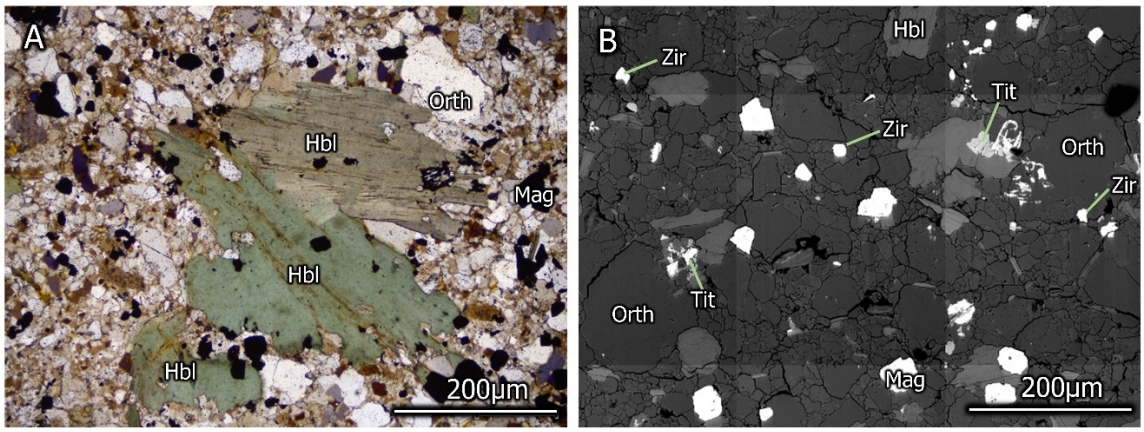

Figure 3: A - DAW-SYN: groundmass of fine grain orthoclase and sericite altered muscovite. Magnetite present as rounded inclusions within hornblende and irregular infill. B - DAW-SYN BSE Image: Zircons present bordering larger orthoclase grains within the groundmass with titanite most commonly present as inclusions of hornblende.

4.1.3. DIORITE

Samples KP004 and KP008 have been classified as quartz diorites and are from the same drillhole 55 km north-east of the Kanmantoo mine (Figure 1). KP004 is a light-coloured rock with dark minerals of tabular biotite and amphibole. The sample is dominated by plagioclase (visual estimation approximately 70%) with minor irregular quartz and irregular non-magnetic opaque mineral. Titanite and zircon are present as

sub 60 μm and sub 30 μm grains homogenously distributed throughout the sample (Figure 4).

KP008 is dominated by plagioclase (visual estimation approximately 60%) which is less sericite altered than KP004. KP008 also contains muscovite and quartz with minor amphibole, biotite and titanite visible in thin section. MLA imagery identified a single monazite grain, multiple zircon and large titanite grains which reach 2 mm.

KFP001, a surface grab sample located 57 km north-east from Kanmantoo, exhibits abundant sericite alteration with relic minerals indistinguishable. Lighter coloured regions within the sample are large plagioclase phenocrysts reaching 3 mm in length. Darker coloured regions are chlorite alteration with irregular clinopyroxene, irregular quartz, chlorite and euhedral titanite. Titanite was identified during petrography with grains located throughout the chlorite alteration groundmass and no observable preferential alignment. MLA imagery confirmed titanite presence as well as minor sub 20 μm zircon inclusions of plagioclase and two monazite grains.

Two samples, 2721789 and 2721790, are from drillhole KMD-07-01 located 118 km south-east from Kanmantoo are classified as diorites. 2721789 (depth 336.4 – 336.55 m) has strong chlorite altered plagioclase and clinopyroxene groundmass. Altered plagioclase and clinopyroxene are irregular in shape with non-altered plagioclase being tabular reaching 1 mm in length. Green chlorite altered biotite is abundant throughout the groundmass with some larger biotite grains containing inclusions of pyrrhotite. Pyrrhotite is more commonly observed as infill with irregular shape. MLA imagery identified low abundances of titanite and zircon with both minerals being sub 20 μm.

Titanite was most commonly located bordering plagioclase with zircon being an inclusion within biotite.

Sample 2721790 (depth 336.15 – 336.45 m) is compositionally similar to 2721789 with every plagioclase grain being chlorite altered to some extent. Large 200 μm long orthopyroxene grains are non-altered and are surrounded by chlorite within an altered plagioclase and quartz groundmass. Pyrrhotite grains were present reaching 150 μm and also as very fine grain infill. Low abundances of zircon and titanite were identified reaching 20 μm located within the chlorite alteration groundmass.

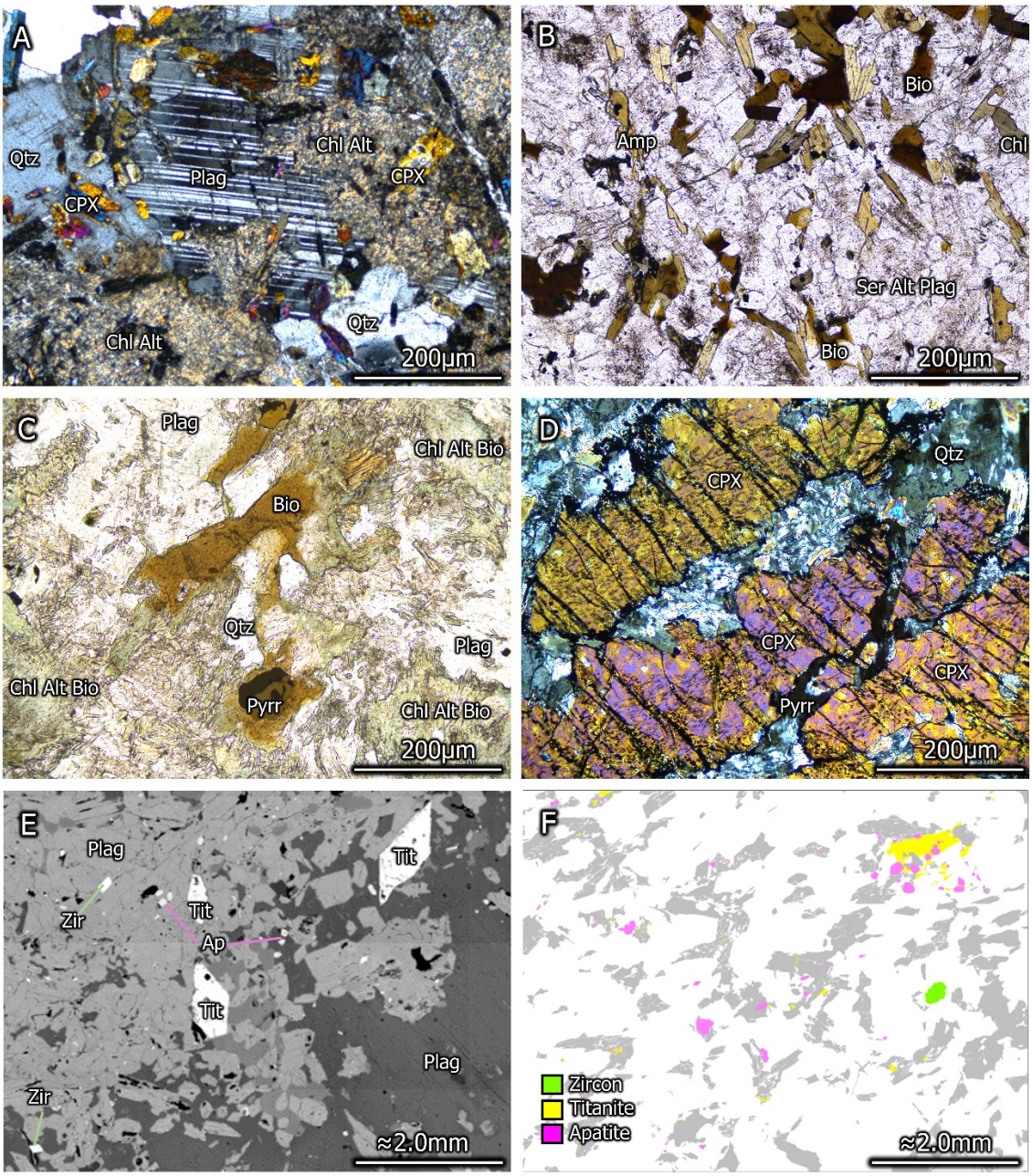

Figure 4: A – KFP001: quartz diorite classification with large irregular plagioclase grains, chlorite alteration of quartz. Titanite and clinopyroxene present as inclusions within irregular quartz and plagioclase. B – KP004: quartz diorite homogenous distribution of sericite altered plagioclase, chlorite, biotite, quartz, amphibole and opaques. C – 2721789: diorite with irregular plagioclase, chlorite altered quartz and chlorite altered biotite often containing inclusions of pyrrhotite. D – 2721790: diorite with chlorite altered quartz, clinopyroxene, irregular plagioclase and irregular pyrrhotite. E – KFP001: BSE image displaying euhedral titanite, euhedral zircon and small apatite clusters. F – KP008: MLA image of irregular titanite with apatite inclusions and the largest zircon grain in sample.

4.1.4. TRURO VOLCANICS

Three samples have been identified as the Truro Volcanics with all samples representing various depths from 130-132 m within drill-hole PADD 31 located south-east 210 km from Kanmantoo (Figure 1). Sample 2721785 (132.75 – 133.00 m depth) is chlorite altered resulting in much of the relic groundmass material being undistinguishable. Calcite (visual abundance approximately 40%) grains are the largest within the sample reaching 1 mm with minor minerology being green chlorite replaced biotite, infill unidentified opaques (nonmagnetic) and unidentified high birefringent grains. MLA imagery identified titanite present as small irregular grains reaching 200 μm in length located bordering calcite and green chlorite altered biotite (Figure 5).

Sample 2721796 (depth 132.00 – 132.75 m) is a porphyritic basalt abundant in amygdales. Smaller 500 μm amygdales are round in shape and filled with chlorite, while larger 5-8 mm amygdales are filled with carbonate. One section of the sample believed to represent a large amygdale, is filled with a mesh of calcite crystals. Within the basaltic groundmass are plagioclase laths and minor biotite. Titanite was identified within the basaltic groundmass with no grains being identified as inclusions of the amygdale infill. All titanite grains are of similar size reaching 80 μm.

Sample 2721787 (depth 130.35 – 130.55 m) is a dark porphyritic rock containing veining of quartz and calcite. Calcite crystals reaching 800 μm are surrounded with a 200 μm border of zeolite. 100 μm pyrrhotite grains are present within this zeolite border on the edge of the calcite crystals, occasionally fully surrounding the calcite crystal. The groundmass is composed of very fine grained hematite alteration, biotite, plagioclase

and zeolite. A small number of sub 100 µm titanite grains were identified within the hematite altered groundmass.

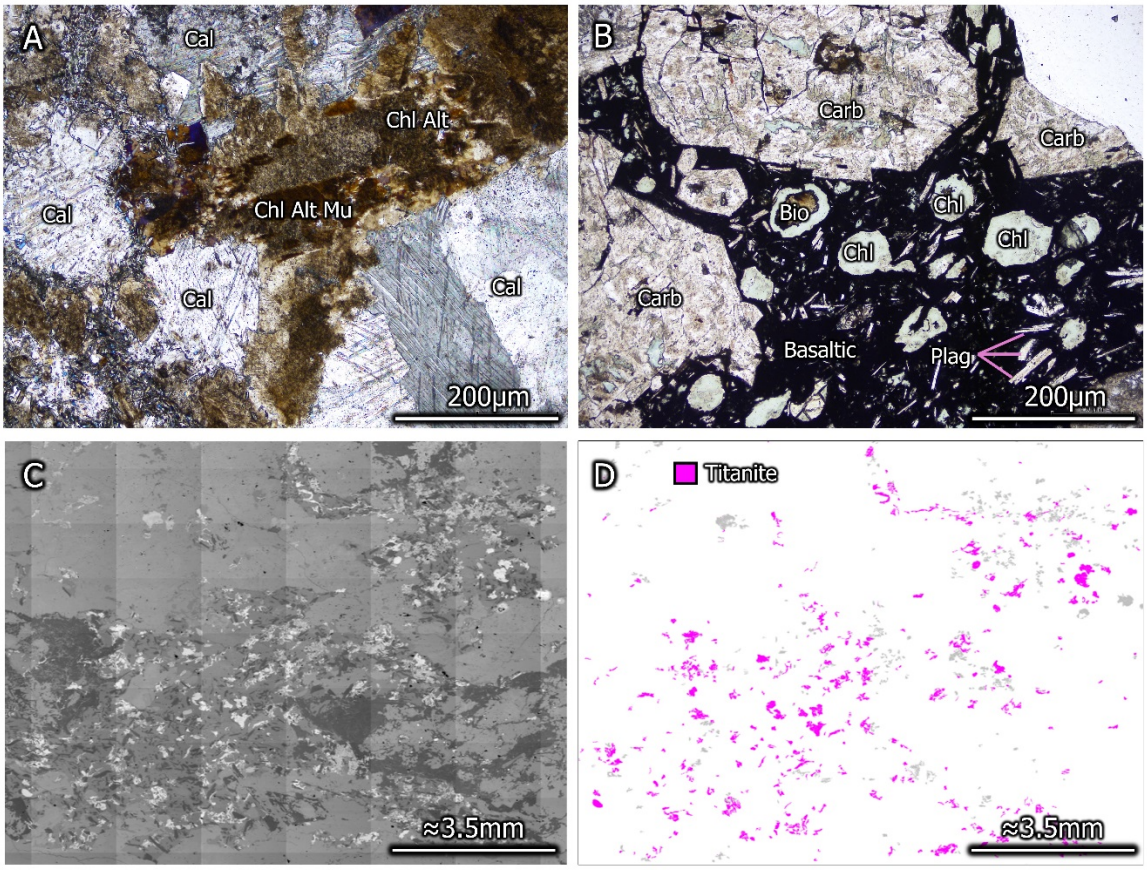

Figure 5: A – 2721785: Brown chlorite alteration surrounding calcite grains. B – 2721786: Vesicular porphyritic basalt filled with carbonate material and chlorite of which often contains biotite inclusions. Plagioclase laths abundant within basaltic groundmass. C/D – 2721785: BSE and MLA imagery displaying abundance of titanite (pink) located within the chlorite alteration as well as calcite inclusions. Sample 2721786 contains a similar titanite abundance throughout the sample (not pictured).

4.2. LA-ICP-MS

Eight samples were subject to laser ablation inductively coupled plasma mass spectrometry focussing on grains of titanite (202 analyses), zircon (98 analyses) and monazite (22 analyses). Two runs were completed with all primary and secondary standards producing ages within acceptable ranges for LA-ICP-MS. Refer to Appendix D for full catalogue of completed analyses and plotting.

Table 1: List of thin sections with rock classification and abundance of dating minerals.

		Dating Mineral Grain Count		
Sample	**Classification**	**Titanite**	**Zircon**	**Monazite**
KFP001	Quartz Diorite	**5901**	**87**	**2**
KP001	Altered Granite	99	679	35
KP004	Quartz Diorite	**1989**	**1297**	0
KP008	Quartz Diorite	**728**	**671**	1
2721785	Truro Volcanics	**2241**	0	0
2721786	Truro Volcanics	**4843**	0	0
2721787	Truro Volcanics	86	0	0
2721788	Altered Granite	396	**67**	0
2721789	Diorite	15	2	0
2721790	Diorite	49	16	0
2721791	Altered Granite	26	29	16
2721792	Altered Granite	8	13	3
KM2-STH-G	Altered Granite	58	23	6
KM2-HWY-G	Altered Granite	47	1	8
DAW-SYN	Syenite	628	**118**	10

4.2.1. TITANITE U-PB GEOCHRONOLOGY

All 15 samples contained titanite, but only five samples (Table 1) contained more than 50 grains of titanite of 50 μm or larger. These five samples were analysed for titanite U-Pb geochronology with 230 in situ analyses being completed resulting in 199 final analyses after data processing, bracketing and reduction. Titanite within all five samples did not exhibit any spatial arrangement as all grains were distributed throughout the whole sample thin section. Upon completing data reduction and bracketing, it was found that four grains contained quartz inclusions, resulting in decreased U-Pb signal strength and increased analytical errors. For inclusions of very small size, bracketing was implemented and for larger inclusions, the spot analysis was removed from the data set. The size of the 230 titanite grains were 50 μm in size (the minimum required size) but due to grain alignment, 27 titanite grain analysis was removed from the data set as the received U-Pb signal was insufficient, because of the laser penetrating completely through the titanite grain. A complete dataset of titanite U-Pb geochronology of samples and standards is located in Appendix G.

All five titanite dated samples exhibited a common lead trend (Figure 6). These samples were therefore plotted using a Tera-Wasserburg (Tera & Wasserburg, 1972) concordia diagram in order to calculate lower intercept ages, interpreted to reflect the timing of titanite crystallisation. Two distinct trends can be distinguished (Table 2): KP samples north-east of Kanmantoo with similar age values of 486.4 ± 2.8 Ma, 486.9 ± 4.4 Ma, and 478.4 ± 6.4 Ma with samples located south-east of Kanmantoo being potentially older with dates of 530.0 ± 23 Ma and 511.0 ± 43 Ma.

Table 2: List of samples with completed titanite U-Pb geochronology

Sample	Initial Spot Count	Removed (Inclusions)	Removed (Signal Error)	Final Spot Count	Lower Intercept Age
KFP001	48	1	3	44	486.4 ± 2.8 Ma
KP004	49	0	7	42	486.9 ± 4.4 Ma
KP008	53	3	2	48	478.4 ± 6.4 Ma
2721785	46	0	10	36	530.0 ± 23 Ma
2721786	34	0	5	29	511.0 ± 43 Ma

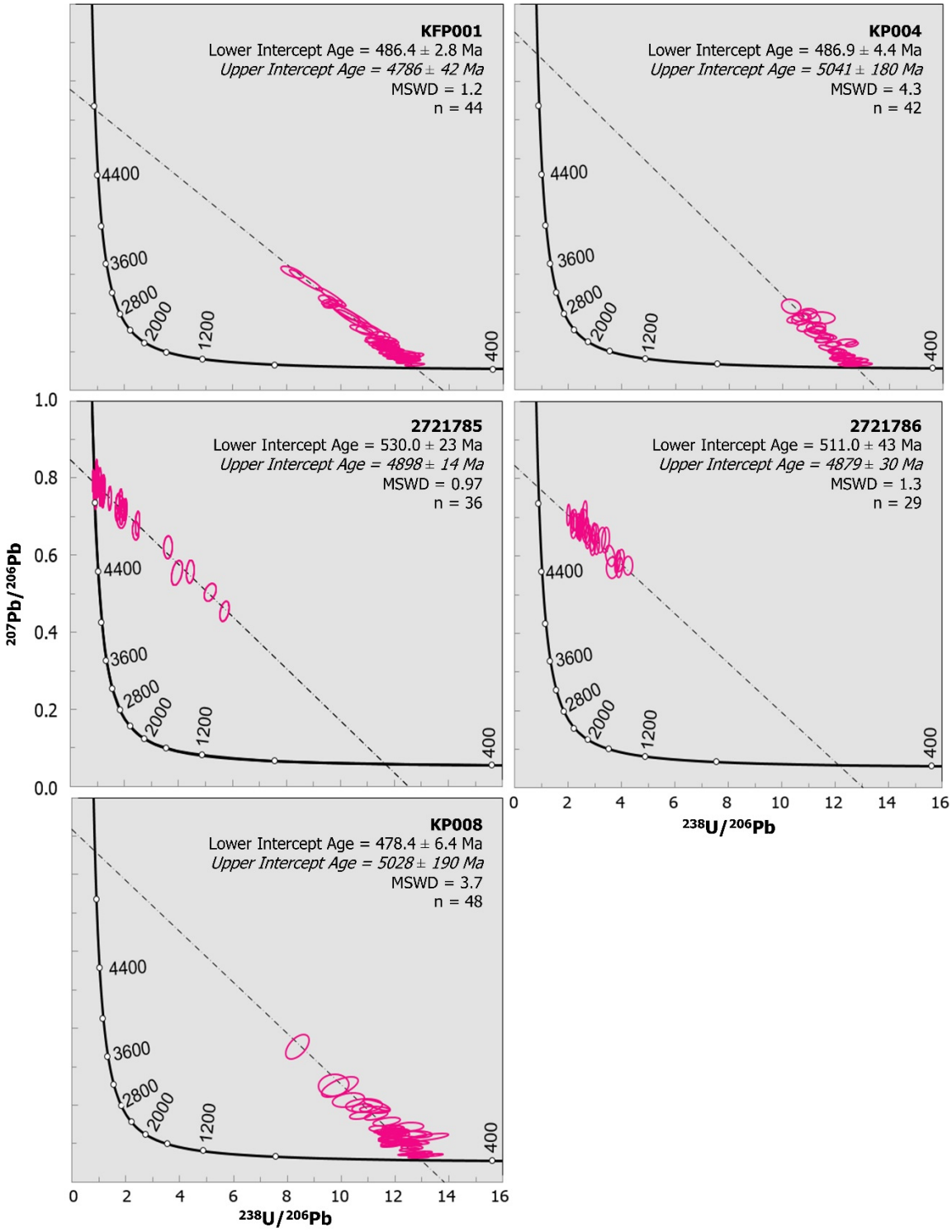

Figure 6: Titanite U-Pb geochronology Tera-Wasserburg plots. Data-point error ellipses are 2σ.

4.2.2. ZIRCON U-PB GEOCHRONOLOGY

Twelve samples contained zircon with only five samples occupying zircon grains larger than 20 μm. From the 72 spot analyses completed, 60 final analyses remained after bracketing and reduction. Zircon was observed to be abundant within many samples distributed throughout the whole of the sample thin section, but could not be analysed because of small grain sizes. These small grains would result in U-Pb signal errors as multiple minerals would be captured rather than one single zircon grain, or laser penetration would exceed the thickness of the small grain capturing the mineralogy beneath. Because of this grain size issue, 12 spot analyses were unable to be bracketed and were therefore removed from the dataset. Multiple spot analyses of which were bracketed introduced large error into the data set as only a small proportion of U-Pb signal remained. This error affected the final date within multiple samples and resulted in a relatively large uncertainty on the calculated age. Samples KP004 and KP008 had a small abundance of zircon grains with all grains within KP004 containing quartz inclusions (Table 3). These spot analyses were retained in order to calculate an age even when not well constrained or concordant. Sample KFP001 data presents possible evidence for minor Pb-loss, making age calculations using a concordia diagram difficult. A weighted mean age of 492.8 ± 5.2 Ma is considered to be the best estimate for the age of this sample. Sample 2721788 located south-east of Kanmantoo has concordant calculated age on a Wetherill Age (Wetherill, 1956) of 484.5 ± 3.1 Ma (Figure 7). Sample DAW-SYN located 7 km north-west of Kanmantoo occupies zircons with uranium fractionation. The fractionation was plotted using a Tera-Wasserburg diagram to visualise both upper and lower age intercepts. DAW-SYN has an upper intercept age of 1212.0 ± 58 Ma and lower intercept of 501.0 ± 58 Ma.

Table 3: List of samples with completed zircon U-Pb geochronology

Sample	Initial Spot Count	Removed (Inclusions)	Removed (Signal Error)	Final Spot Count	Weighted Mean Age
KFP001	27	0	6	21	492.8 ± 5.2 Ma
KP004	5	*all 5 have inc.*	0	5	294.0 ± 150 Ma
KP008	8	0	1	7	284.0 ± 120 Ma
					Wetherill Concordant Age
2721788	14	0	1	13	484.5 ± 3.1 Ma
					Tera-Wasserburg Intercept Ages
DAW-SYN	18	0	4	14	1212.0 ± 58 Ma
DAW-SYN	18	0	4	14	501.0 ± 58 Ma

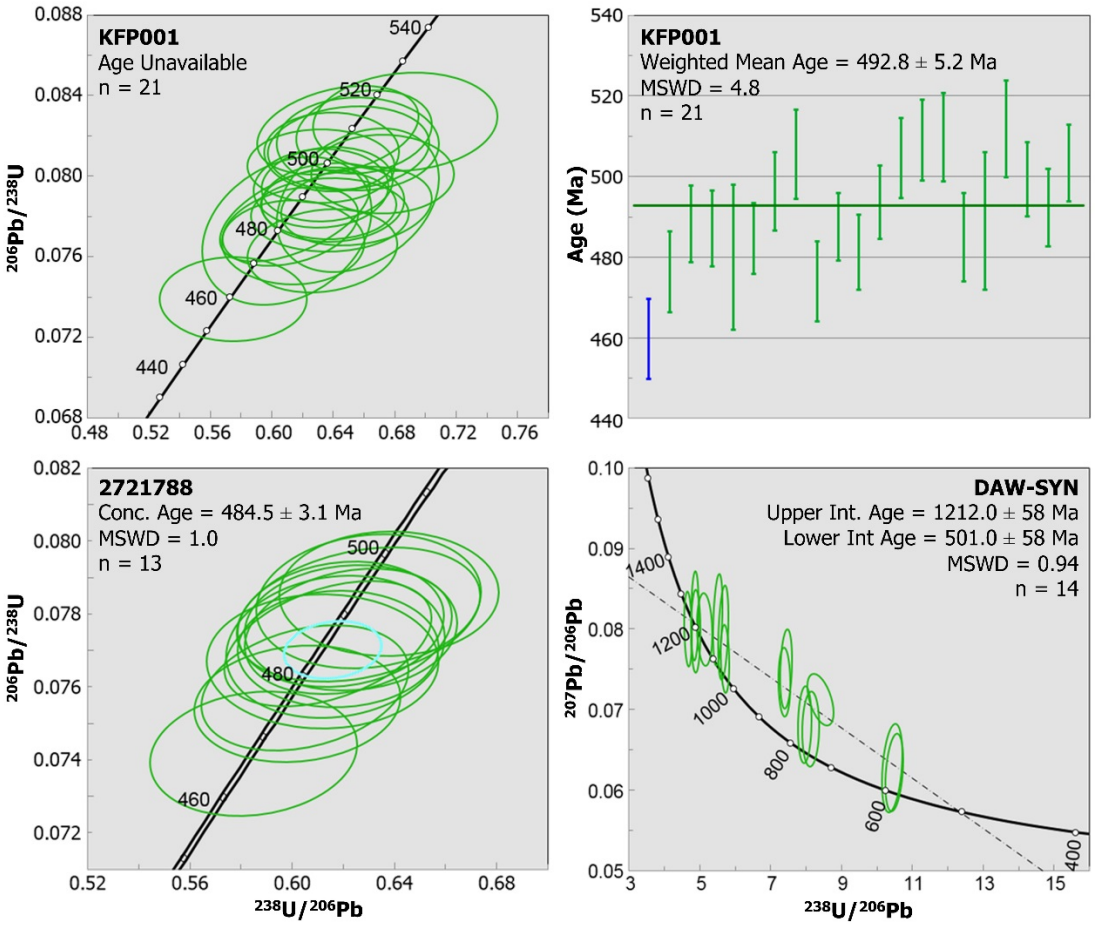

Figure 7: Zircon U-Pb geochronology plots for three of five analysed samples. KP004 and KP008 not displayed due to large error rendering data inaccurate. Data-point error ellipses/bars are 2σ. Sample KFP001 data presented on weighted mean age diagram. Sample 2721788 data presented on Wetherill Concordant Age diagram. Sample DAW-SYN presented on Tera-Wasserburg Intercept diagram.

4.2.3. MONAZITE U-PB GEOCHRONOLOGY

From the eight samples containing monazite grains, with sample KP001 is the only sample to contain multiple grains 15 µm or larger. Twenty-two spot analysis from KP001 were initially taken with five analysis being removed due to U-Pb signal error (laser penetration through mineral) (Table 4). Monazite grains were located throughout the whole sample, however the remaining 17 analyses are situated within only five grains because of size constraints. KP001 spot analysis is partially discordant with a Wetherill intercept age of 469.0 ± 23 Ma and a weighted mean average age of 473.0 ± 18 Ma (Figure 8).

Table 4: List of samples with completed monazite U-Pb geochronology

Sample	Initial Spot Count	Removed (Common Pb)	Removed (Signal Error)	Final Spot Count	Weighted Mean Age
KP001	22	0	5	17	473.0 ± 18 Ma
					Wetherill Age
KP001	22	0	5	17	469.0 ± 23 Ma

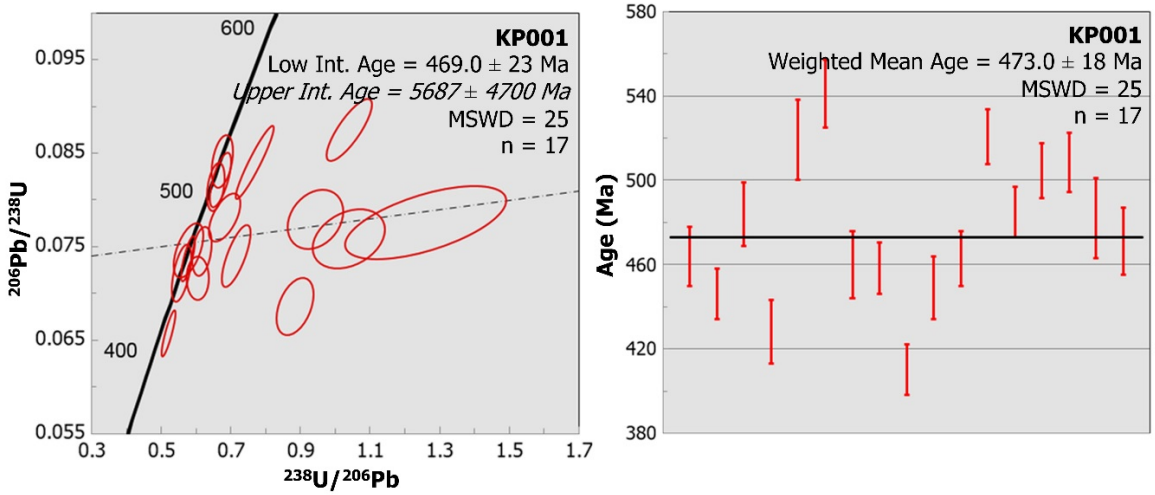

Figure 8: Sample KP001 Monazite U-Pb geochronology using Wetherill and weighted mean methods. Data-point error ellipses/bars are 2σ.

4.2.4. MONAZITE TRACE ELEMENT ANALYSIS

Monazite trace element data was collected simultaneously with U-Pb geochronology data. Sample KP001 was the only sample from the data set which contained sufficiently sized monazite grains that were utilised for U-Pb geochronology. Therefore, only this sample underwent monazite trace element analysis. Data from sample KP001 was overlaid and compared to Kanmantoo Cu-Au mine samples of chlorite alteration, felsic veins and two regional samples (KMT1 and BKDK1) (Figure 9). KP001 has low values of LREE similar to the most distal existing regional sample BKDK1 but much lower HREE enrichment. KP001 on average has the lowest recorded LREE and HREE of all four existing samples. KP001 exhibits variable Y_2O_3 and Th/U weight percentages and the lowest recorded Gd/Lu and Eu/Eu* values indicating KP001 results are not consistent with hydrothermal monazite formation.

4.2.5. PYRITE TRACE ELEMENT ANALYSIS

Previous studies have identified visible Au and overall Au anomalism within sections of S11 drill core. Booth (2018) identified abundances of Au within pyrite grain structure within Kanmantoo Cu-Au deposit. This same pyrite-Au relationship will be investigated within two samples (2721791 and 2721792) from drillhole S11 of which contain abundant pyrite grains. Quantitative ablation line analysis covering the exposed surface of 10 pyrite grains were completed to find zonation variances in elemental abundances throughout the grain. All pyrite grains contain significant variable abundance of Co, Ni, As and Bi with minor Cu, Ag, Au and Pb (Figure 10). Pyrite grains from sample 2721791 have zonation highlighted with near grain centre enrichment of Co and Ni exceeding 1000 ppm on average, reaching near 10000 ppm within grain 2721791 A 1. Regions with enrichment in Co and Ni contain relative depletion most noticeably of Bi,

but also Ag, Cu and Pb. Bi abundance on average ranged from 50-100 ppm at grain boundary to near 0 ppm when Co and Ni are in greatest abundance at the pyrite core. Sample 2721792 also contains zonation highlighted by Co and Ni enriched at pyrite grain core. This relationship between Co/ Ni and Bi is not observed within 2721792 as Bi exhibits enrichment rather than depletion (like that of sample 2721791) when Co and Ni are enriched. Abundances of Ag, Cu and Pb vary in conjunction with Bi, Ni and Co. Singular zonation patterns within 2721792 are not present within the trace element data like those easily distinguishable zonation trends within sample 2721791. Cu abundance is variable within both samples. 2721791 contains two spikes exceeding 1000 ppm with an additional spikes of 12100 ppm and 7500 ppm. 2721792 contains two copper spikes exceeding 1000 ppm with an additional spike reaching 13600 ppm.

Six pyrite trace element maps were created with LA-ICP-MS line scanning from the largest five pyrite grains within samples 2721791 and 2721792. The maps exhibit resolution great enough to observe trace element variation and zonation within the pyrite grains with both ppm (Figure 12) and particle counts (Figure 11) units. Analysing number count maps, all five pyrite grains exhibit zonation, most easily observed viewing the variable abundance of Co and Ni within growth rings surrounding the grains core. Abundances of Au, Ag, Al, Si, Mg, Mn and Zn are minimal with only small abundances present as inclusions with As and Pb occupying low abundances at grain boundaries and fractures. Bi concentrations are variable with highest concentrations present as inclusions with intermediate concentrations bordering grains and within fractures. Major fractures visible within SEM imagery correlate with maximum Cu abundances, the highest concentration visible within this mapping method of 600000 particle counts. Unit mapping (ppm) resulted in much lower resolution final imagery

and created multiple problems with identifying zonation. Grain 2721791-2 (Figure 12) exhibits minor zoning with no definitive specific grain core location. Zonation is recognisable with variations in Co and Ni from below detection limit to above 1000 ppm. Cu abundance hot spots are visible reaching 8000 ppm, but it is unknown if this is a correlation with grain fracture. Inclusions of Bi (2000 ppm), Ca (2000 ppm) and Ag (200 ppm) are present throughout the pyrite grain.

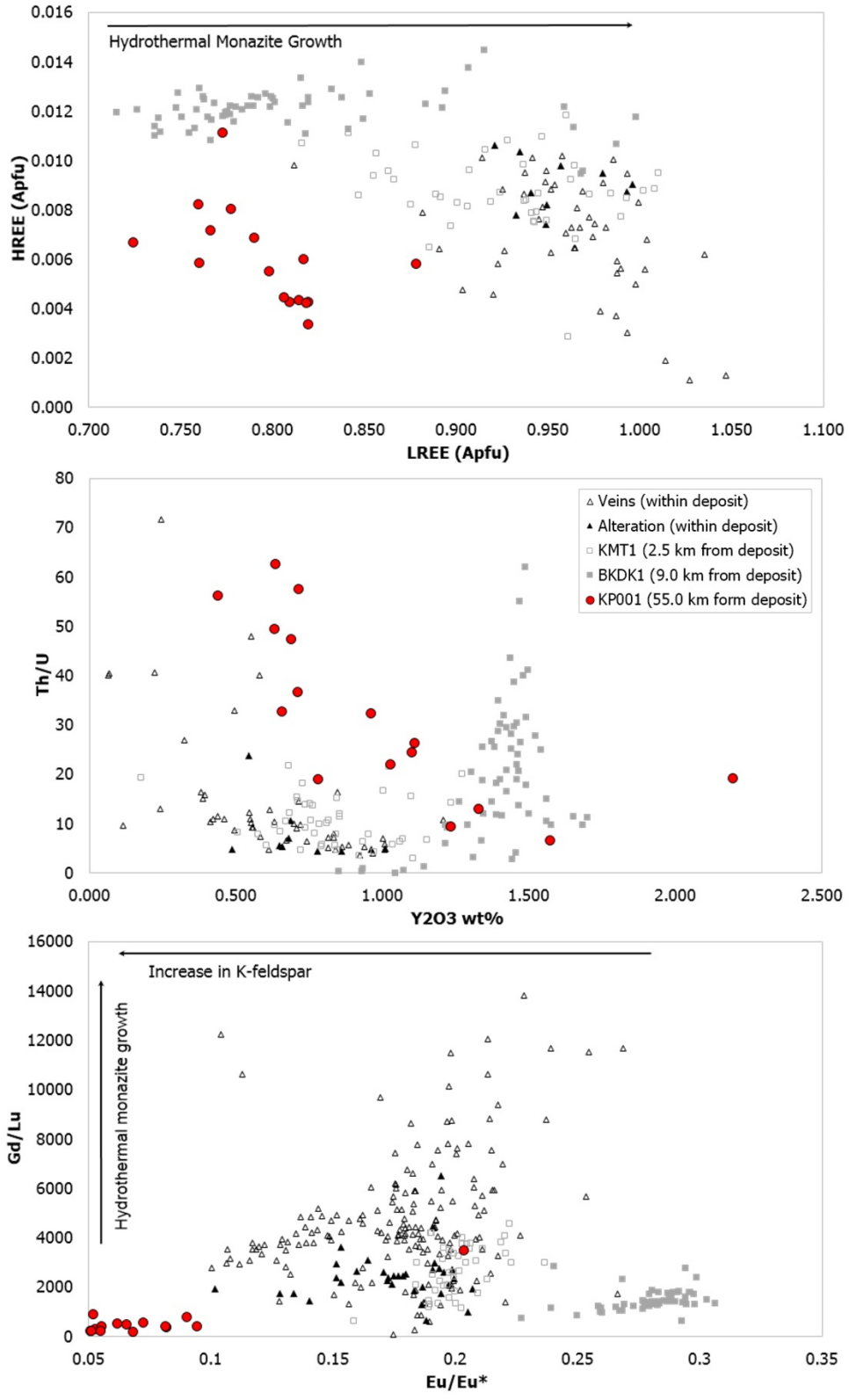

Figure 9: Graph recreated from Kimpton (2018) containing sample KP001 overlay of vein, alteration and proximal sample trace element chemistry. Plot of HREE vs LREE (Apfu = atoms per formula unit) (Poitrasson, Chenery, & Shepherd, 2000). Th/U vs Y_3O_3 and Gd/Lu vs Eu/Eu*, where Eu*=((Sm+Gd)/2) (Rubatto, Hermann & Buick, 2006).

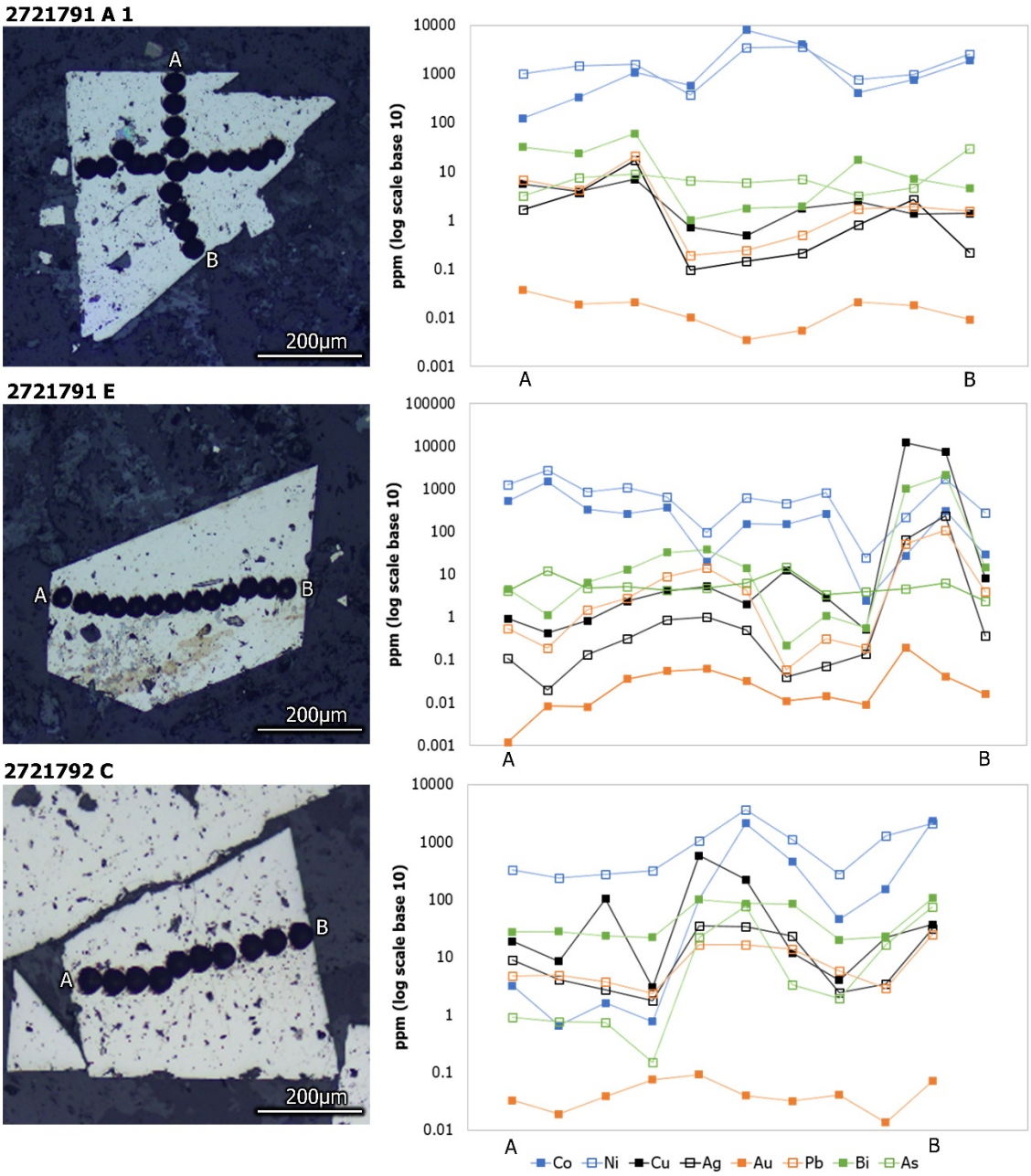

Figure 10: Quantitative ablation line spot analysis of three pyrite grains from samples 2721791 and 2721792 displaying the variation in trace element chemistry across each grain.

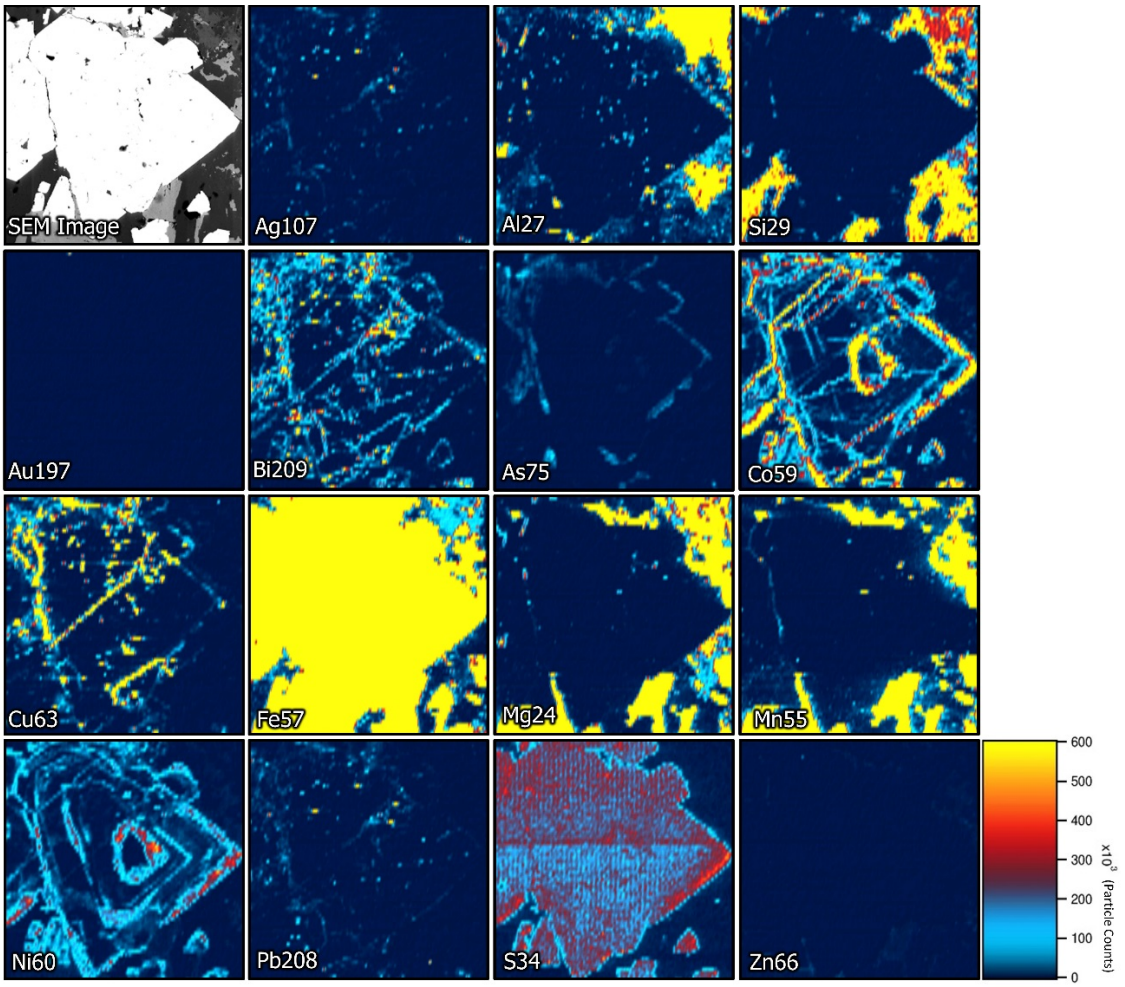

Figure 11: Semi quantitative trace element map of pyrite within sample 2721792 (specific grain 2721792-3) to display variation in chemistry throughout the entire grain. Zonation is present within the grain highlighted best by changes in Co and Ni abundance (all individual element maps utilising the same scale of number of particle counts).

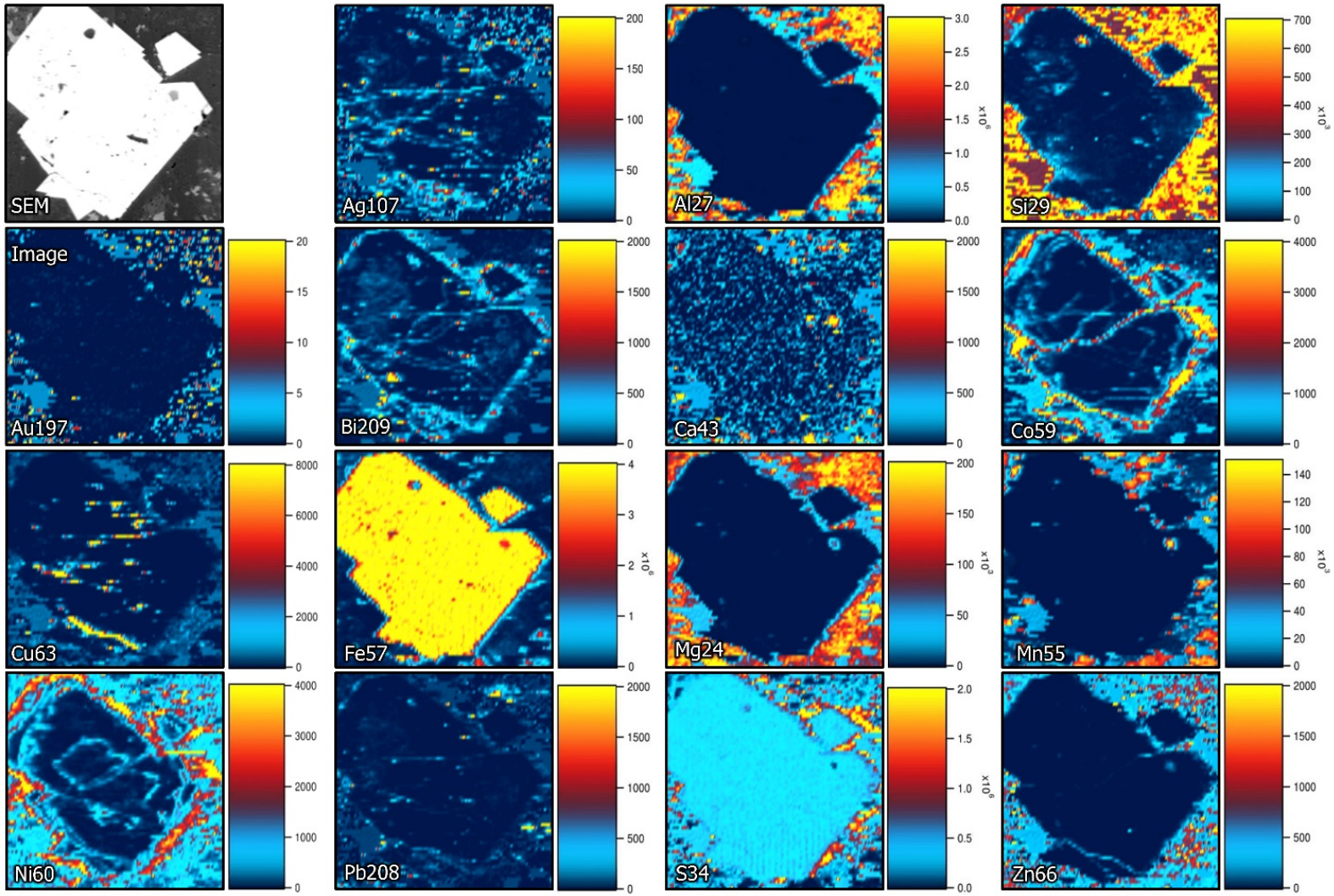

Figure 12: Semi quantitative trace element map of pyrite within sample 2721791 (specific grain 2721791-2) to display variation in chemistry throughout the entire grain. Zonation is present within the grain highlighted best by changes in Ni abundance (all individual element maps utilising separate scale of ppm).

4.3. Extended sample set classifications

4.3.1. SAMPLE CLASSIFICATIONS

The data for 720 additional samples within the sample area of interest were provided by Prof. John Foden. The data set has been collected over a prolonged period and represents data from multiple University of Adelaide honours and PhD level studies. The data set was collected using multiple techniques, which have not been fully listed. However, the data is considered fit for purpose and the samples have been individually classified using the following schemes:

1. Tectonic Classification of Mafic Igneous Rocks (Cabanis & Lecolle, 1989).
2. TAS Plutonic (Middlemost, 1994).

Utilising ioGAS 7.1 geochemical software, all 720 additional samples were plotted within the two classification schemes (Figure 13 and Figure 14). Table 5 displays the number of samples of which have been classified within each scheme. All nine possible rock-types were represented by the sample set for tectonic classification with 14 categories of a possible 19 being represented in the data for TAS plutonic classification. Refer to Appendix A to identify each individual sample classification.

Table 5: Tectonic classification of mafic igneous rocks and TAS plutonic classifications of extended sample set displaying the number of samples classified into each category.

Tectonic Classification of Mafic Igneous Rocks (Cabanis & Lecolle, 1989)		TAS Plutonic (Middlemost, 1994)	
Classification	**No. of Samples**	**Classification**	**No. of Samples**
Alkaline	74	Alkalic Basalt/ Alkalic Gabbro	50
Arc calc-alkaline	267	Diorite	56
Arc tholeiite	16	Foid-gabbro	24
Arc transitional	33	Foid-monzodiorite	1
Back arc	26	Foidolite	4
Enriched MORB	17	Gabbro	133
Weakly enriched MORB	48	Gabbroic diorite	44
Late to post orogenic intra-continental domains	173	Granite	231
N-MORB	11	Granodiorite	68
Undetermined	55	Monzodiorite	38
		Monzogabbro	29
		Monzonite	19
		Peridotgabbro	15
		Quartz monzonite	5
		Undetermined	3

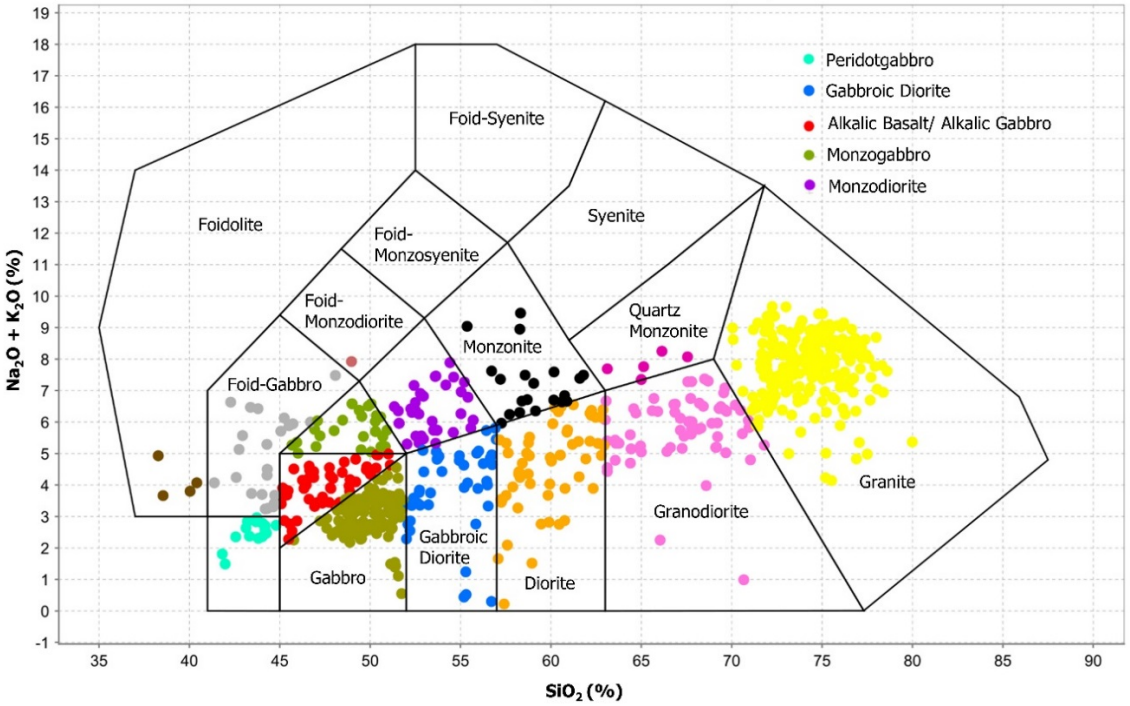

Figure 13: TAS Plutonic diagram created with ioGAS 7.1 software displaying classification of 720 samples within the extended sample data set. Samples are categorised into 14 different rock classifications with three samples being undetermined because of data collection errors.

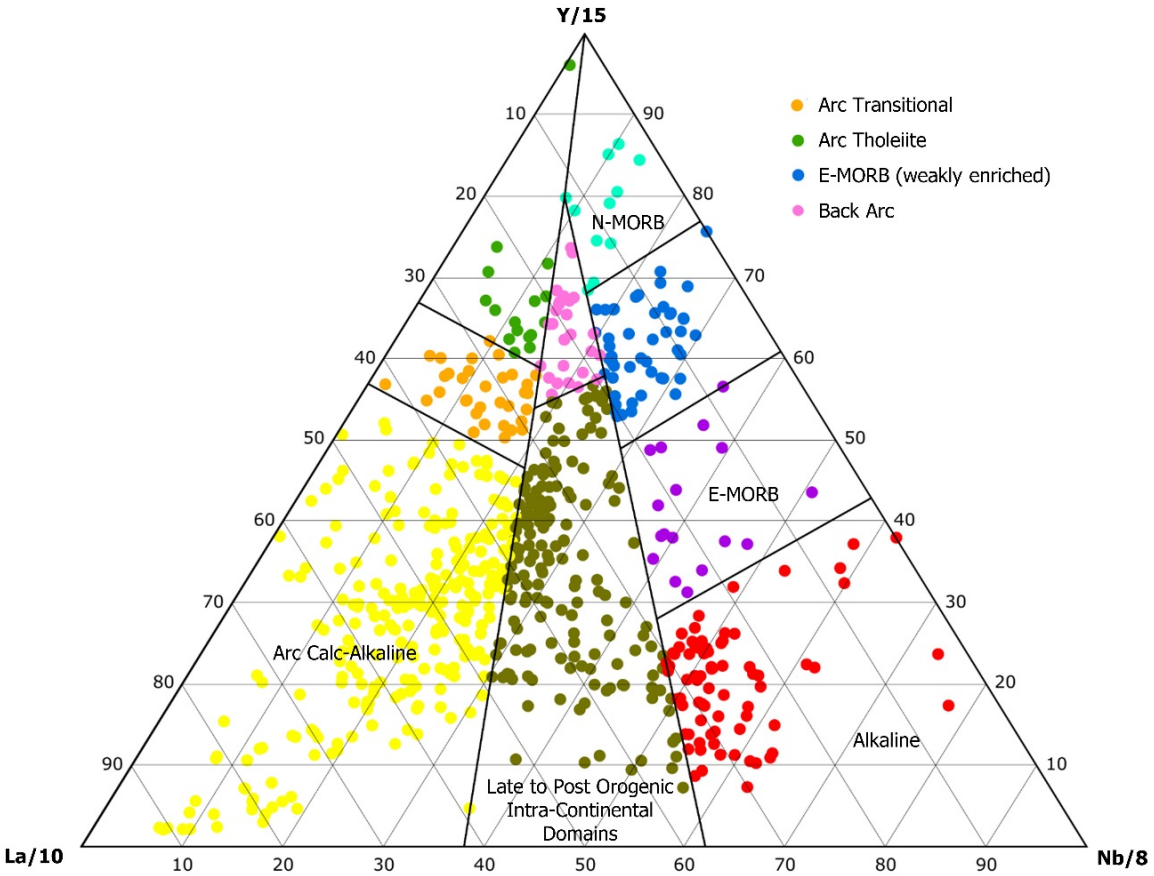

Figure 14: 720 extended analysis samples plotted on a tectonic classification of mafic igneous rocks plot using ioGAS 7.1. Samples are categorised into nine classifications with 55 samples being undetermined (grey) due to plotting outside of the tectonic ternary diagram.

4.3.2. SAMPLE SPATIAL DISTRIBUTION

The 720 classified samples were spatially plotted using the Geographic Coordinate System WGS 1984 on ArcMap 10.5.1 to identify any trends between sample classification and location. A distinctive belt of samples is visible because of the spatial limitations of the original dataset.

Tectonic Classification of Mafic Igneous Rocks:

Observing the most abundant classifications, there is no definitive segregation or pattern associate with geographical location (Figure 15). It can be hypothesised that there are three zones of intrusive material for arc calc-alkaline, alkaline and late- to post-orogenic intra-continental domains residing in the north, central and south of the sample area. However, it is more possible these three zones are present because of the spatial constrictions of the dataset primarily because of samples not being taken as regularly between these zones.

TAS Plutonic Classification:

Three distinct regions of granite classified samples are present located within the north, south and centre of the sample area. The highest concentration of granite is located within the south of the sample area with one single coastal sample residing ~60 km away from the centre of the main cluster. Gabbro classified samples are present throughout the whole sample area but are dominantly concentrated (125 samples) in close proximity to the Kanmantoo Cu-Au mine and in the north of the sample area. Central region occupies five gabbro samples with only three samples being located in the south. The third most abundant classification; granidiorite, exhibits the same trend as gabbro with greater concentrations in the north reducing to the south.

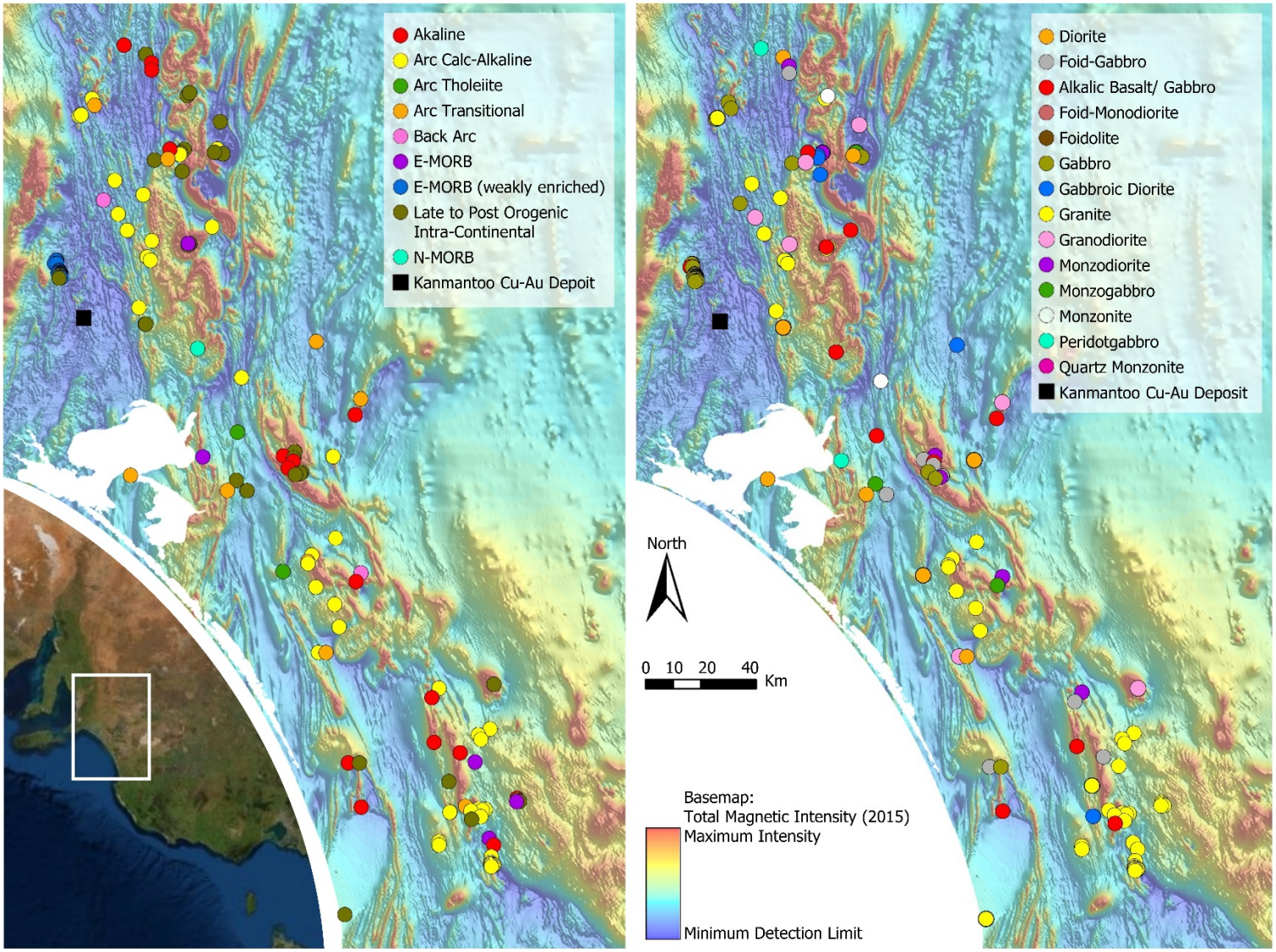

Figure 15: Spatial distribution of igneous samples created using ArcMap 10.5.1 displaying the locations of all 720 samples provided by Professor John Foden with colour overlay of two rock classifications. Total magnetic intensity basemap sourced from the Department of Primary industries and Resources, South Australia.

5. DISCUSSION

This study has identified multiple magmatic events within the sampled Delamerian affected terrains and aimed to identify Delamerian-aged intrusives, which may have acted as heat sources for related hydrothermal systems. This study also aims to draw comparison between the lithologies, mineralogy and possible economic mineralisation between the sample locations and areas which these magmatic events have affected. The geochronology of each sample will then be placed into the context of the Delamerian Orogeny.

5.1. Geochronology

5.1.1. MINERALOGY HABIT AND RELIABILITY FOR ABSOLUTE AGES

This investigation used a combination of zircon, titanite and monazite minerals identified within the sample set. Titanite proved to be the most reliable and the most abundant dating mineral, and often exhibiting euhedral structure and grain sizes exceeding 50 μm. Over 100 individual titanite grains were identified within five thin sections, allowing for a larger sample set, assisting data reduction and bracketing. Titanite produced U-Pb Tera-Wasserburg lower intercept ages with errors ranging from 2.8 Ma to 43.0 Ma, the lowest average error in comparison to monazite and zircon. Apatite grains were present in nearly every sample, but previous apatite geochronology (Kimpton, 2018) demonstrated that error margins were too large for apatite to be considered for this investigation. Monazite and zircon were less abundant throughout the sample suite and with ~85% of identified monazite and zircon grains being too small for ablation. Strong overprint sericite alteration resulted in many zircon and monazite

grains being indistinguishable, but also the very fine grain texture within most samples is indicative of fast cooling and therefore reduced time for mineral growth.

5.1.2. TITANITE U-PB GEOCHRONOLOGY INFERENCES

Five samples were successfully dated using titanite U-Pb dating from two different regions within the field area, with all exhibiting common Pb trends. Samples KFP001, KP004 and KP008 located within the Hillgrove Resources Kanappa drilling project north-east 55 km from the Kanmantoo mine exhibit Tera-Wasserburg lower intercept ages of 486.4 ± 2.8 Ma, 486.9 ± 4.4 Ma and 478.4 ± 6.4 Ma. These three samples are from 1.8 km of each other and have analogous ages with Kanmantoo Cu-Au mine samples BK25A and BK25B, samples dated by Kimpton (2018) at 485.35 ± 2.46 Ma and 483.43 ± 2.52 Ma. This succinct age range is comparably different to samples 2721785 and 2721786 from drill hole PADD 31 located 210 km south-east from Kanmantoo which returned less accurately constrained ages of 530 ± 23 Ma and 511 ± 43 Ma. These two samples contain the greatest common Pb abundances resulting in discordant data and resulted in a poorly constrained lower age intercept of which could still represent the same ~480 Ma Kanappa drilling project samples.

5.1.3. ZIRCON U-PB GEOCHRONOLOGY INFERENCES

Five samples were dated utilising zircon U-Pb geochronology with two samples (KP004 and KP008) being unstable because of small ablation sample counts and errors associated with inclusions resulting in age errors exceeding 100 Ma. Sample KFP001 is the only sample to host grains of zircon and titanite suitable for analysis. Zircon geochronology provided a weighted mean age of 492.8 ± 5.2 Ma in range of the error overlap of titanite geochronology data. Similarly aged sample 2721788, located south-

east of Kanmantoo exhibits a concordant Wetherill age of 484.5 ± 3.1 Ma, the only concordant date achieved via zircon U-Pb geochronology in this study. This sample represents an undeformed altered granite of similar age to an undeformed andesite (478.8 ± 5 Ma) located at ~134 m depth within drill hole PADD 28 (Foden, 2015). Zircon geochronology from this investigation further supports the presence of an undeformed volcanic suite located within south-east South Australia of which has no current established stratigraphic name in South Australia.

In comparison, sample DAW-SYN contains uranium fractionation, and therefore two concordia intercepts of which are not caused by common lead abundances as displayed in every titanite U-Pb diagram. It is interpreted that the two intercepts for the DAW-SYN sample represent the initial emplacement of the original rock unit (1212 ± 58 Ma) and the subsequent Delamerian metamorphism (501 ± 58 Ma). Rocks that have undergone multiphase tectono-metamorphic events is generally not comprised of homogenous zircons but much more likely will contain multi-core zircons with magmatic overgrowths and possible metamorphic overgrowths (Kröner, Wan, Liu & Liu, 2014). As the zircons within DAW-SYN are very small, it is possible that overgrowths and zonation regions were all sampled together resulting in the differences of chemistry and uranium fractionation present within the produced Tera-Wasserburg Concordia diagram. Ireland, Flottmann, Fanning, Gibson & Preiss (1998) recorded two main age peaks of detrital zircons from within with three units of the Kanmantoo Group sediments, one peak ranging from 900 – 1200 Ma coinciding with the upper age intercept of the DAW-SYN sample concordia diagram. These zircons are from the Grenville Orogen (orogen cycle 1350 – 1000 Ma), a Mesoproterozoic, long lived orogen which was associated with the assembly of Rodinia and currently represents the

largest set of detrital zircons distributed throughout the Kanmantoo Group sediments (McLelland, Daly & McLelland, 1996). It is hypothesised that with the influx of hydrothermal and igneous material of the forming DAW-SYN remobilised these Kanmantoo Group detrital zircons into the new location within DAW-SYN.

5.1.4. MONAZITE U-PB GEOCHRONOLOGY INFERENCES

Only sample KP001 contained enough suitably sized monazite grains for ablation and produced the youngest age from the sample area with weighted mean of 473 ± 18 Ma and Wetherill 469 ± 23 Ma. However, caution should be used when interpreting the relevance of this date because of the relatively large associated error.

5.2. Identified magmatic events

This study has identified two separate aged magmatic events, the oldest occurring approximately 520 Ma (termed Pre-Delamerian Magmatism) with the second occurring 490 – 480 Ma (termed Syn-Delamerian Magmatism) and the possibility of a third occurring ~471 Ma (termed Post-Delamerian Magmatism), which is consistent with the literature (Foden et al., 2006; Foden et al., 2019; Kimpton, 2018).

5.2.1. PRE-DELAMERIAN MAGMATISM (520 MA)

Evidence for Pre-Delamerian Magmatism within this investigation is spatially confined to a single drill hole, PADD 31, which is the southernmost sample within the data set. Petrography from this investigation and core logging data provided by the Australian Stratigraphic Database identified the intrusive within PADD 31 as the Truro Volcanics. The thickness of this intrusive is variable reaching 490 m at many locations and includes 13 different petrographically distinguishable units (Forbes, Coats & Daily,

1972). Samples 2721785 and 2721786 contain fine grained dark green/grey basalt and andesite flows abundant with chlorite, calcite and carbonate material, corresponding to the Truro Volcanics C4 unit (main phase) outlined by Forbes et al. (1972). Zircon U-Pb dates from this study correlate well with previous dating of the Truro Volcanics published by Cooper, Jenkins, Compston & Williams (1992) at 526 ± 4 Ma and most recently by Jenkins, Cooper & Compston (2002) at 522 ± 2 Ma. The Truro Volcanics precede the onset of the Kanmantoo Group sedimentation and represents evidence of renewed crustal extension and intra-cratonic rifting (Cooper et al., 1992). This magmatic stage represents pre-D1 Delamerian deformation with studies completed by Belperio et al. (1998) suggesting extension of the Normanville Group, where the Truro Volcanics are housed, could have reached the Victorian border with progressive changes in Early Cambrian slope environments and continental shelfs. It is also hypothesised that the Murray Basin region was the only location of volcanism during the late Early Cambrian. Therefore, it is recognised that the Kanmantoo Group sediments represent the onset of a new tectono-sedimentary cycle within the region (Daily, 1956) postdating this Pre-Delamerian Magmatism.

5.2.2. SYN-DELAMERIAN MAGMATISM (~490 – 480 MA)

Evidence for Syn-Delamerian Magmatism is represented by four samples from three locations and include hydrothermal zircon and titanite U-Pb ages of 486.9 ± 4.4 Ma (KP004), 486.4 ± 2.8 Ma (KFP001), 484.5 ± 3.1 Ma (2721788) and 478.4 ± 6.4 Ma (KP008). Samples from this investigation hosting Syn-Delamerian Magmatism are confined to the Kanappa Drilling region (samples beginning KP or KFP) located 55 km north-east of Kanmantoo, but also at a single location situated 224 km south-east of

Kanmantoo, the eastern most sample within the data set. Three Kanappa samples (KFP001, KP004 and KP008) are classified as quartz diorites. The presence of hydrothermal chlorite alteration at location KFP001 implies there has been movement of heated aqueous fluids likely transported via fractures and fault zones (Meyer & Hemley, 1967), and is common in all ore systems (Berger, 1999). Sample 2721788, also represents Syn-Delamerian Magmatism, but is chemically and texturally different to the Kanappa samples. Two distinctive intrusive materials and textures are present within the sample, indicating at least two stages of igneous activity. This sample is from a depth of approximately 155 m and contains rounded quartz grains exhibiting berlin blue chlorite alteration indicating the presence of hydrothermal alteration. Furthermore, very fine (sub 0.1 mm) pyrrhotite is present throughout the sample but only in one of the two intrusive compositions. Original hand samples of KP004, KP008 and KFP001 have been recorded to exhibit minor pyrrhotite and chalcopyrite mineralisation in the form of wispy infill veining reaching 2 mm in width (Taylor, 2019). Although these mineralised veins were not identified within thin section petrography from this study, the mineralisation temporally associated with Syn-Delamerian Magmatism and the age correlation to U-Pb dating completed at the Kanmantoo Cu-Au mine provides insight into prospectivity and further broad scale mineralisation potential of intrusive rocks of this age. Sample geochronology demonstrates this Syn-Delamerian Magmatism stage occurred during Delamerian D2 through to post D3 (post-peak metamorphism), the same deformation stage of which the Kanmantoo deposit was emplaced (Kimpton, 2018), and represents a magmatic stage with enhanced prospectivity.

5.2.3. POST-DELAMERIAN MAGMATISM

Evidence for Post-Delamerian Magmatism is provided by sample KP001, collected from the same drillhole as samples KP004 and KP008. U-Pb monazite geochronology of both Wetherill age and weighted mean age place this intrusive at 469 ± 23 Ma and 473 ± 18 Ma. It is possible that this sample represents Syn-Delamerian Magmatism especially given its overlapping errors and proximal location to other Kanappa samples dating from this stage. However, petrographic comparisons between these samples show that KP001 is compositionally different to those samples representing Syn-Delamerian Magmatism. Sulphides were not found within this sample but the presence of magnetite (10 – 20 μm) allows for some heightened prospectivity given the association of magnetite and many hydrothermal ore systems, including Kanmantoo (Kimpton, 2018). Taking into consideration the petrological differences between Syn- and Post-Delamerian Magmatism, this Post-Delamerian Magmatism sample represents a magmatic event which occurred at ~471 Ma and represents the youngest magmatic event recorded by this investigation occurring post-peak Delamerian Metamorphism (D3). Foden (2019) displayed a comparative age range between 486.1 ± 1 Ma (Kongal Rocks) and 470.1 ± 1 Ma (Monteith Granite) concluding this age range (Table 6) supports convergent deformation ceased around 490 Ma during this stage of the Delamerian Orogeny (Foden et al., 2006; Foden et al., 2019).

Table 6: Concordia ages from Foden (2019) correlating with sample KP001 from this investigation, providing supporting evidence of Post-Delamerian Magmatism representing the possible final minor stages of the Delamerian Orogeny.

Sample	Age (Ma)
Kongal Rocks	486.1 ± 1
Mannum Granite	482.7 ± 2
Marcollat Granite	478.2 ± 0.8
Mt Monster porphyry	472.5 ± 1
PADD 28 undeformed granodiorite	475.2 ± 1
Monteith Granite	470.1 ± 1

5.3. Hydrothermal exploration guides with monazite trace elements

Research conducted by Kimpton (2018) using monazite trace displayed there was a strong vector relationship towards the Kanmantoo Cu-Au deposit in which LREE were enriched with depletion of Y. Monazite with hydrothermal origins can be differentiated from metamorphic origins through the analysis of trace elements and radiogenic distributions (Figure 9) (Poitrasson et al., 2000; Seydoux-Guillaume et al., 2012). Sample KP001, the only sample containing sufficient monazite for analysis, exhibits a different trace element trend to that of Kanmantoo vein and alteration hydrothermal monazite grains. KP001 monazite grains exhibit relative depletion in Eu, Gd, Lu and depletion in LREE and Y. This geochemical signature provides evidence the monazite in KP001 are likely metamorphic in origin (Poitrasson et al., 2000; Seydoux-Guillaume et al., 2012).

5.4. Sulphide mineralisation composition

Quantitative ablation line spot analysis and semi-quantitative geochemical maps were created for five pyrite grains across two samples (2721791 and 2721792) from drillhole S11. Visible Au has previously been identified within this drill core, but was not identified within samples 2721791 and 2721792. These samples were selected because of the presence of relatively large pyrite grains which may have hosted free Au. Quantitative spot analysis across the largest pyrite grains within each sample identified trace levels of Au (average 20 ppm), Ag (average 200 ppm) and Bi (average 2000 ppm) are present within all grains analysed. Cu is the most abundant trace metal in the pyrite grains and reaches a maximum of 8000 ppm, present as micro-inclusions and pyrite grain fracture infill. The distribution of these elements appears to be affected by zonation (growth) halos which display varying relative abundances of Co and Ni. A

positive relationship between Bi and Au is recorded at many Au mines around the world (Yunsheng, Liandeng & Huihuang, 2005). This relationship is also present within both samples analysed in this project with Au concentrations in pyrite reaching ~20 ppm in locations of bismuth enrichment of up to ~500 ppm. However, the areas within the pyrite grains which contain the highest Bi do not contain the highest Au abundances. The trace Au present appears to be chemically bound as a solid solution or as sub-microscopic inclusions within the analysed pyrite grains.

5.5. Additional prospectivity studies

Cu and Au fertility identification methods developed by Loucks (2014) utilising trace and major element geochemistry of known prospective and non-prospective samples have been utilised in conjunction with various additional samples from the Kanappa drilling project within deposit scale proximity to samples KP004, KP008 and KFP001. Kanappa drilling samples from two drill holes plot in two zones with over half of all samples being situated within regions of known Cu and Au prospective intrusive chemistry (Figure 16). Similarly, trace element geochemical studies developed by Wells, Meffre, Cooke & Steadman (2019) utilising Zr and Y cut off values of 120 ppm and 12.5 ppm formed a fertility window which identified 100% of all mineralised samples within the Northparkes district of central western NSW. Using this same identification method from Wells et al. (2019), geochemical data provided by Prof. J Foden was spatially plotted to find 31 fertile samples within the sample area of this investigation. Most importantly, 13 are fertile samples located with 4.5 km of pyrite mineralised samples 2721791 and 2721792 (within 13 km of the Kanappa drilling project). These fertile samples on average are classified as gabbroic diorites and granites

with tectonic classifications of arc calc-alkaline and late- to post-orogenic intra-continental domains. The locations of these fertile samples may indicate the presence of a greater area of prospective intrusions and related hydrothermal systems (Figure 17) surrounding the existing Kanappa drilling project.

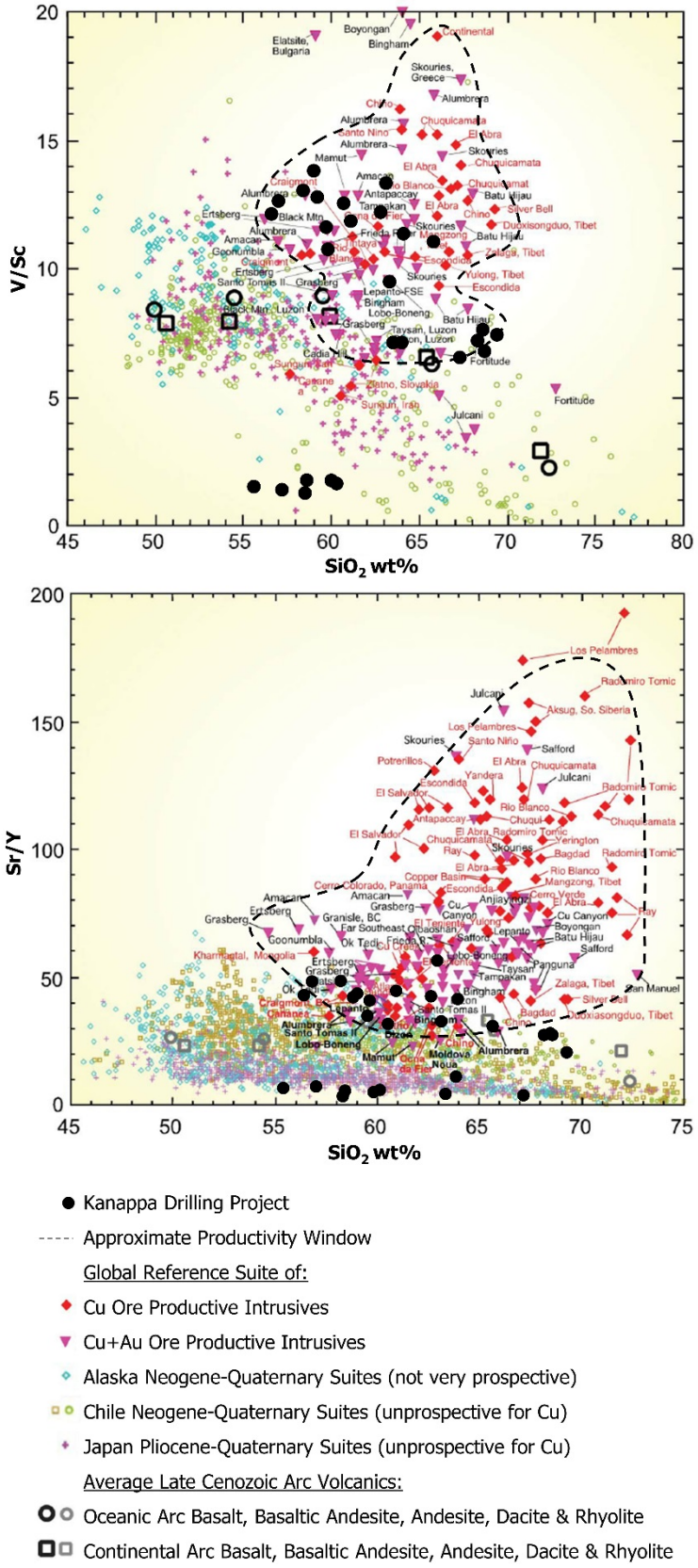

Figure 16: Cu-Au fertility plots from Loucks (2014) with overlaid samples from the Kanappa drilling project located 55 km north-east from the Kanmantoo deposit. Sr/Y is comparably different to V/Sc when comparing both Au and Cu fertility. V/Sc is resistant to disturbances caused by hydrothermal alteration and is therefore best suited for Cu prospective intrusive identification in comparison to Au (Loucks, 2014).

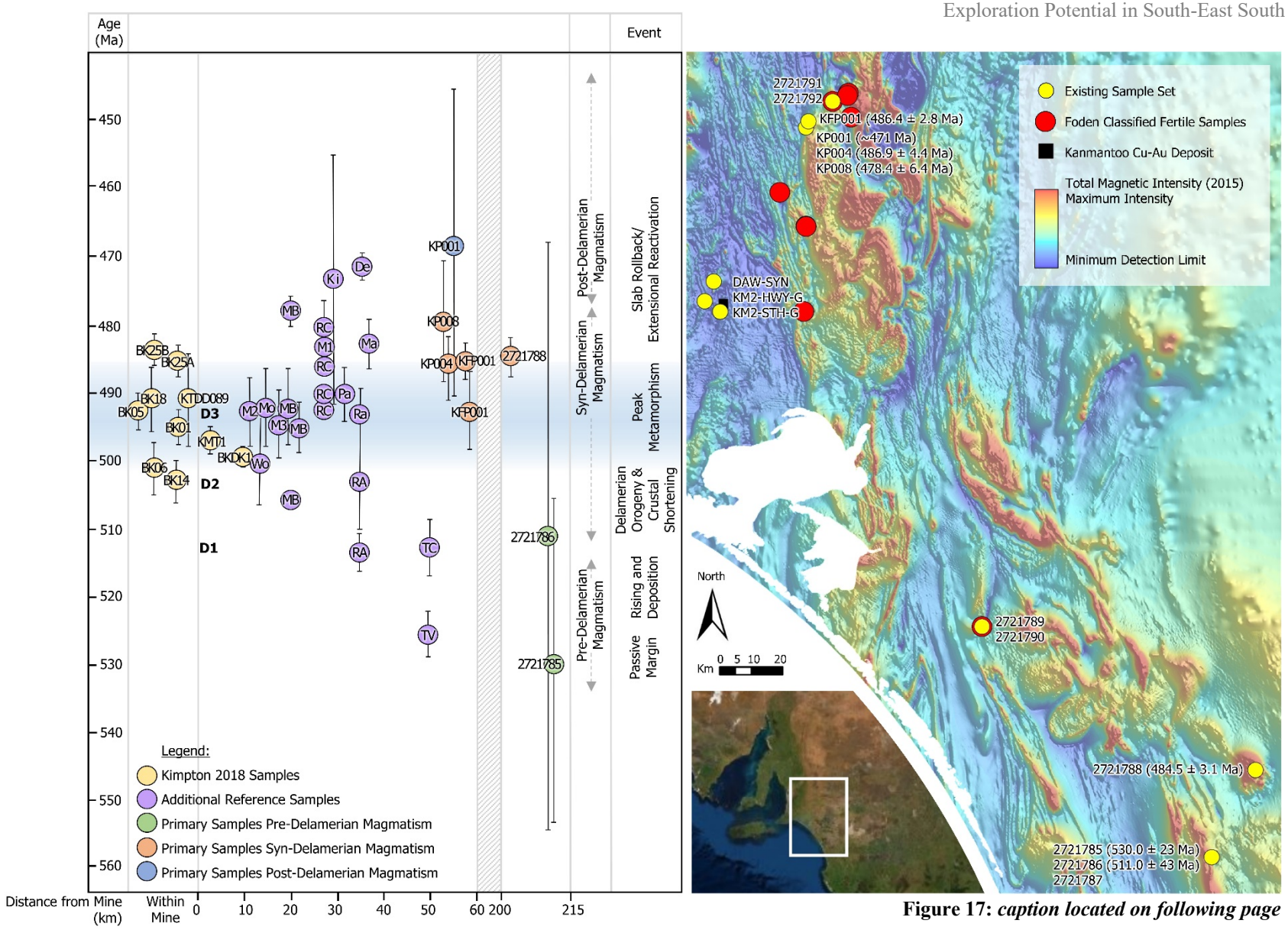

Figure 17: ***caption located on following page***

Figure 17: Time plot recreated from Kimpton (2018) displaying spatial relation of original sample set of this investigation with Kimpton (2018) Kanmantoo mine samples, with associated map of specific original and additional fertile sample geographic locations. The highest density of fertile samples being located surrounding 2721791 and 2721792 further indicates that the mineralisation identified in this area may be of broader scale. Additional fertile samples located between the Kanappa drilling program and the Kanmantoo deposit indicate a mineralised belt may be present between these 2 locations. Metamorphic isograds defined by Preiss (1995). Time plot sample identification from Kimpton (2018) BK05 (492.8±2.94 Ma), BK25B (483.43±2.52 Ma), BK18 (491.17±5.54 Ma), BK06 (501.1±4.04 Ma), BK25A (485.35±2.46 Ma), KTDD089 (491.06±7.03 Ma), BK01 (495.11±2.79 Ma), BK14 (503.44±3.32 Ma), KMT1 (496.98±2.18 Ma), BKDK1 (499.09±1.54 Ma). Additional reference sample ages: monazite U-Pb Kanmantoo group metasediments (Stinear, 2017): M1 (438.5±4.3 Ma), M2 (492.4±5.3 Ma), M3 (493.8±5.3 Ma). U-Pb geochronology (Cooper et al., 1992): TV Truro Volcanics (526±4 Ma). Regional igneous intrusive and metamorphic ages (Burtt & Phillips, 2003; Foden et al., 2006; Foden, Sandiford, Dougherty-Page & Williams, 1999; Foden et al., 2002; George, 2018; Milnes, Compston & Daily, 1977; Turner & Foden, 1996): Tc Tanunda Creek (513.4±4 Ma), Ra Rathjen (514±4 Ma, 503±7 Ma), MB Murray Bridge (506±1 Ma, 495.37±4.14 Ma, 495.2±3.7 Ma, 492±6 Ma, 478±2 Ma), Wo Woodside Dykes (500±7 Ma), Mo Monarto (492±6 Ma), BH Black Hill (487±5 Ma), PC Petrel Cove (497.8±2.6). Ar-Ar Cooling Ages (Turner et al., 1996): Ra (493±5 Ma), Pa (490±4 Ma), Rc (480±4 Ma). Ages defining tectonic regimes and mineralisation by (Griessmann, 2011; Jenkins et al., 2002): Ki Kitticoola Au (473±19 Ma), De Deloraine Au (471.3±4.1 Ma). Tectonic regimes and other age boundaries sourced from Jenkins et al. (2002) and Griessmann (2011) with total magnetic intensity basemap sourced from the Department of Primary industries and Resources, South Australia.

5.6. Delamerian Orogeny

It has been widely recognised the Delamerian Orogeny provided an environment spanning millions of years with the potential for generating intrusive units. These units could mobilise hydrothermal fluids and transport metals resulting in metal accumulations such as the Kanmantoo Cu-Au deposit (Kimpton, 2018). Two samples located over 200 km south of Kanmantoo representing part of the Truro volcanics, represent the first identified magmatic stage within this investigation and were emplaced during the onset of Delamerian-related tectonism (Cooper et al., 1992; Jenkins et al., 2002). The presence of this early magmatism located south of Kanmantoo suggests early pluton development may have initiated in the south before migrating north. Syn-Delamerian Magmatism, represented by samples from the Kanappa Drilling region in this study, contains the greatest on average abundance of pyrite and pyrrhotite mineralisation for a single location. The Syn-Delamerian Magmatism stage is interpreted to have taken place between ~490 – 480 Ma during late D3 post peak

metamorphism (Griessmann, 2011; Jenkins et al., 2002), and is the same stage in which the Kanmantoo Cu-Au deposit was emplaced (Kimpton, 2018). These metamorphic conditions may be responsible for the minor sulphide mineralisation present within the Kanappa region, supported with monazite trace element studies of this location concluding monazite is not of hydrothermal origin. Post-Delamerian Magmatism, the most recent magmatic stage occurring 486 - ~469 Ma, is represented by a single sample from this investigation and by six additional samples dated by Foden et al. (2019) from various locations (including those samples not confined by the sample space of this investigation). These post-Delamerian samples are interpreted to represent Delamerian slab rollback and extensional reactivation (Griessmann, 2011; Jenkins et al., 2002). This broad scale extensional environment is the probable cause of which multiple spatially distant locations contain intrusive and extrusive rock spanning approximately 15 Mys.

6. CONCLUSION

- This study has identified Delamerian Age intrusives throughout south-east South Australia with a strike length of over 200km north to south.
- The intrusive samples from this investigation are interpreted to represent three magmatic stages associated with the Delamerian Orogeny.
- Pre-Delamerian Magmatism, represented by samples 2721785 and 2721786, contains intrusives from the Truro Volcanics and took place at approximately 520 Ma.
- Syn-Delamerian Magmatism outlined within this investigation occurs between ~490 – 480 Ma (late D3 post peak Delamerian metamorphism) and contains

minor pyrrhotite and pyrite mineralisation and is represented by samples KFP001, KP004, KP008 and 2721788.

- Post-Delamerian Magmatism, represented by sample KP001 dated within this investigation at ~471 Ma, contains minor pyrite and pyrrhotite mineralisation and possibly represents an event in conjunction with the final minor stages of the Delamerian Orogeny.
- Hydrothermal-related mineralisation is associated throughout the sample set. However, within the sample set of this project, geochemistry, petrography and geochronology data indicate the highest prospectivity to be located ~60 km north-east of Kanmantoo within post-peak Delamerian metamorphism age intrusives of the Syn-Delamerian Magmatism stage outlined within this investigation.
- Titanite U-Pb geochronology was most effective on this Delamerian sample suite due to grain sizes exceeding 50 μm and grain counts exceeding 50 per thin section.
- Zircon geochronology of sample 2721788 provides further evidence of an undeformed volcanic suite at ~484 – 478 Ma located in south-east South Australia with no current established stratigraphic name in South Australia.
- The presence of Delamerian-aged intrusive units within the same age range as the intrusive-related Kanmantoo deposit, indicates potential for syn-orogenic mineralisation within the greater unexposed Delamerian-affected terrains of South Australia and represent an under explored and possibly highly prospective metallogenic belt.

7. FUTURE RESEARCH

Future research continuing the expansion of South Australian intrusive knowledge would be benefitted by geophysical studies detecting heat transference and conductivity in order to identify the proximal limitations between intrusive heat sources and deposit locations.

8. ACKNOWLEDGEMENTS

My supervisors Dr Richard Lilly, Peter Rolley, Professor John Foden, the team at Adelaide Microscopy including Benjamin Wade and Sarah Gilbert, past Kanmantoo research student Ben Kimpton, and student colleges at the University of Adelaide are thanked for their support, scientific opinions and insights. This project would not have been possible without the support and funding provided by Hillgrove Resources Limited and the associated staff and geology team including Daniel Woolford and Hayden Arbon. Insight into data processing and filtration was provided by the Department of Earth Sciences at the University of Adelaide including Mitchell Bockmann, Brad Cave and Megan Williams. The University of Adelaide and Adelaide Microscopy have provided training, analytical equipment and software essential for the completion of this study.

REFERENCES

BELPERIO, A., PREISS, W., FAIRCLOUGH, M., GATEHOUSE, C., GUM, J., HOUGH, J., & BURTT, A. (1998). Tectonic and metallogenic framework of the Cambrian Stansbury Basin - Kanmantoo Trough South Australia. *Journal of Australian Geology & Geophysics, 17*, 183-200.

BERGER, B. (1999). *Geochemistry*: Hydrothermal Alteration, SpringerLink.

BERRY, R., & CRAWFORD, A. (1988). The tectonic significance of Cambrian allochthonous mafic-ultramafic complexes in Tasmania. *Australian Journal of Earth Sciences, 35*(4), 523-533. doi:10.1080/08120098808729467

BOOTH, M. (2018). *Distribution and mineralogical association of Au at the Kanmantoo Cu-Au deposit.* (Honours Thesis), The University of Adelaide,

BURTT, A. (2003). Kanmantoo Trough. In *South Australian Mineral Explorers Guide* (pp. 3-29).

BURTT, A., & PHILLIPS, D. (2003). Ar/Ar dating of a pegmatite, Kinchina Quarry, Murray Bridge, South Australia. *MESA Journal, 28*, 50-52.

CABANIS, B., & LECOLLE, M. (1989). Le diagramme La/10-Y/15-Nb/8: Un outil pour la discrimination des series volcaniques et lamise en evidence des processus demelange et/ou de contamination crustale. *Compte Rendus de I'Académie des Sciences Series II, 309*, 2023-2029.

CONEY, P., EDWARDS, A., HINE, R., MORRISON, F., & WINDRIM, D. (1990). The regional tectonics of the Tasman orogenic system, eastern Australia. *Journal of Structural Geology, 12*(5/6), 519-543.

COOPER, J., JENKINS, R., COMPSTON, W., & WILLIAMS, I. (1992). Ion-probe zircon dating of a mid-Early Cambrian Tuff in South Australia. *Journal of the Geological Society, London, 149*, 185-192. doi:149.2.0185

CRAWFORD, A., & BERRY, R. (1991). Tectonic implications of Late Proterozoic-Early Palaeozoic igneous rock associations in western Tasmania. *Tectonophysics, 214*, 37-56.

DAILY, B. (1956). The Cambrian in South Australia. In: EI Sistema Cambrico, su paleogeografia y el problema de su base. *20th International Geological Congress, 2,* 91-147*,* Retrieved from: International Geological Congress.

FODEN, J. (2015). *Delamerian Orogeny.* Paper presented at the Broken Hill Confrence, Broken Hill.

FODEN, J., ELBURG, M., DOUGHERTY-PAGE, J., & BURTT, A. (2006). The Timing and Duration of the Delamerian Orogeny: Correlation with the Ross Orogen and Implications for Gondwana Assembly. *Journal of Geology, 114*, 189-210. doi:0022-1376/2006/11402-0004

FODEN, J., ELBURG, M., TURNER, S., CLARK, C., BLADES, M., COX, G., COLLINS, A. WOLFF, K., & GEORGE, C. (2019). *(In Review) Cambro-Ordovician Magmatism in the Delamerian Orogeny: Implications for Tectonic Development of the Southern Gondwanan Margin*. Gondwana Research.

FODEN, J., SANDIFORD, M., DOUGHERTY-PAGE, J., & WILLIAMS, I. (1999). Geochemistry and geochronology of the Rathjen Gneiss:implications for the early tectonic evolution of theDelamerian Orogen. *Australian Journal of Earth Sciences, 46*, 337-389.

FODEN, J., SONG, S. H., TURNER, S., ELBURG, M., SMITH, P., STELDT, B. V. D., & PENGLIS, D. V. (2002). Geochemical evolution of lithospheric mantle beneath S.E. South Australia. *Chemical Geology, 182*, 663-695. doi:S0009-2541 01 00347-3

FORBES, B., COATS, R., & DAILY, B. (1972). *Quarterly Geological Notes*, *The Geological Survey of South Australia, 44.*

GEORGE, C. (2018). *Adakitic rocks of Kanchina and their relationship to Gondwana subduction (Honours Thesis).* The University of Adelaide, Australia,

GRIESSMANN, M. (2011). *Gold mineralosation in the Adelaide fold belt*. (Doctoral Dissertation). The University of Adelaide, Australia.

IRELAND, T. R., FLOTTMANN, T., FANNING, C. M., GIBSON, G. M., & PREISS, W. V. (1998). Development of the early Paleozoic Pacific margin of Gondwana from detrital-zircon ages across the Delamerian orogen. *Geology, 26*(3), 243-246.

JACKSON, S., PEARSON, N., GRIFFIN, W., & BELOUSOVA, E. (2004). The application of laser ablation-inductively coupled plasma-mass spectrometry to in situ U–Pb zircon geochronology. *Chemical Geology, 211*, 47-69.

JAGO, J., GUM, J., HAINES, P., & BURTT, A. (2003). Stratigraphy of the Kanmantoo Group: a critical element of the Adelaide Fold Belt and the Palaeo-Pacific plate margin, Eastern Gondwana. *Australian Journal of Earth Sciences, 50*, 343-363. doi:10.1046/j.1440-0952.2003.00997

JENKINS, R., COOPER, C., & COMPSTON, W. (2002). Age and biostratigraphy of Early Cambrian tuffs from SE Australia and southern China. *Journal of the Geological Scienty of London, 159*, 645-658.

KIMPTON, B. (2018). *The geological relatioship between Kanmantoo Cu-Au deposit mineralisation, hydrothermal metasomatism and igneous intrusives.* (Honours Thesis), The University of Adelaide,

KRÖNER, A., WAN, Y., LIU, X., & LIU, D. (2014). Dating of zircon from high-grade rocks: Which is the most reliable method? *Geoscience Frontiers, 5*(4), 515-523. doi:10.1016/j.gsf.2014.03.012

LOUCKS, R. R. (2014). Distinctive composition of copper-ore-forming arc magmas. *Australian Journal of Earth Sciences, 61*(1), 5-16. doi:10.1080/08120099.2013.865676

LYONS, N. (2012). *Evidence for magmatic hydrothermal mineralisation at Kanmantoo Copper deposit, South Australia.* (Honours Thesis), The University of Adelaide,

MCLELLAND, J., DALY, J., & MCLELLAND, J. (1996). The Grenville Orogenic Cycle (ca. 1350-1000 Ma): an Adirondack perspective. *Tectonophysics, 265*, 1-28.

MEYER, C., & HEMLEY, J. (1967). Wall rock alteration, *Geochemistry of Hydrothermal Ore Deposits,* 166-235*,* Published: New York

MIDDLEMOST, E. (1994). Naming materials in the magma/igneous rock system. *Earth Science Reviews, 37*(3-4), 215-224. doi:10.1016/0012-8252(94)90029-9

MILNES, A., COMPSTON, W., & DAILY, B. (1977). Pre- to syn-tectonic emplacement of early Palaeozoic granites in south-eastern South Australia. *Journal of the Geophysical Society of Australia, 24*.

OLIVER, N., DIPPLE, G., CARTWRIGHT, I., & SCHILLER, J. (1998). Fluid flow and metasomatism in the genesis of the amphibolite-facies, pelite-hosted Kanmantoo copper despoit, South Australia. *American Journal of Science, 298*, 181-218.

PARKER, A. (1986). Tectonic development and metallogeny of the Kanmantoo Trough in South Australia. *Ore Geology Reviews, 1*, 203-212. doi:0169-1368(86)90009-0

PATON, C., HELLSTROM, J., PAUL, B., WOODHEAD, J., & HERGT, J. (2011). Iolite: Freeware for the visualisation and processing of mass spectrometric data. *Journal of Analytical Atomic Spectrometry, 26*(12). doi:10.1039/c1ja10172b

PAYNE, J. L., HAND, M., BAROVICH, K. M., & WADE, B. P. (2008). Temporal constraints on the timing of high-grade metamorphism in the northern Gawler Craton: implications for assembly of the Australian Proterozoic. *Australian Journal of Earth Sciences, 55*(5), 623-640. doi:10.1080/08120090801982595

POITRASSON, F., CHENERY, S., & SHEPHERD, T. (2000). Electron microprobe and LA-ICP-MS study of monazite hydrothermal alteration:Implications for U-Th-Pb geochronology and nuclear ceramics. *Geochimica et Cosmochimica Acta, 64*(19), 3283-3297.

PREISS, W. (1995). *Early and Middle Paleozoic Orogenesis: Delamerian Orogeny* (Vol. 2, The Phanerozoic). South Australia: Geological Survey, Bulletin 54.

ROLLEY, P., & WRIGHT, M. (2017). Kanmantoo copper deposits. In *Australia Ore Deposits* (Vol. Monograph 32, pp. 667-670). Melbourne, Australia: Australasian Institute of Mining and Metallurgy.

RUBATTO, D., HERMANN, J., & BUICK, I. S. (2006). Temperature and Bulk Composition Control on the Growth of Monazite and Zircon During Low-pressure Anatexis (Mount Stafford, Central Australia). *Journal of Petrology, 47*(10), 1973-1996. doi:10.1093/petrology/egl033

SCHILLER, J. (2000). Structural geology, metamorphism and origin of the Kanmantoo copper deposit, South Australia. *The University of Adelaide*, 1-252.

SCHOENE, B. (2014). U–Th–Pb Geochronology. In *Treatise on Geochemistry* (pp. 341-378).

SECCOMBE, P., SPRY, P., BOTH, R., JONES, M., & SCHILLER, J. (1985). Base metal mineralization in the Kanmantoo Group, South Australia: A Regional Sulfur Isotope Study. *Economic Geology, 80*, 1824-1843.

SEYDOUX-GUILLAUME, A., MONTEL, J., BINGEN, B., BOSSE, V., PARSEVEL, P. D., PAQUETTE, J., JANOTS, E., & WIRTH, R. (2012). Low-temperature alteration of monazite: Fluid mediated coupled dissolution-precipitation, irradiation damage, and disturbance of the U-Pb and Th-Pb chronometers. *Chemical Geology, 330-331*, 140-158.

SLAMA, J., KOSLER, J., CONDOM, D., CROWLEY, J., GERDES, A., HANCHAR, J., HORSTWOOD, M., MORRIS, G., NASDALA, L., NORBERG, N., SCHALTEGGER, U., SCHOENE, B., TURBRETT, M., & WHITEHOUSE, M. (2008). Plesovice zircon - A new natural reference material for U-Pb and Hf isotopic microanalysis. *Chemical Geology, 249*, 1-35.

SPANDLER, C., HAMMERLI, J., SHA, P., HILBERT-WOLF, H., HU, Y., ROBERTS, E., & SCHMITZ, M. (2016). MKED1: A new titanite standard for in situ analysis of Sm–Nd isotopes and U–Pb geochronology. *Chemical Geology, 425*, 110-126. doi:10.1016/j.chemgeo.2016.01.002

SPRY, P. (1976). *Base metal mineralisation in the Kanmantoo Group, SA: The South Hill, Bremer and Wheal Ellen Areas,* (Honours Thesis), The University of Adelaide, Australia.

STINEAR, M. (2017). *Refining the physical and temporal record of metamorphism during the Delamerian Orogeny* (Honours Thesis). The University of Adelaide, Australia.

TAYLOR, R. (2019). *Petrology and observations concerning 15 samples from the Kanappa prospect, (Kanmantoo region) South Australia.* Retrieved from C/o 15 Burns Street, Invermary, Launceston, Tasmania, 7248

TERA, F., & WASSERBURG, G. J. (1972). U-Th-Pb systematics in lunar highland samples from the Luna 20 and Apollo 16 missions. *Earth and Planetary Science Letters, 17*, 36-51.

TOTEFF, S. (1999). *Cambrian sediment-hosted exhalative base metak mineralisation, Kanmantoo Trough, South Australia*. Retrieved from Geological Survey of South Australia:

TOTT, K. A., SPRY, P. G., POLLOCK, M. V., KOENIG, A., BOTH, R. A., & OGIERMAN, J. (2019). Ferromagnesian silicates and oxides as vectors to metamorphosed sediment-hosted Pb-Zn-Ag-(Cu-Au) deposits in the Cambrian Kanmantoo Group, South Australia. *Journal of Geochemical Exploration, 200*, 112-138. doi:10.1016/j.gexplo.2019.01.015

TURNER, S., & FODEN, J. (1996). Petrogenesis of late-Delamerian A-type granites and granophyre, South Australia: magma mingling in the Mannum granite, South Australia. *Mineralogy and Petrology, 56*(147-169).

TURNER, S., KELLEY, S., VANDERBERG, A., FODEN, J., SANDIFORD, M., & FLOTTMANN, T. (1996). Source of the Lachlan fold belt flysch linked to convective removal of the lithosphere mantle and rapid exhumation of the Delamerian-Ross fold belt. *Geology, 24*, 941-944.

WELLS, T., MEFFRE, S., COOKE, D., & STEADMAN, J. (2019). *New indicators of, and methods to assess magmatic fertility in the Northparkes district*. Paper presented at the AGCC 2018, Adelaide.

WETHERILL, G. (1956). Discordant Uranium-Lead Ages, I. *Transactions, American Geophysical Union, 37*(3), 320-326.

WIEDENBECK, M., ALLW, P., CORFU, F., GRIFFIN, W., MEIER, M., OBERLI, F., VONQUADT, A., RODDICK, J., & SPEIGEL, W. (1995). 3 Natural Zircon Standards for U-Th-Pb, Lu-Hf, Trace-Element and REE Analyses. *Geostandards Newsletter, 19*, 1-23.

YUNSHENG, R., LIANDENG, L., & HUIHUANG, Z. (2005). *Gold deposits rich in bismuth minerals: An important type of gold deposits*. Paper presented at the Mineral Deposit Research: Meeting the Global Challenge.

APPENDIX A: DETAILED SAMPLE INFORMATION

Appendix Table 1: Primary data set sample location and parameters

Sample	Drill Hole	Depth	Easting	Northing
2721785	PADD 31	132.75 - 133.00m	433241.96	5988578.05
2721786	PADD 31	132.00 - 132.75m	433241.96	5988578.05
2721787	PADD 31	130.35 - 130.55m	433241.96	5988578.05
2721788	PADD 28	155.65 - 155.90m	443201.00	6008676.98
2721789	KMD-07-01	336.40 - 336.55m	379614.00	6041096.00
2721790	KMD-07-01	336.15 - 336.45m	379614.00	6041096.00
2721791	S11	580.90 - 580.11ft	342900.00	6162660.00
2721792	S11	582.00 - 582.20ft	342900.00	6162660.00
KM2-STH-G		Surface Grab	317469.87	6113094.47
DAW-SYN		Surface Grab	315816.16	6120088.00
KM2-HWY-G		Surface Grab	313804.34	6115444.03
KP008		224.4 - 224.55m	336771.00	6156461.00
KP004		154.10 - 154.22m	336771.00	6156461.00
KP001		87.65 - 87.75m	336771.00	6156461.00
KFP001		Surface Grab	337297.00	6157887.00

Appendix Table 2: Sample data sourced from Foden (2019) supplied by Hillgrove Resources of which has been classified using ioGAS 7.1 geochemical software for the following: Tectonic Classification of Mafic Igneous Rocks (Cabanis & Lecolle, 1989), TAS Plutonic (Middlemost, 1994). All samples were also geochemically sorted using Microsoft Excel to create Figure 17.

Sample Name	Easting	Northing	Drill Hole Depth (m) or area location	Intrusive 1 Volcanic 2 Foliated 1 Unfoliated 2	Tectonic Classification of Mafic Igneous Rocks (Cabanis and Lecolle 1989)	TAS Plutonic Classification (Middlemost 1994)
-564	346361	6164091	Black Hill		Arc calc-alkaline	Alkalic basalt/ alkalic
-379	153309	6010977			Arc calc-alkaline	Granite
-379	140076	6012073			Arc calc-alkaline	Granite
-378	140076	6012073			Arc transitional	Granite
52	338795	6162285			Enriched MORB	Alkalic basalt/ alkalic
53	338795	6162285			Enriched MORB	Alkalic basalt/ alkalic
54	338795	6162285			Enriched MORB	Gabbro
58	338795	6162285			Late- to post-orogenic intra-	Alkalic basalt/ alkalic
63	338795	6162285			Late- to post-orogenic intra-	Gabbro
64	338795	6162285			Late- to post-orogenic intra-	Gabbro
65	338795	6162285			Enriched MORB	Alkalic basalt/ alkalic
69	338795	6162285			Enriched MORB	Gabbro

77	338795	6162285			Late- to post-orogenic intra-	Alkalic basalt/ alkalic
79	338795	6162285			Late- to post-orogenic intra-	Gabbro
85	338795	6162285			Late- to post-orogenic intra-	Alkalic basalt/ alkalic
91	338795	6162285			Late- to post-orogenic intra-	Gabbro
92	338795	6162285			Late- to post-orogenic intra-	Gabbro
93	337460	6189155			Late- to post-orogenic intra-	Monzogabbro
120	328918	6196408			Alkaline	Gabbro
121	328918	6196408			Alkaline	Peridotgabbro
122	328918	6196408			Alkaline	Peridotgabbro
123	328918	6196408			Late- to post-orogenic intra-	Peridotgabbro
124	328918	6196408			Alkaline	Foid-gabbro
126	335604	6193830			Alkaline	Gabbro
127	335604	6193830			Late- to post-orogenic intra-	Diorite
132	337405	6191230			Alkaline	Monzodiorite
133	337405	6191230			Alkaline	Monzodiorite
134	337405	6191230			Alkaline	Foid-gabbro
135	337405	6191230			Alkaline	Monzonite
136	337405	6191230			Alkaline	Monzonite
137	337405	6191230			Alkaline	Monzodiorite
140	423636	6376968			Arc calc-alkaline	Granodiorite
151	423636	6376968			Arc calc-alkaline	Diorite
152	423636	6376968			Arc calc-alkaline	Diorite
154	423636	6376968			Arc calc-alkaline	Diorite
156	423636	6376968			Arc calc-alkaline	Monzonite
163	423636	6376968			Arc calc-alkaline	Diorite
167	423636	6376968			Arc calc-alkaline	Granodiorite
1007	337460	6189155			Alkaline	Monzogabbro
1009	337460	6189155			Alkaline	Foid-gabbro
1013	328918	6196408			Alkaline	Peridotgabbro
1014	330879	6141180			Arc calc-alkaline	Granite
1014	330879	6141180			Arc calc-alkaline	Granite
2000	439503	5969978			Arc calc-alkaline	Granite
2001	442104	5995571	2	2	Arc calc-alkaline	Granite
2002	451052	5974492	1	2	Late- to post-orogenic intra-	Granite
2003	442487	5956793	1	2	Arc calc-alkaline	Granite
2006	387107	6043572	1	1	Arc calc-alkaline	Granite
2007	388186	6046030	1	1	Arc calc-alkaline	Granite
2009	442104	5963627	1	2	Enriched MORB	Granite
2011	443449	5961701	1	2	Alkaline	Granite
6064	349493	6137590			Arc calc-alkaline	Monzodiorite
6832	349493	6137590			Arc calc-alkaline	Monzodiorite
6833	349493	6137590			Late- to post-orogenic intra-	Monzodiorite
22072	241261	6029961			Arc calc-alkaline	Granite
208394	399332	5941046			Unclassified	Granodiorite
208409	399332	5941046			Unclassified	Granodiorite
208410	399332	5941046			Unclassified	Granodiorite
1004-1	330879	6141180			Arc calc-alkaline	Granite
1004-15	330879	6141180			Arc calc-alkaline	Granite
1004-16	330879	6141180			Late- to post-orogenic intra-	Granite
1004-17	330879	6141180			Late- to post-orogenic intra-	Granite
1004-2	330879	6141180			Late- to post-orogenic intra-	Granite
1004-21	330879	6141180			Late- to post-orogenic intra-	Granite
1004-23	330879	6141180			Late- to post-orogenic intra-	Granite
1004-3	330879	6141180			Alkaline	Granite
1004-32	330879	6141180			Arc calc-alkaline	Granite
1004-33	330879	6141180			Arc calc-alkaline	Granite
1004-34	330879	6141180			Arc calc-alkaline	Granite
1004-35	330879	6141180			Late- to post-orogenic intra-	Granite
1004-36	330879	6141180			Arc calc-alkaline	Granite
1004-37	330879	6141180			Arc calc-alkaline	Granite
1004-38	330879	6141180			Late- to post-orogenic intra-	Granite
1004-39	330879	6141180			Late- to post-orogenic intra-	Granite
1004-4	330879	6141180			Late- to post-orogenic intra-	Granite
1004-5	330879	6141180			Arc calc-alkaline	Granite
1004-6	330879	6141180			Late- to post-orogenic intra-	Granite
1004-7	330879	6141180			Late- to post-orogenic intra-	Granite
1131-1	310645	6127845			Weakly enriched MORB	Gabbro
1131-10	310145	6128215			Weakly enriched MORB	Gabbro
1131-11	310165	6128135			Weakly enriched MORB	Gabbro
1131-12	310825	6127960			Weakly enriched MORB	Gabbro
1131-13	310790	6128105			Unclassified	Gabbro
1131-14	310385	6127555			Weakly enriched MORB	Gabbro
1131-15	310405	6127470			Weakly enriched MORB	Gabbro
1131-16	310930	6128130			Weakly enriched MORB	Gabbro
1131-17	310890	6128255			Weakly enriched MORB	Gabbro
1131-18	310815	6128325			Weakly enriched MORB	Gabbro
1131-19	310545	6126580			Late- to post-orogenic intra-	Gabbro
1131-2	310775	6127660			Weakly enriched MORB	Gabbro

1131-20	309464	6131765				Weakly enriched MORB	Gabbro
1131-21	309380	6131750				Weakly enriched MORB	Gabbro
1131-22	309590	6131885				Unclassified	Gabbro
1131-23	309605	6131975				Weakly enriched MORB	Gabbro
1131-24	309040	6130920				Weakly enriched MORB	Alkalic basalt/ alkalic
1131-25	309165	6130955				Late- to post-orogenic intra-	Gabbro
1131-26	309390	6130925				Late- to post-orogenic intra-	Gabbro
1131-27	309405	6130930				Weakly enriched MORB	Gabbro
1131-28	309565	6131010				Weakly enriched MORB	Gabbro
1131-29	309650	6130940				Weakly enriched MORB	Gabbro
1131-3	310840	6127555				Weakly enriched MORB	Gabbro
1131-30	309725	6130855				Weakly enriched MORB	Gabbro
1131-31	336872	6113494				Back arc	Monzogabbro
1131-32	336872	6113494				Weakly enriched MORB	Alkalic basalt/ alkalic
1131-33	336872	6113494				Weakly enriched MORB	Gabbro
1131-4	311055	6126810				Weakly enriched MORB	Gabbro
1131-5	311010	6126940				Weakly enriched MORB	Gabbro
1131-6	310781	6127405				Late- to post-orogenic intra-	Gabbro
1131-7	310465	6128755				Weakly enriched MORB	Gabbro
1131-8	310475	6128885				Weakly enriched MORB	Gabbro
1131-9	310470	6128835				Weakly enriched MORB	Gabbro
1154-10	425422	5991558	70.3-79.5	2	1	Arc calc-alkaline	Monzodiorite
1154-11	425422	5991558	70.3-79.5	2	1	Arc calc-alkaline	Monzodiorite
1154-12	424652	6004578		2	2	Alkaline	Monzodiorite
1154-13	424652	6004578		2	2	Alkaline	Monzodiorite
1154-14	424652	6004578		2	2	Alkaline	Monzodiorite
1154-15	426771	6007378	205.3-214.6	2	2	Alkaline	Monzogabbro
1154-16	426771	6007378	205.3-214.6	2	2	Alkaline	Monzogabbro
1154-17	426771	6007378	205.3-214.6	2	2	Alkaline	Foid-gabbro
1154-18	426771	6007378	205.3-214.6	2	2	Late- to post-orogenic intra-	Foid-gabbro
1154-19	436771	5969177	81.0-86.5	2	1	Arc calc-alkaline	Diorite
1154-20	436771	5969177	81.0-86.5	2	1	Late- to post-orogenic intra-	Diorite
1154-21	436771	5969177	81.0-86.5	2	1	Late- to post-orogenic intra-	Diorite
1154-22	436771	5969177	81.0-86.5	2	1	Arc calc-alkaline	Diorite
1154-24	388780	6109083				Late- to post-orogenic intra-	Foidolite
1154-25	388780	6109083				Alkaline	Alkalic basalt/ alkalic
1154-26	388780	6109083				Late- to post-orogenic intra-	Gabbro
1154-27	388780	6109083				Alkaline	Gabbro
1154-29	400801	6087569				Alkaline	Monzodiorite
1154-30	388780	6109083				Alkaline	Alkalic basalt/ alkalic
1154-34	400801	6087569				Arc tholeiite	Gabbroic diorite
1154-35	400801	6087569				Back arc	Gabbroic diorite
1154-36	400801	6087569				Arc tholeiite	Gabbroic diorite
1154-38	400801	6087569				N-MORB	Gabbroic diorite
1154-39	400801	6087569				Back arc	Gabbroic diorite
1154-40	400801	6087569				N-MORB	Gabbroic diorite
1154-41	400801	6087569				N-MORB	Gabbroic diorite
1154-42	388780	6109083				Arc tholeiite	Gabbroic diorite
1154-44	388780	6109083				Back arc	Gabbro
1154-45	388780	6109083				Arc tholeiite	Gabbro
1154-46	400801	6087569				N-MORB	Gabbroic diorite
1154-49	400801	6087569				Back arc	Gabbroic diorite
1154-50	400801	6087569				Back arc	Gabbroic diorite
1154-51	388780	6109083				Back arc	Alkalic basalt/ alkalic
1154-52	388780	6109083				Back arc	Gabbro
1154-53	382939	6069664				Arc tholeiite	Alkalic basalt/ alkalic
1154-54	382939	6069664				Back arc	Alkalic basalt/ alkalic
1154-55	384340	6069994				Back arc	Monzogabbro
1154-56	384340	6069994				Weakly enriched MORB	Alkalic basalt/ alkalic
1154-57	384340	6069994				Alkaline	Gabbro
1154-58	384340	6069994				Alkaline	Foid-gabbro
1154-59	384340	6069994				Late- to post-orogenic intra-	Foid-gabbro
1154-60	384796	6070393				Late- to post-orogenic intra-	Foid-gabbro
1154-61	384796	6070393				Alkaline	Foid-gabbro
1154-62	380735	6071595				Enriched MORB	Peridotgabbro
1154-63	380735	6071595				Late- to post-orogenic intra-	Alkalic basalt/ alkalic
1154-64	380735	6071595				Late- to post-orogenic intra-	Alkalic basalt/ alkalic
1154-65	382661	6076411				Late- to post-orogenic intra-	Alkalic basalt/ alkalic
1154-66	382661	6076411				Late- to post-orogenic intra-	Alkalic basalt/ alkalic
1154-67	382352	6074497				Late- to post-orogenic intra-	Peridotgabbro
1154-68	382352	6074497				Alkaline	Foid-gabbro
1154-69	379240	6075154				Alkaline	Unclassified
1154-7	430301	5971186				Arc transitional	Alkalic basalt/ alkalic
1154-70	379240	6075154				Late- to post-orogenic intra-	Foid-gabbro
1154-72	401595	6038448				Late- to post-orogenic intra-	Foid-gabbro
1154-73	401595	6038448				Late- to post-orogenic intra-	Foid-gabbro
1154-74	401595	6038448				Late- to post-orogenic intra-	Foid-gabbro
1154-75	403043	6040969				Late- to post-orogenic intra-	Gabbro

1154-76	403043	6040969				Arc calc-alkaline	Monzodiorite
1154-77	403043	6040969				Late- to post-orogenic intra-	Monzogabbro
1154-78	403043	6040969				Late- to post-orogenic intra-	Gabbroic diorite
1154-8	430301	5971186				Arc transitional	Gabbro
1154-81	394291	6075154	50.6-50.7	2	1	Arc calc-alkaline	Monzonite
1154-82	394291	6075154	51.6-51.7	2	1	Arc calc-alkaline	Monzonite
1154-83	394291	6075154	51.6-51_7	2	1	Arc calc-alkaline	Monzonite
1154-84	382237	6073633				Late- to post-orogenic intra-	Foid-gabbro
1154-85	382237	6073633				Alkaline	Foid-gabbro
1154-86	354951	6074507				Arc tholeiite	Alkalic basalt/ alkalic
1154-87	354951	6074507				Arc transitional	Monzogabbro
1154-89	354951	6074507				Late- to post-orogenic intra-	Monzodiorite
1154-90	365328	6081965				Arc transitional	Unclassified
1155-CG1afR	180204	6005081				Arc calc-alkaline	Granite
1155-CG1bmeR	180204	6005081				Arc calc-alkaline	Granodiorite
1155-CG2	180204	6005081				Arc calc-alkaline	Granodiorite
1155-CG8meR	180204	6005081	KI	1	2	Arc calc-alkaline	Monzogabbro
1155-CH1	233291	6022859	KI	1	2	Weakly enriched MORB	Peridotgabbro
1155-CH11R	233291	6022859				Arc calc-alkaline	Granodiorite
1155-CH13	233291	6022859				Arc calc-alkaline	Granite
1155-CH13aR	233291	6022859				Arc calc-alkaline	Granite
1155-CH14	233291	6022859				Arc calc-alkaline	Granite
1155-CH15	233291	6022859				Arc calc-alkaline	Granite
1155-CH17	233291	6022859				Late- to post-orogenic intra-	Granite
1155-CH18	233291	6022859				Arc calc-alkaline	Granodiorite
1155-CH19	233291	6022859				Arc calc-alkaline	Granodiorite
1155-CH2	233291	6022859				Arc calc-alkaline	Granodiorite
1155-CH21R	233291	6022859				Arc calc-alkaline	Granite
1155-CH22	233291	6022859				Late- to post-orogenic intra-	Granodiorite
1155-CH23	233291	6022859	KI	1	2	Late- to post-orogenic intra-	Gabbro
1155-CH27	233291	6022859	KI	1	2	Weakly enriched MORB	Gabbro
1155-CH28	233291	6022859	KI	1	2	Weakly enriched MORB	Gabbro
1155-CH37R	233291	6022859				Arc calc-alkaline	Granite
1155-CH38	233291	6022859				Arc calc-alkaline	Granite
1155-CH3R	233291	6022859				Late- to post-orogenic intra-	Granite
1155-CH48	233291	6022859	KI	1	2	Late- to post-orogenic intra-	Gabbro
1155-CH50	233291	6022859	KI	1	2	Late- to post-orogenic intra-	Gabbro
1155-CH53	233291	6022859	KI	1	2	Late- to post-orogenic intra-	Gabbro
1155-CH54	233291	6022859	KI	1	2	Weakly enriched MORB	Gabbro
1155-CH56	233291	6022859	KI	1	2	Late- to post-orogenic intra-	Gabbro
1155-CH58	233291	6022859	KI	1	2	Late- to post-orogenic intra-	Gabbro
1155-CH7	233291	6022859	KI	1	2	Late- to post-orogenic intra-	Gabbro
1155-CW1	241261	6029961				Arc transitional	Granite
1155-CW2	241060	6029624				Late- to post-orogenic intra-	Granite
1155-CW3	241261	6029961				Arc calc-alkaline	Granite
1155-CW4	241261	6029961				Arc calc-alkaline	Granite
119104-0-01	343470	6165590	110.2-110.5	1	1	Back arc	Peridotgabbro
119104-0-03	343470	6165590	148.8-149.1	1	1	Weakly enriched MORB	Peridotgabbro
119104-0-04	343470	6165590	169.5-170	1	1	Unclassified	Peridotgabbro
119104-0-05	343470	6165590	179.8-180.1	1	1	Late- to post-orogenic intra-	Peridotgabbro
119104-0-06	343470	6165590	181.8-182.1	1	1	Weakly enriched MORB	Alkalic basalt/ alkalic
339-A	442775	5955446		1	2	Arc calc-alkaline	Granite
339-BA	438926	5972182		1	2	Arc calc-alkaline	Granite
339-BC	440850	5972086		1	2	Arc calc-alkaline	Granite
339-DA	434980	5972952		1	2	Arc transitional	Granite
339-DB	436616	5971605		1	2	Arc calc-alkaline	Granite
339-DC	439984	5971797		1	2	Arc calc-alkaline	Granite
339-E	443256	5955831		1	2	Arc calc-alkaline	Granite
339-GA	427088	5962462		1	2	Arc calc-alkaline	Granite
339-KF	450186	5974396		1	2	Enriched MORB	Granite
339-LA	442679	5955831		1	2	Arc calc-alkaline	Granite
339-MC	439379	5992483		2	2	Arc calc-alkaline	Granite
5-540	359652	6164511				Late- to post-orogenic intra-	Granite
5-619	359562	6164511				Late- to post-orogenic intra-	Granite
5-625	359604	6164511				Late- to post-orogenic intra-	Granite
5-677	358684	6174039				Late- to post-orogenic intra-	Granodiorite
6-456	356649	6142675				Enriched MORB	Granite
7-716	357880	6165857				Arc calc-alkaline	Granite
7-722	357880	6165857				Late- to post-orogenic intra-	Granodiorite
779/19	337183	6133316				Arc calc-alkaline	Granite
779/2/13	336872	6113494				Back arc	Gabbro
779/2/14	336872	6113494				Back arc	Gabbro
779/2/15	336872	6113494				Late- to post-orogenic intra-	Gabbro
779/2/18	336872	6113494				Back arc	Gabbro
779/20	337149	6133417				Unclassified	Monzogabbro
779/20	337137	6133418	Reedy Creek			Unclassified	Monzogabbro
779/21	337149	6133417				Unclassified	Monzodiorite
779/21	337137	6133418	Reedy Creek			Unclassified	Monzodiorite

779/23	337149	6133417			Unclassified	Foid-gabbro
779/25	337149	6133417			Unclassified	Monzodiorite
779/25	337137	6133418	Reedy Creek		Unclassified	Monzodiorite
779/3	337149	6133417			Unclassified	Monzogabbro
779/3	337137	6133418	Reedy Creek		Unclassified	Monzogabbro
779/30	337149	6133417			Unclassified	Monzodiorite
779/30	337137	6133418	Reedy Creek		Unclassified	Monzodiorite
779/31	337149	6133417			Unclassified	Monzodiorite
779/31	337137	6133418	Reedy Creek		Unclassified	Monzodiorite
779/32	337149	6133417			Unclassified	Monzogabbro
779/35	337183	6133316			Unclassified	Granodiorite
779/36	337149	6133417			Unclassified	Monzogabbro
779/36	337137	6133418	Reedy Creek		Unclassified	Monzogabbro
779/4	337183	6133316			Arc calc-alkaline	Granite
779/43	337149	6133417			Unclassified	Monzodiorite
779/43	337183	6133316			Unclassified	Monzodiorite
779/5	337149	6133417			Unclassified	Monzogabbro
779/5	337137	6133418	Reedy Creek		Late- to post-orogenic intra-	Monzogabbro
779/51	337183	6133316			Arc calc-alkaline	Quartz monzonite
779/52	337183	6133316			Late- to post-orogenic intra-	Granodiorite
779/54	337183	6133316			Arc calc-alkaline	Monzonite
779/6	337183	6133316			Arc calc-alkaline	Granite
779/66	337183	6133316			Arc calc-alkaline	Granodiorite
779/7	337183	6133316			Arc calc-alkaline	Monzonite
779-63	349493	6137590			Arc calc-alkaline	Monzogabbro
848-13	337007	6113502			Unclassified	Granite
848-14	337007	6113502			Unclassified	Granite
848-18	346571	6164642			Unclassified	Gabbro
848-30	337007	6113502			Unclassified	Granite
848-32	337007	6113502			Unclassified	Granite
848-40	337007	6113502			Unclassified	Granite
848-59	241060	6029624			Unclassified	Granite
861/116	541214	5852327			Arc calc-alkaline	Gabbroic diorite
861/121	541214	5852327			Arc calc-alkaline	Monzodiorite
861/123	541214	5852327			Arc calc-alkaline	Granodiorite
861/130	541214	5852327			Arc calc-alkaline	Diorite
861/41	541214	5852327			Late- to post-orogenic intra-	Granodiorite
861/54	541214	5852327			Alkaline	Granodiorite
861/80	541214	5852327			Late- to post-orogenic intra-	Monzonite
861/86	541214	5852327			Arc calc-alkaline	Diorite
861/87	541214	5852327			Late- to post-orogenic intra-	Diorite
861/90	505000	5939701		1 2	Arc calc-alkaline	Granite
861/99	541214	5852327			Alkaline	Granodiorite
861-1	399332	5941046			Arc calc-alkaline	Granodiorite
861-17	437737	5985916		1 2	Enriched MORB	Granite
861-93	349533	6137100			Late- to post-orogenic intra-	Granite
861-95	349640	6137546			Arc calc-alkaline	Granite
86-SG1	348463	6181677			Late- to post-orogenic intra-	Granite
876 -2-543	346571	6164642	Black Hill		Arc calc-alkaline	Gabbro
876-1035	346361	6164091	Black Hill		Late- to post-orogenic intra-	Alkalic basalt/ alkalic
876-11-750	346571	6164642	Black Hill		Late- to post-orogenic intra-	Diorite
876-11-875	346571	6164642	Black Hill		Arc calc-alkaline	Gabbro
876-11-938	346571	6164642	Black Hill		Late- to post-orogenic intra-	Gabbroic diorite
876-12-391	347286	6159046	Black Hill		Late- to post-orogenic intra-	Monzodiorite
876-18-426	347286	6159046	Black Hill		Arc calc-alkaline	Peridotgabbro
876-18-677	347286	6159046	Black Hill		Late- to post-orogenic intra-	Gabbroic diorite
876-19-1031	346319	6164049	Black Hill		Late- to post-orogenic intra-	Gabbro
876-19-1233	346503	6164049	Black Hill		Arc calc-alkaline	Gabbroic diorite
876-19-1278	346361	6164091	Black Hill		Late- to post-orogenic intra-	Gabbroic diorite
876-19-1310	346361	6164091	Black Hill		Arc calc-alkaline	Gabbro
876-19-536	346361	6164091	Black Hill		Arc calc-alkaline	Gabbro
876-19-768	346361	6164091	Black Hill		Late- to post-orogenic intra-	Gabbro
876-19-801	346571	6164642	Black Hill		Late- to post-orogenic intra-	Gabbro
876-2-451	346361	6164091	Black Hill		Arc calc-alkaline	Gabbro
876-2-590	346361	6164091	Black Hill		Arc calc-alkaline	Gabbro
876-2-648	346361	6164091	Black Hill		Late- to post-orogenic intra-	Gabbro
876-2-732	346361	6164091	Black Hill		Arc calc-alkaline	Gabbro
876-2-823	346361	6164091	Black Hill		Arc calc-alkaline	Gabbro
876-3-750	357081	6164890	Black Hill		Late- to post-orogenic intra-	Gabbro
876-3-801	357081	6164890	Black Hill		Back arc	Gabbro
876-5-629	359652	6164511	Black Hill		Late- to post-orogenic intra-	Gabbro
876-6-377	356649	6142675	Black Hill		Arc calc-alkaline	Alkalic basalt/ alkalic
876-6-440	356649	6142675	Black Hill		Late- to post-orogenic intra-	Alkalic basalt/ alkalic
876-6-441	356649	6142675	Black Hill		Arc calc-alkaline	Alkalic basalt/ alkalic
876-7-510	357880	6165857	Black Hill		Late- to post-orogenic intra-	Gabbro
876-7-554	357880	6165857	Black Hill		Arc calc-alkaline	Gabbro
876-7-569	357880	6165857	Black Hill		Arc calc-alkaline	Gabbro
876-7-634	357880	6165857	Black Hill		Late- to post-orogenic intra-	Gabbro

876-7-676	357880	6165857	Black Hill			Late- to post-orogenic intra-	Gabbroic diorite
876-7-707	357880	6165857	Black Hill			Late- to post-orogenic intra-	Alkalic basalt/ alkalic
876-7-743	357880	6165857	Black Hill			Late- to post-orogenic intra-	Gabbroic diorite
876-9-364	357880	6165857	Black Hill			Arc calc-alkaline	Monzogabbro
876-c1	365328	6081965				Arc calc-alkaline	Alkalic basalt/ alkalic
876-C4B	395307	6051116				Arc calc-alkaline	Granite
87-AH1	319470	6180158				Weakly enriched MORB	Alkalic basalt/ alkalic
87-AH2	319470	6180158				Arc calc-alkaline	Gabbro
87-AH3	323525	6150053				Arc tholeiite	Gabbro
87-AH4	323525	6150053				Back arc	Gabbro
88-PG11	442594	5956187		1	2	Arc calc-alkaline	Granite
88-RG1	328093	6145988				Arc calc-alkaline	Granite
88-TC1	316238	6175331				Arc calc-alkaline	Granite
88-TC2	316238	6175331				Arc calc-alkaline	Granite
88-TC3	316238	6175331				Arc calc-alkaline	Granite
88-TC4	315651	6174995				Arc transitional	Gabbroic diorite
88-TC5	315651	6174995				Arc calc-alkaline	Gabbro
88-WS1	310775	6127660				Arc calc-alkaline	Gabbro
898-309	328093	6145988				Arc calc-alkaline	Granite
898-350	323525	6150053				Arc transitional	Gabbro
898-367	323525	6150053				Arc tholeiite	Gabbro
898-369	323525	6150053				Back arc	Gabbro
90-ang4	320246	6178284				Arc transitional	Gabbro
90-CH2(1)	335560	6151890				Late- to post-orogenic intra-	Alkalic basalt/ alkalic
90-CH2(2)	335560	6151890				Late- to post-orogenic intra-	Alkalic basalt/ alkalic
90-CH3	335560	6151890				Late- to post-orogenic intra-	Alkalic basalt/ alkalic
90-CH5	335560	6151890				Arc calc-alkaline	Granodiorite
90-PE1	290072	6064959				Arc calc-alkaline	Granite
91-CYH1	122166	6010307				Arc calc-alkaline	Granite
929-26	154111	6012261				Arc calc-alkaline	Granodiorite
A1109 11	326857	6155970				Arc calc-alkaline	Granite
A1109/13	423636	6376968				Arc calc-alkaline	Quartz monzonite
A1109/14	423636	6376968				Arc calc-alkaline	Diorite
A1109/7	350102	6137630				Late- to post-orogenic intra-	Granite
A1109/8	349682	6137378				Arc calc-alkaline	Granite
A1109-123	283014	6058790				Arc calc-alkaline	Granite
A1109-4	290072	6064959				Arc calc-alkaline	Granite
A1109-5	334885	6118365				Arc calc-alkaline	Granite
A1109-6	337137	6133418				Late- to post-orogenic intra-	Granite
bcm2 M2	337007	6113502				Arc calc-alkaline	Granite
BCv33	283005	6058843				Arc calc-alkaline	Granite
BCv35	285198	6061888				Arc calc-alkaline	Granodiorite
BH- 597	357081	6164890	Black Hill			Arc calc-alkaline	Diorite
BH-750	357081	6164890	Black Hill			Late- to post-orogenic intra-	Diorite
bvs 1008	328918	6196408				Alkaline	Peridotgabbro
CG 18 1	337007	6113502		1		Arc calc-alkaline	Granite
CG 18 11	337007	6113502		1		Late- to post-orogenic intra-	Gabbro
CG 18 12	337007	6113502		1		Arc calc-alkaline	Granite
CG 18 13	337007	6113502		1		Late- to post-orogenic intra-	Gabbro
CG 18 14	337007	6113502		1		Arc calc-alkaline	Granite
CG 18 16	337007	6113502		1		Back arc	Gabbro
CG 18 17	337007	6113502		1		Weakly enriched MORB	Gabbro
CG 18 18	337007	6113502		1		Arc calc-alkaline	Granite
CG 18 19	337007	6113502		1		Unclassified	Granite
CG 18 2	337007	6113502		1		Arc calc-alkaline	Granite
CG 18 21	337007	6113502		1		Arc calc-alkaline	Granite
CG 18 24	337007	6113502		1		Arc calc-alkaline	Granite
CG 18 25	337007	6113502		1		Back arc	Gabbro
CG 18 26	337007	6113502		1		Weakly enriched MORB	Gabbro
CG 18 28	337007	6113502		1		Arc calc-alkaline	Granite
CG 18 29	337007	6113502		1		Weakly enriched MORB	Gabbro
CG 18 3	337007	6113502		1		Arc calc-alkaline	Granite
CG 18 31	337007	6113502		1		Arc calc-alkaline	Granite
CG 18 4	337007	6113502		1		Arc calc-alkaline	Granite
CG 18 6	337007	6113502		1		Arc calc-alkaline	Granite
CG 18 6 Rpt	337007	6113502		1		Arc calc-alkaline	Granite
CG 18 8	337007	6113502		1		Arc calc-alkaline	Granite
CH90-1	335560	6151890				Arc calc-alkaline	Gabbro
CH90-2	335560	6151890				Arc calc-alkaline	Gabbro
CH90-3	335560	6151890				Arc calc-alkaline	Gabbro
CH90-4	335560	6151890				Arc calc-alkaline	Gabbroic diorite
CH90-5	233291	6022859				Arc calc-alkaline	Granite
COP55-01	368453	6064778	74.1-74.2	1	1	Late- to post-orogenic intra-	Monzodiorite
COP55-02	368453	6064778	76.0-76.2	1	1	Late- to post-orogenic intra-	Monzodiorite
COP56-01	366291	6098108	109.7-109.9	2	1	Arc transitional	Gabbroic diorite
COP56-02	366291	6098108	111.0-111.15	2	1	Back arc	Diorite
COP57-01	365171	6067778	185.8-186.0	2	1	Alkaline	Alkalic basalt/ alkalic
COP57-02	365171	6067778	190.3-190.5	2	1	Late- to post-orogenic intra-	Foidolite

COP58-01	362521	6064678				Late- to post-orogenic intra-	Diorite
F0706 FO606	352868	6106504		1	2	Alkaline	Monzogabbro
F0707 FO607	352868	6106504		1	2	Alkaline	Alkalic basalt/ alkalic
F0708 FO608	352868	6106504		1	2	Alkaline	Alkalic basalt/ alkalic
F0709 FO609	352868	6106504		1	2	Late- to post-orogenic intra-	Granite
GM/153	423636	6376968				Arc calc-alkaline	Diorite
Granite	337007	6113502				Arc calc-alkaline	Granite
JF07-100	386964	6044148		1	1	Arc transitional	Granite
JF07-101	386964	6044148		1	1	Arc calc-alkaline	Granite
JF07-102	386964	6044148		1	1	Arc transitional	Granite
JF07-104	395272	6031670		1	1	Arc calc-alkaline	Granite
JF07-105	396645	6025056		1	1	Arc calc-alkaline	Granite
JF07-106	396645	6025056		1	1	Arc calc-alkaline	Granite
JF07-107	396645	6025056		1	1	Arc calc-alkaline	Granite
JF07-108	438634	5993813		2	2	Arc calc-alkaline	Granite
JF07-109	438634	5993813		2	2	Arc calc-alkaline	Granite
JF07-110	450411	5974957		1	2	Alkaline	Granite
JF07-111	450411	5974957		1	2	Enriched MORB	Granite
JF07-112	450411	5974957		1	2	Alkaline	Granite
JF07-113	450411	5974957		1	2	Enriched MORB	Granite
JF07-114a	450411	5974957		1	2	Enriched MORB	Granite
JF07-114b	450411	5974957		1	2	Late- to post-orogenic intra-	Granite
JF07-115	450265	5975367		1	2	Alkaline	Granite
JF07-116	442594	5956187		1	2	Arc calc-alkaline	Granite
JF07-117	442594	5956187		1	2	Arc calc-alkaline	Granite
JF07-118	442594	5956187		1	2	Arc calc-alkaline	Granite
JF07-119	442594	5956187		1	2	Arc calc-alkaline	Granite
JF07-120	442594	5956187		1	2	Arc calc-alkaline	Granite
JF07-121	427139	5961572		1	2	Enriched MORB	Granite
JF07-122	427139	5961572		1	2	Arc calc-alkaline	Granite
Ki--29	154111	6012261				Arc calc-alkaline	Granite
KI89-10	233291	6022859				Arc calc-alkaline	Granite
KI89-2	125315	6012358				Arc calc-alkaline	Granite
KI89-3	125315	6012358				Arc calc-alkaline	Granite
KI89-4	116934	6009291				Arc calc-alkaline	Granite
KI89-5	154111	6012261				Arc calc-alkaline	Granite
KI89-6	154111	6012261				Arc calc-alkaline	Granite
KI89-7	154111	6012261				Enriched MORB	Granite
KI89-8	153309	6010977				Arc calc-alkaline	Granite
KI89-9	241261	6029961				Arc calc-alkaline	Granite
kism-07	153309	6010977				Late- to post-orogenic intra-	Granite
KiSM-34	154111	6012261				Arc calc-alkaline	Granite
KMD-07-01	379614	6041096	277.35			Arc calc-alkaline	Alkalic basalt/ alkalic
KMD-07-01	379614	6041096	336.4			Late- to post-orogenic intra-	Alkalic basalt/ alkalic
KMD-07-01	379614	6041096	336.15			Late- to post-orogenic intra-	Alkalic basalt/ alkalic
KMD-07-01	379614	6041096	372.8			Late- to post-orogenic intra-	Alkalic basalt/ alkalic
KMD-07-01	379614	6041096	354.4			Arc calc-alkaline	Diorite
KMD-07-01	379614	6041096	343.3			Late- to post-orogenic intra-	Foid-gabbro
KMD-07-01	379614	6041096	294.4			Arc transitional	Foidolite
KMD-07-01	379614	6041096	326.47			Arc calc-alkaline	Gabbro
KMD-07-01	379614	6041096	337			Late- to post-orogenic intra-	Gabbro
KMD-07-01	379614	6041096	317.15			Late- to post-orogenic intra-	Gabbro
KMD-07-01	379614	6041096	313.25			Late- to post-orogenic intra-	Gabbro
KMD-07-01	379614	6041096	342.5			Late- to post-orogenic intra-	Gabbro
KMD-07-01	379614	6041096	367.4			Late- to post-orogenic intra-	Gabbro
KMD-07-01	379614	6041096	377.5			Arc calc-alkaline	Gabbroic diorite
KMD-07-01	379614	6041096	351.2			Arc calc-alkaline	Gabbroic diorite
KMD-07-01	379614	6041096	334.7			Arc calc-alkaline	Gabbroic diorite
KMD-07-01	379614	6041096	287.85			Late- to post-orogenic intra-	Gabbroic diorite
KMD-07-01	379614	6041096	340			Arc calc-alkaline	Granite
KMD-07-01	379614	6041096	285.8			Arc calc-alkaline	Granite
KMD-07-01	379614	6041096	284			Late- to post-orogenic intra-	Granite
KMD-07-01	379614	6041096	283.6			Late- to post-orogenic intra-	Granite
KMD-07-01	379614	6041096	285.1			Arc calc-alkaline	Granodiorite
KMD-07-01	379614	6041096	341.3			Late- to post-orogenic intra-	Granodiorite
KMD-07-01	379614	6041096	359.6			Late- to post-orogenic intra-	Monzodiorite
KMD-07-01	379614	6041096	293.3			Late- to post-orogenic intra-	Monzonite
KTH1-01	429938	5980113	49.6-49-8	2	1	Late- to post-orogenic intra-	Granite
KTH1-02	429938	5980113	51.1-51.2	2	1	Late- to post-orogenic intra-	Granite
KTH12-01	436771	5969177	82.4-82.6	2	1	Late- to post-orogenic intra-	Diorite
KTH12-02	436771	5969177	82.7-82.8	2	1	Late- to post-orogenic intra-	Diorite
KTH12-03	436771	5969177	84.3-84.45	2	1	Arc calc-alkaline	Diorite
KTH2-01	430374	5971192				Weakly enriched MORB	Granite
KTH2-02	430374	5971192				Back arc	Granite
KW08-1	349149	6182518				Late- to post-orogenic intra-	Granite
KW08-10	352868	6106504		1	2	Alkaline	Quartz monzonite
KW08-11	352868	6106504		1	2	Late- to post-orogenic intra-	Monzonite
KW08-12	352868	6106504		1	2	Alkaline	Quartz monzonite

KW08-13	352868	6106504		1	2	Late- to post-orogenic intra-	Granite
KW08-14	352868	6106504		1	2	Arc calc-alkaline	Granite
KW08-15	352868	6106504		1	2	Late- to post-orogenic intra-	Granite
KW08-16	352868	6106504		1	2	Arc calc-alkaline	Granite
KW08-17	352868	6106504		1	2	Arc calc-alkaline	Granite
KW08-2	349149	6182518				Late- to post-orogenic intra-	Monzonite
KW08-3	349149	6182518				Arc calc-alkaline	Granite
KW08-4	349149	6182518				Late- to post-orogenic intra-	Granite
KW08-5	349448	6137616				Late- to post-orogenic intra-	Granite
KW08-6	349448	6137616				Late- to post-orogenic intra-	Granite
KW08-7	349448	6137616				Late- to post-orogenic intra-	Monzodiorite
KW08-8	349448	6137616				Late- to post-orogenic intra-	Monzodiorite
KW08-9	349448	6137616				Arc calc-alkaline	Granite
LD3-01	459556	5931261	117.8-118			Alkaline	Diorite
LD3-02	459556	5931261	160.8-161			Late- to post-orogenic intra-	Granodiorite
LD3-03	459556	5931261	217-217.2			Late- to post-orogenic intra-	Granodiorite
LD3-04	459556	5931261	240.5-240.7			Late- to post-orogenic intra-	Granodiorite
LD3-05	459556	5931261	264.2-264.4			Late- to post-orogenic intra-	Granite
LD3-06	459556	5931261	280.2-280.5			Late- to post-orogenic intra-	Granodiorite
LD3-07	459556	5931261	303.9-304.1			Late- to post-orogenic intra-	Gabbroic diorite
LD3-08	459556	5931261	320.4-320.7			Late- to post-orogenic intra-	Granodiorite
M/7	337007	6113502				Alkaline	Granite
M/8	337007	6113502				Arc calc-alkaline	Granite
M161-01	333235	6068679	158.0-158.2	1	2	Late- to post-orogenic intra-	Granite
m9	337007	6113502				Arc calc-alkaline	Granite
MG10	349493	6137590				Arc calc-alkaline	Alkalic basalt/ alkalic
MG7	349493	6137590				Enriched MORB	Alkalic basalt/ alkalic
MTR10-01	399863	5985278	164.9-165.1	2	1	Late- to post-orogenic intra-	Monzogabbro
MTR10-02	399863	5985278	166-166.2	2	1	Late- to post-orogenic intra-	Monzodiorite
MTR12	392822	6017478	119.25			Arc transitional	Diorite
MTR12-01	392821	6017477	119-119.2	2	1	Arc tholeiite	Monzodiorite
MTR12-02	392821	6017477	119.9-120.2	2	1	Back arc	Monzodiorite
MTR12-03	392821	6017477	122.1-122.2	2	1	Arc tholeiite	Monzodiorite
MTR12-04	392821	6017477	122.8-123.0	2	1	N-MORB	Diorite
MTR13-01	390521	6017477	156.3-156.5	2	1	Arc calc-alkaline	Granite
MTR13-02	390521	6017477	159.9-160.2	2	1	Arc transitional	Granodiorite
MTR13-03	390521	6017477	161.2-161.5	2	1	Arc transitional	Granodiorite
MTR13-04	390521	6017477	158.6-158.7	2	1	Arc calc-alkaline	Granodiorite
MTS/1/02	640013	5897854				Arc transitional	Granodiorite
MTS/2/02	640013	5897854				Arc calc-alkaline	Diorite
MTS/3/02	640013	5897854				Arc tholeiite	Gabbroic diorite
MTS/4/02	640013	5897854				Late- to post-orogenic intra-	Granodiorite
MTS/5/02	640013	5897854				Arc transitional	Granite
MTS/6/02	640013	5897854				Arc calc-alkaline	Diorite
PADD28	443201	6008677	155.65			Late- to post-orogenic intra-	Granodiorite
PADD28-01	443201	6008676	133.9-134.1	1	2	Arc calc-alkaline	Monzonite
PADD28-02	443201	6008676	134.1-134.2	1	2	Arc calc-alkaline	Gabbroic diorite
PADD28-03	443201	6008676	136.0-136.2	1	2	Arc calc-alkaline	Diorite
PADD28-04	443201	6008676	136.2-136.3	1	2	Arc calc-alkaline	Diorite
PADD28-05	443201	6008676	147.8-148	1	2	Arc calc-alkaline	Monzonite
PADD28-06	443201	6008676	151.5-151.7	1	2	Late- to post-orogenic intra-	Monzonite
PADD28-07	443201	6008676	152.4-152.6	1	2	Arc calc-alkaline	Monzonite
PADD28-08	443201	6008676	152.6-152.8	1	2	Arc calc-alkaline	Monzonite
PADD28-09	443201	6008676	153.3-153.5	1	2	Late- to post-orogenic intra-	Monzonite
PADD28-10	443201	6008676	154.3-154.5	1	2	Arc calc-alkaline	Granite
PADD28-11	443201	6008676	154.9-155.1	1	2	Late- to post-orogenic intra-	Granite
PADD28-12	443201	6008676	144.8-145	1	2	Arc calc-alkaline	Granodiorite
PADD31	433241	5988578	113.4	2	2	Alkaline	Alkalic basalt/ alkalic
PADD31	433241	5988578	123.5	2	2	Alkaline	Alkalic basalt/ alkalic
PADD31	433241	5988578	132	2	2	Alkaline	Foid-gabbro
PADD31	433241	5988578	121.93	2	2	Alkaline	Gabbroic diorite
PADD31	433241	5988578	130.35	2	2	Alkaline	Monzogabbro
PADD31	433241	5988578	120.45	2	2	Alkaline	Peridotgabbro
PADD31-01	433241	5988578	111.3-111.4	2	2	Late- to post-orogenic intra-	Monzogabbro
PADD31-02	433241	5988578	112.4-112.6	2	2	Alkaline	Monzogabbro
PADD31-03	433241	5988578	113.1-113.2	2	2	Alkaline	Alkalic basalt/ alkalic
PADD31-04	433241	5988578	114.9-115.0	2	2	Alkaline	Alkalic basalt/ alkalic
PADD31-05	433241	5988578	116.8-117.0	2	2	Alkaline	Unclassified
PADD31-06	433241	5988578	121.0-121.2	2	2	Alkaline	Peridotgabbro
PADD31-07	433241	5988578	123.4-123.6	2	2	Alkaline	Gabbro
PADD31-08	433241	5988578	128.05-128.2	2	2	Alkaline	Monzogabbro
PADD31-09	433241	5988578	128.8-129.0	2	2	Alkaline	Foid-gabbro
PADD31-10	433241	5988578	129.4-129.6	2	2	Alkaline	Foid-gabbro
PADD32-01	403878	5972405		1	2	Late- to post-orogenic intra-	Monzogabbro
PADD32-03	403878	5972405		1	2	Arc calc-alkaline	Granite
PADD32-04	403878	5972405		1	2	Arc calc-alkaline	Granite
PADD33-01	403196	5985269	109.0-109.15	2	1	Alkaline	Alkalic basalt/ alkalic
PADD33-02	403196	5985269	115.0-115.2	2	1	Alkaline	Foid-gabbro

PADD33-03	403196	5985269	117.4-117.6	2	1	Alkaline	Alkalic basalt/ alkalic
PADD33-04	403196	5985269	120.1-120.3	2	1	Alkaline	Monzogabbro
PADD33-05	403196	5985269	121.3-121.4	2	1	Alkaline	Foid-gabbro
PADD33-06	403196	5985269	124.7-124.9	2	1	Alkaline	Foid-monzodiorite
PADD33-07	403196	5985269	127.7-127.9	2	1	Alkaline	Foidolite
PD1-01	389521	6036677		1	1	Arc calc-alkaline	Granite
PEG	337007	6113502				Weakly enriched MORB	Granite
PG11	442583	5956312		1	2	Arc calc-alkaline	Granite
PG4-01	442734	5958339		1	2	Arc calc-alkaline	Granite
PG4-01	442734	5958339		1	2	Arc calc-alkaline	Granite
PG4-02	442734	5958339		1	2	Arc calc-alkaline	Granite
PG4-02	442734	5958339		1	2	Arc calc-alkaline	Granite
PG5-01	443519	5955907		1	2	Arc calc-alkaline	Granite
PG5-01	443519	5955907		1	2	Arc calc-alkaline	Granite
PG5-02	443519	5955907		1	2	Arc calc-alkaline	Granite
PG5-02	443519	5955907		1	2	Arc calc-alkaline	Granite
R126 L375	316238	6175331				Late- to post-orogenic intra-	Granite
R14 L1	316238	6175331				Late- to post-orogenic intra-	Granodiorite
R145 L472	316186	6175408				Back arc	Alkalic basalt/ alkalic
R146 L471	316238	6175331				Enriched MORB	Granite
R147A L475	316238	6175331				Arc calc-alkaline	Granite
R148 L477	316238	6175331				Arc calc-alkaline	Granite
R149 L478	316238	6175331				Arc calc-alkaline	Granite
R15 L85	316238	6175331				Late- to post-orogenic intra-	Granodiorite
R150 L479	316238	6175331				Arc calc-alkaline	Granite
R151 L480	316238	6175331				Arc calc-alkaline	Granite
R152 L481	316238	6175331				Arc calc-alkaline	Granite
R154 L75	316238	6175331				Arc calc-alkaline	Granite
R156 L75	316186	6175408				Weakly enriched MORB	Gabbroic diorite
R157 L75	316238	6175331				Arc calc-alkaline	Granite
R158 L75	316238	6175331				Arc calc-alkaline	Granite
R159 L75	316238	6175331				Late- to post-orogenic intra-	Diorite
R16 L85	316238	6175331				Arc calc-alkaline	Diorite
R161 L75	316186	6175408				Arc transitional	Gabbro
R162 L75	316186	6175408				Weakly enriched MORB	Gabbro
R164 L75	316186	6175408				Weakly enriched MORB	Gabbro
R165 L76	316238	6175331				Arc calc-alkaline	Granite
R166 L76	316238	6175331				Arc calc-alkaline	Granite
R167 L76	316186	6175408				Weakly enriched MORB	Gabbro
R168 L76	316238	6175331				Late- to post-orogenic intra-	Gabbroic diorite
R169 L76	316238	6175331				Arc calc-alkaline	Granite
R17 L133	316186	6175408				Weakly enriched MORB	Gabbro
R170 L76	316238	6175331				Arc calc-alkaline	Granite
R171 L76	316186	6175408				N-MORB	Gabbro
R172 L76	316186	6175408				Weakly enriched MORB	Gabbro
R173 L483	316186	6175408				Arc tholeiite	Gabbro
R174 L482	316186	6175408				Weakly enriched MORB	Gabbro
R175 L482	316186	6175408				Arc transitional	Gabbro
R176 L483	316238	6175331				Arc calc-alkaline	Granite
R177 L483	316186	6175408				Arc tholeiite	Gabbro
R178 L483	316186	6175408				Weakly enriched MORB	Gabbro
R179 L483	316186	6175408				Weakly enriched MORB	Gabbro
R180 L483	316238	6175331				Arc calc-alkaline	Granite
R181 L483	316186	6175408				Arc transitional	Gabbro
R182 L483	316186	6175408				N-MORB	Gabbro
R36 L64	316238	6175331				Arc tholeiite	Diorite
R99 L248	316238	6175331				Late- to post-orogenic intra-	Granite
RC/2B	338097	6132423				Arc calc-alkaline	Granite
RC/2C	338097	6132423				Arc calc-alkaline	Granite
S10-01	347842	6165607	392-392_9	1	1	Late- to post-orogenic intra-	Granodiorite
S10-02	347842	6165607	414-415	1	2	Arc calc-alkaline	Granite
S10-03	347842	6165607	468.3-469	1		Late- to post-orogenic intra-	Quartz monzonite
S10-04	347842	6165607	487_6-488_4	1		Late- to post-orogenic intra-	Granite
S10-05	347842	6165607	499_4-500_3	1		Late- to post-orogenic intra-	Monzonite
S10-06	347842	6165607	532_9-534	1		Alkaline	Granite
S10-07	347842	6165607	569_8-570_10	1		Late- to post-orogenic intra-	Monzodiorite
S10-08	347842	6165607	607_8-608_2	1		Alkaline	Granite
S10-09	347842	6165607	646_6-647	1		Alkaline	Granite
S10-10	347842	6165607	648_6-649_8	1		Late- to post-orogenic intra-	Granite
S10-11	347842	6165607	651-652	1		Alkaline	Granite
S10-12	347842	6165607	683-683_9	1		Late- to post-orogenic intra-	Monzodiorite
S11	342900	6162660	177.01			Late- to post-orogenic intra-	Diorite
S11	342900	6162660	202.23			Late- to post-orogenic intra-	Gabbro
S11	342900	6162660	198.91			Late- to post-orogenic intra-	Gabbro
SJF11	338419	6138208				Late- to post-orogenic intra-	Diorite
SJF12	337149	6133417				Unclassified	Gabbro
SJF2	337149	6133417				Unclassified	Gabbro
SJF5	337149	6133417				Unclassified	Monzodiorite

SJF6	337137	6133418				Arc calc-alkaline	Granite
SJF7	337137	6133418				Arc calc-alkaline	Granodiorite
SJF9	337137	6133418				Arc calc-alkaline	Granite
SS2000-11	139019	6011815				Arc calc-alkaline	Granite
SS2000-12	139019	6011815				Arc calc-alkaline	Granite
SS2000-13	139019	6011815				Arc calc-alkaline	Granodiorite
SS2000-15	139019	6011815				Arc calc-alkaline	Granite
SS2000-16	139019	6011815				Arc calc-alkaline	Granite
TA	399332	5941046				Unclassified	Granodiorite
v43	285198	6061888				Arc calc-alkaline	Granite
v53	285198	6061888				Arc calc-alkaline	Granite
VB2000-1	154065	6011956				Arc transitional	Granite
VB2000-3	153630	6011956				Alkaline	Granite
VB2000-4	153309	6010977				Late- to post-orogenic intra-	Granite
VB2000-5	153313	6011959				Arc calc-alkaline	Granodiorite
VB2000-6	153313	6011959				Arc calc-alkaline	Granite
VB2000-7	153473	6011955				Late- to post-orogenic intra-	Granodiorite
VIC 01	668752	5862256				Unclassified	Gabbro
VIC 02	668752	5862256				Unclassified	Gabbro
VIC 03	668752	5862256				Unclassified	Gabbro
VIC 04	668752	5862256				Unclassified	Gabbroic diorite
VIC 05	668752	5862256				Unclassified	Gabbroic diorite
VIC 06	668752	5862256				Unclassified	Gabbroic diorite
VIC 07	668752	5862256				Unclassified	Gabbro
VIC 08	668752	5862256				Unclassified	Gabbro
VIC 09	643406	5835528				Unclassified	Granodiorite
VIC 10	643406	5835528				Arc calc-alkaline	Granodiorite
VIC 11	643406	5835528				Arc calc-alkaline	Granodiorite
VIC 12	643406	5835528				Unclassified	Granodiorite
VIC 14	644320	5832795				Arc calc-alkaline	Diorite
VIC 16	644320	5832795				Arc calc-alkaline	Diorite
VIC 17	644320	5832795				Arc calc-alkaline	Diorite
VIC 19	644320	5832795				Arc calc-alkaline	Granodiorite
VIC 21	645536	5827792				Arc calc-alkaline	Diorite
VIC 22	645536	5827792				Arc calc-alkaline	Diorite
VIC 23	645536	5827792				Late- to post-orogenic intra-	Diorite
VIC 24	645958	5828058				Arc calc-alkaline	Diorite
VIC 25	645958	5828058				Arc calc-alkaline	Diorite
VIC 26	645958	5828058				Arc calc-alkaline	Granodiorite
VIC 27	645958	5828058				Arc calc-alkaline	Granodiorite
VIC 28	645958	5828058				Arc calc-alkaline	Diorite
VIC 30	649949	5875013				Arc calc-alkaline	Diorite
VIC 31	649949	5875013				Arc calc-alkaline	Gabbroic diorite
VIC 33	649751	5873618				Arc calc-alkaline	Granodiorite
VIC 34	649751	5873618				Arc calc-alkaline	Granodiorite
VIC 34A	649751	5873618				Arc calc-alkaline	Granodiorite
VIC 35	649751	5873618				Arc calc-alkaline	Granodiorite
VIC 36	639809	5897845				Arc transitional	Diorite
VIC 37	639809	5897845				Arc transitional	Gabbroic diorite
VIC 38	639809	5897845				Arc calc-alkaline	Granodiorite
VIC 39	639758	5897748				Arc transitional	Granite
VIC 40	639758	5897748				Arc tholeiite	Granite
VIC 41	639758	5897748				Arc transitional	Granodiorite
VIC 42	639739	5897724				Arc calc-alkaline	Diorite
VIC 43	639598	5897573				Unclassified	Diorite
VIC 45	639598	5897573				Arc transitional	Diorite
VIC 46	639598	5897573				Unclassified	Granodiorite
VIC 47	640013	5897854				Arc tholeiite	Diorite
VIC 48	640013	5897854				Arc transitional	Granodiorite
VIC 49	640013	5897854				Arc transitional	Diorite
VIC 50	640013	5897854				Arc transitional	Diorite
VIC 51	648991	5883264				Arc calc-alkaline	Granodiorite
VIC 52	648991	5883264				Arc calc-alkaline	Granodiorite
VIC 53	648991	5883264				Arc transitional	Granodiorite
VIC 54	648991	5883264				Unclassified	Granodiorite
VIC 55	648999	5883264				Unclassified	Diorite
VIC 56	648999	5883264				Arc calc-alkaline	Diorite
VIC 57	648999	5883264				Arc calc-alkaline	Gabbroic diorite
VIC 58	649090	5883227				Arc calc-alkaline	Gabbroic diorite
VIC 59	649090	5883227				Arc transitional	Gabbroic diorite
VIC 60	649050	5883464				Unclassified	Gabbro
VIC 61	649050	5883464				Arc calc-alkaline	Gabbroic diorite
VIC 62	649038	5883632				Unclassified	Diorite
VIC 63	649038	5883632				Arc calc-alkaline	Diorite
VIC 64	649002	5883682				Arc calc-alkaline	Gabbroic diorite
VIC 65	649002	5883682				Arc calc-alkaline	Gabbroic diorite
VIC/1/02	640013	5897854				Alkaline	Foid-gabbro
WYN1-01	402421	6092278	147.1 -155.8	2	2	N-MORB	Monzogabbro

WYN1-02	402421	6092278	147.1 -155.8	2	2	N-MORB	Alkalic basalt/ alkalic
WYN1-03	402421	6092278	147.1 -155.8	2	2	N-MORB	Alkalic basalt/ alkalic
WYN1-04	402421	6092278	147.1 -155.8	2	2	N-MORB	Alkalic basalt/ alkalic
WYN1-05	402421	6092278	147.1 -155.8	2	2	Back arc	Gabbroic diorite
WYN1-06	402421	6092278	147.1 -155.8	2	2	Back arc	Granodiorite
WYN1-07	402421	6092278	147.1 -155.8	2	2	Back arc	Granodiorite
WYN1-08	402421	6092278	147.1 -155.8	2	2	Unclassified	Gabbro

Appendix Table 3: A second additional data set provided by Hillgrove Resources containing geochemical information for samples within the Kanappa Drilling region used to create fertility diagram Figure 16.

Sample	SiO2	Sr	Y	Sr/Y	V	Sc	V/Sc
	wt%	ppm	ppm		ppm	ppm	
KNP199	62.7	626	14.7	42.58503	98	8	12.25
KNP200	64	635	15.3	41.50327	97	8.5	11.41176
KNP201	59.1	689	15.8	43.60759	113	8.8	12.84091
KNP202	65.7	572	18.5	30.91892	91	8.2	11.09756
KNP203	61	693	15.5	44.70968	100	8.4	11.90476
KNP204	59.7	720	17.6	40.90909	95	8.8	10.79545
KNP205	63	695	12.3	56.50407	87	6.5	13.38462
KNP206	58.3	860	17.7	48.58757	110	8.4	13.09524
KNP207	56.5	855	19.9	42.96482	123	10.1	12.17822
KNP208	56.9	923	19.1	48.32461	118	9.3	12.68817
KNP209	63.2	595	18.2	32.69231	83	8.7	9.54023
KNP211	63.9	156.5	14.1	11.09929	91	12.7	7.165354
KNP212	67.2	60.6	15.7	3.859873	81	12.3	6.585366
KNP213	63.4	69.3	15.8	4.386076	101	14.1	7.163121
KNP214	59.6	618	17.7	34.91525	112	9.6	11.66667
KNP215	58.9	739	17.5	42.22857	122	8.8	13.86364
KNP216	60.6	574	18.1	31.71271	97	7.7	12.5974
KNP432	36.7	724	17.7	40.90395	35	5.7	6.140351
KNP433	69.3	500	24.3	20.57613	53	7.1	7.464789
KNP434	68.5	531	18.9	28.09524	46	6	7.666667
KNP435	68.2	494	18	27.44444	42	5.8	7.241379
KNP436	68.6	537	19.6	27.39796	43	6.3	6.825397
KNP461	57.1	1090	151	7.218543	18.8	13.2	1.424242
KNP462	55.5	1005	151	6.655629	20.6	13.3	1.548872
KNP463	60.2	733	125	5.864	18.5	11.1	1.666667
KNP464	59.9	689	136	5.066176	22	12.3	1.788618
KNP465	58.5	694	125	5.552	21.2	11.8	1.79661
KNP467	58.4	364	106	3.433962	13.2	10.2	1.294118

APPENDIX B: PETROGRAPHIC DESCRIPTIONS

Petrographic descriptions from the 15 sample primary data set used throughout this investigation.

KFP001
Location: 337297E 6157887N
Depth: Surface Grab

Variable distribution of minerals throughout sample. As seen in physical thin section, darker regions are chlorite alteration which often surround those lighter regions of plagioclase. Plagioclase forms largest grains up to 3mm. Clinopyroxene present along with minor chlorite and titanite form much of the alteration groundmass of which surrounds those much larger plagioclase grains.
Proportions: Chlorite alteration 30%, Plagioclase 30%, Quartz 15%, CPX 21%, Titanite 2%, Chlorite 2%.
Classification: Quartz Diorite

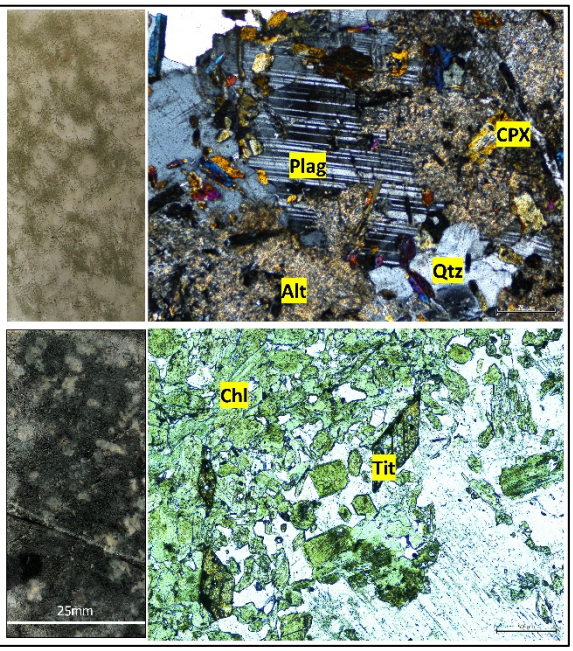

KP001
Location: 336771E 6156461N
Depth: 87.65 – 87.75m

Quartz dominated with some regions exhibiting grains of preferred crystal habit, however generally irregular grains. Relatively homogenous distribution of minerals throughout with sericite alteration present appearing to dominantly replace potassium feldspar and minor muscovite. Biotite infill present with irregular shape.
Proportions: Quartz 48%, sericite Alteration (K-Feld) 40%, Biotite 6%, Chlorite 2%, Titanite 2%, Muscovite 2%.
Classification: Minor Altered Granite

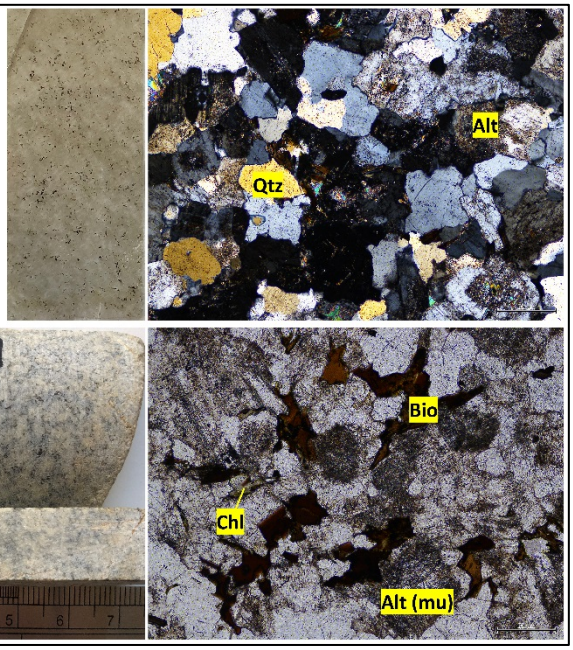

KP004
Location: 336771E 6156461N
Depth: 154.2 – 154.22m

Homogenous distribution of minerals throughout sample. Dominating mineral being plagioclase of which often does not show obvious characteristic twinning due to minor sericite alteration. Biotite and chlorite throughout often difficult to distinguish, chlorite being more regular and tabular with biotite being irregular shaped. Slight alteration throughout affecting plagioclase and quartz dominantly.

Proportions: Plagioclase 70%, Biotite 13%, Quartz 10%, Opaques 2%, Amphibole 5%

Classification: Quartz Diorite

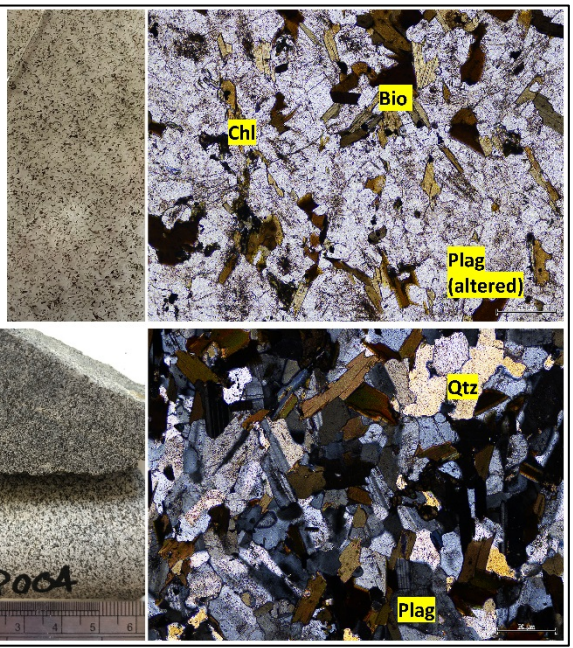

KP008
Location: 336771E 6156461N
Depth: 224.4 – 224.55m

Homogenous distribution of minerals throughout with chlorite being more concentrated in patches 2-3cm in size. Possible preferential grain alignment of deformation as seen in sand sample and top right image with direction NW-SE.

Proportions: Plagioclase 60%, Quartz 10%, Muscovite 15%, Amphibole 5%, Biotite 9%, Titanite 1%

Classification: Quartz Diorite

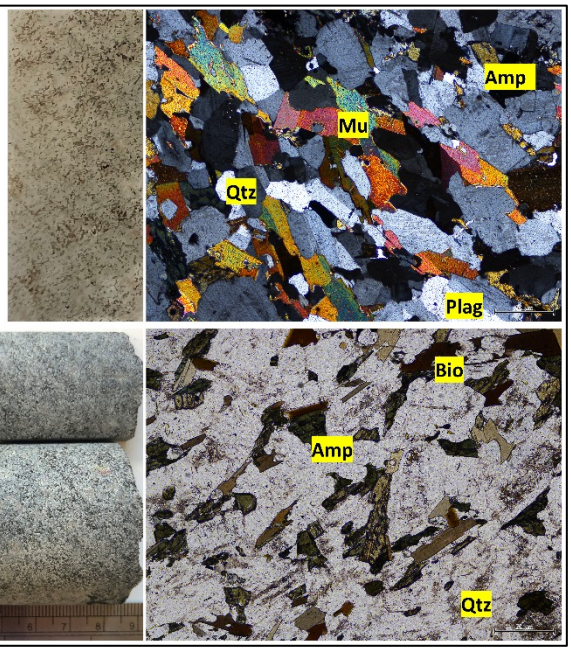

2721785
Drillhole: PADD 31
Depth: 132.75 - 133.00m

Chlorite alteration make up majority of the ground mass. Large calcite phenocrysts within. Chlorite dominant regions, as seen in pink/orange colour of bottom left image and brown in top right image. Green chlorite replacement of biotite located in areas surrounded by chlorite, rarely in close proximity to brown alteration chlorite. Hematite or magnetite present as minor infill.
High birefringent gains found sparsely throughout but dominantly within green chlorite altered biotite, seen in bottom right image.

Proportions: brown chlorite alteration 50%, Calcite 40%, green chlorite replaced biotite 5%, high birefringent grains 2%, opaque 3%.

Classification: Volcanics, Siltstone, 'Truro Volcanics'

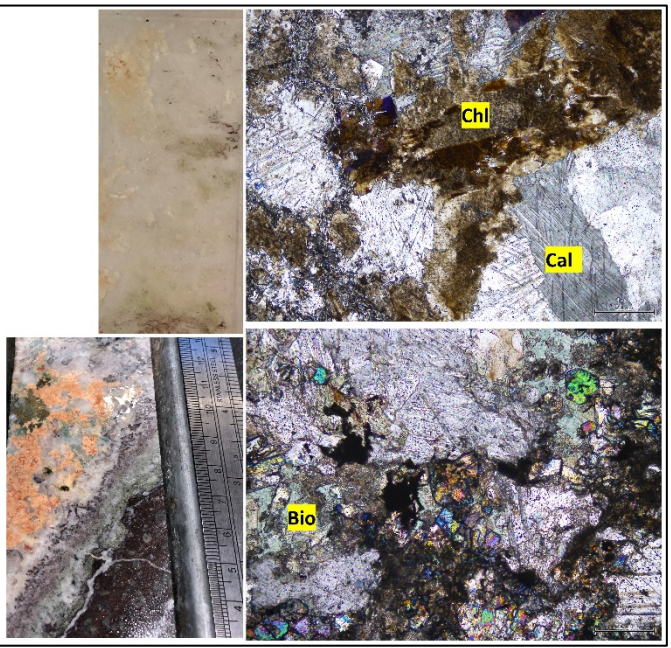

2721786
Drillhole: PADD 31
Depth: 132.00 – 132.75m

Altered porphyritic basalt abundant with vesicles. Two vesicle sizing's with smaller 30µm being more rounded and filled with green chlorite. Larger 5-8mm vesicles filled with carbonate material (image top right). Plagioclase laths are abundant in the groundmass, possibly been replaced by albite. No preferential alignment within the groundmass. Occasional biotite within the ground mass, hard to distinguish. Large chlorite mass (pictured bottom right and present within top left of image top left).

Proportions: basalt groundmass 50%, chlorite 25%, carbonate 18% ,plag laths 5%, biotite 2%.

Classification: Volcanics, 'Truro Volcanics'.

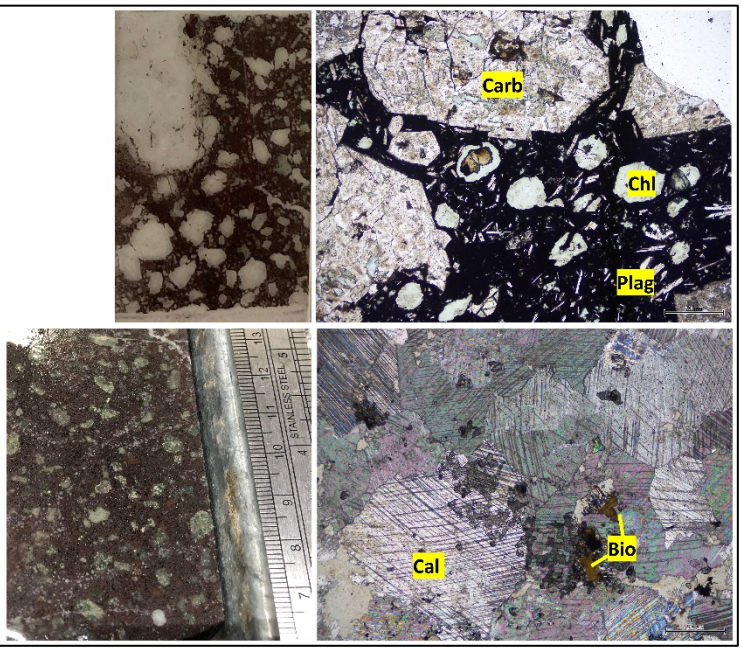

2721787
Drillhole: PADD 31
Depth: 130.35 – 130.55m

Porphyritic texture overall. Quartz with undulose extinction and calcite (bottom right image) form veining through the sample, 1mm wide in some locations. Plagioclase and biotite within the dark hematite altered groundmass form much of the sample. Fibrous zeolite surrounds many calcite and chlorite phenocrysts. Calcite and more commonly chlorite surrounded if not being replaced by very fine grained pyrrhotite.

Proportions: hematite alt groundmass 60%, calcite 15%, chlorite 5%, quartz 5%, plagioclase 5%, zeolite 4%, pyrrhotite 6%.

Classification: Volcanics, 'Truro Volcanics'.

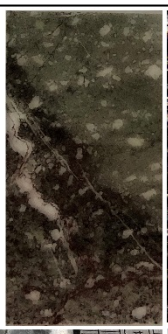
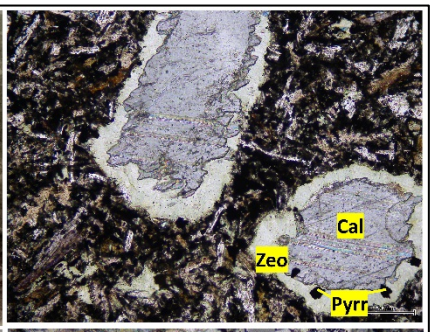

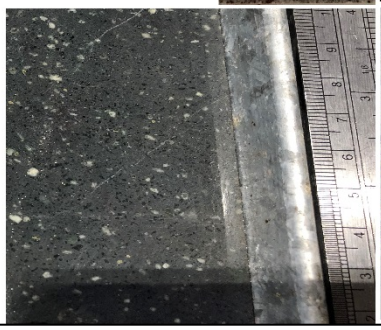
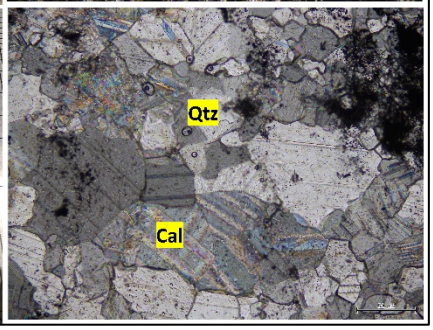

2721788
Drillhole: PADD 28
Depth: 155.65 – 155.90m

Rock comprised of biotite, plagioclase and quartz. Central vein region of the thin section (cream orange in bottom central image) composed of large irregular quartz with smaller plagioclase surrounded by chlorite alteration. Small 25um vein of quartz running the length of the thin section visible in top right image. Iron sulphides (pyrrhotite) homogenously distributed throughout grey regions, with varying grain size.
Proportions: Chlorite alteration 50%, quartz 27%, plagioclase 10%, biotitie 10%, pyrrhotite 3%
Classification: Altered Granite.


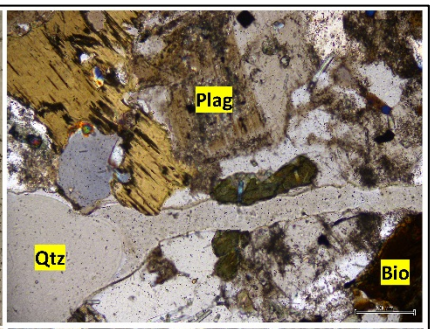

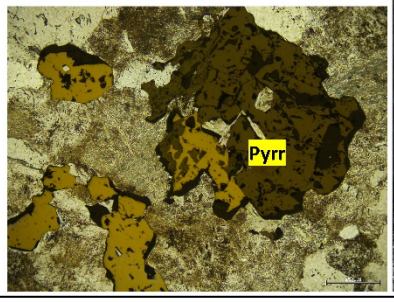


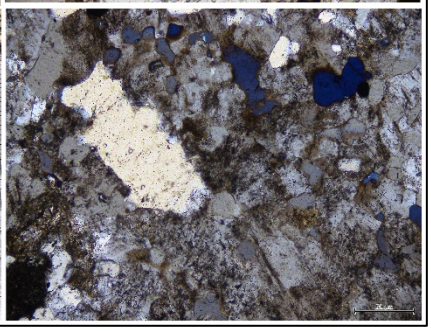

2721789
Drillhole: KMD-07-01
Depth: 336.40 – 336.55m

Strongly chlorite altered groundmass consisting or irregular plagioclase and orthopyroxene. Biotite altered to chlorite and since replaced by pyrrhotite (as displayed in image top right – reflectance on). Irregular shaped pyrrhotite present appearing to replace predominantly chlorite altered phenocrysts (image bottom right). Pyrrhotite not observed within non altered plagioclase.

Proportions: Chlorite altered plagioclase 40%, chlorite altered orthopyroxene 20%, chlorite altered biotite 20%, pyrrhotite 10% non altered plagioclase 10%.

Classification: Diorite


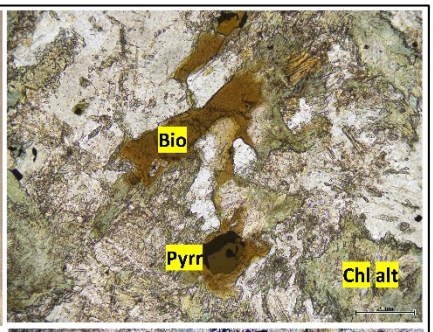

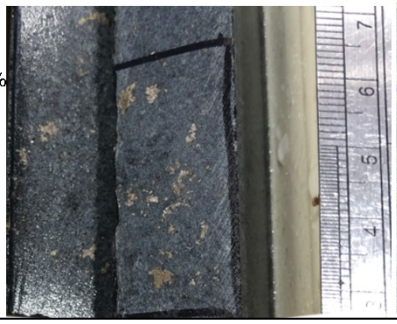
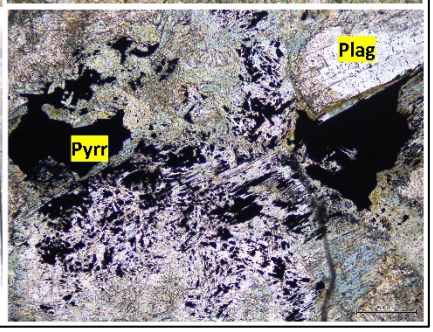

2721790
Drillhole: KMD-07-01
Depth: 336.15 – 336.45m

Chlorite dominated, both as own mineral and altered biotite. Irregular pyrrhotite (top right image – reflectance on) surrounded by chlorite groundmass. Strongly green pink pleochroic orthopyroxene phenocrysts (bottom right image). Chlorite altered and non altered plagioclase fills the groundmass, iron sulphides not found within non altered plagioclase. Chlorite altered quartz phenocrysts 50um homogenously distributed throughout.

Proportions: Chlorite alteration 45%, plagioclase 30%, orthopyroxene 10%, quartz 5%, pyrrhotite 6%, opaques 4%

Classification: Diorite


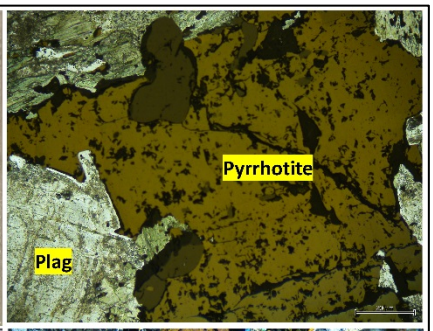


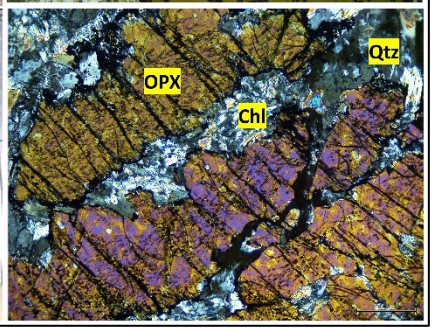

2721791
Drillhole: S11
Depth: 580.90 – 580.11feet

Heavily sericite dominated and altered rock. Sericite altered groundmass encompasses most of the sample. Pyrite with variable structure (top right image) but often exhibiting preferred cubic shape. Quartz fills the groundmass with irregular shape as well as hexagon structure visible in many locations.

Proportions: Sericite altered groundmass 70%, chlorite 10%, quartz 15%, pyrite 5%.

Classification: Altered Granite

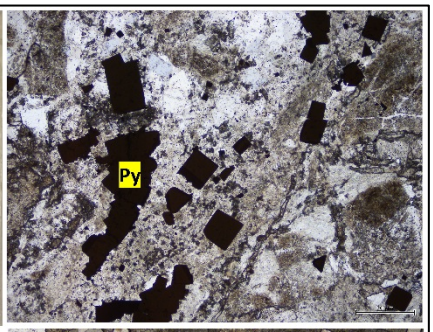

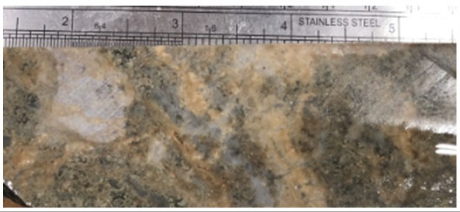

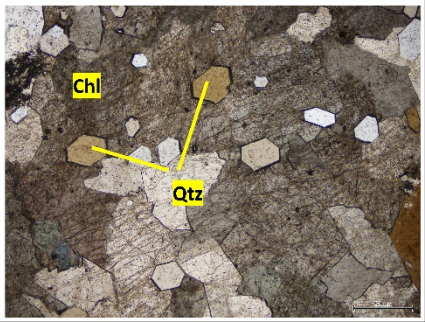

2721792
Drillhole: S11
Depth: 582.00 – 582.20feet

Sericite dominated rock. Sericite altered ground mass filled with quartz phenocrysts that display hexagonal crystal habit and minor non altered plagioclase. Pyrite present (bottom right image – reflectance on) with pyrite cubic growth. Quartz veining present with highly variable shape and width reaching 40um.

Proportions: Sericite altered groundmass 50%, quartz 38%, pyrite 10%, plagioclase 2%.

Classification: Altered Granite

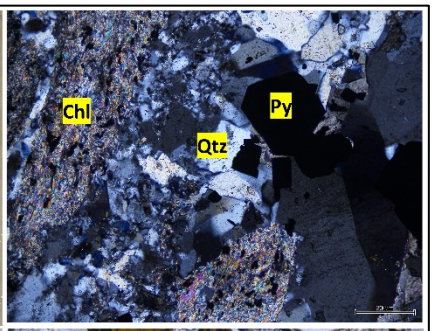

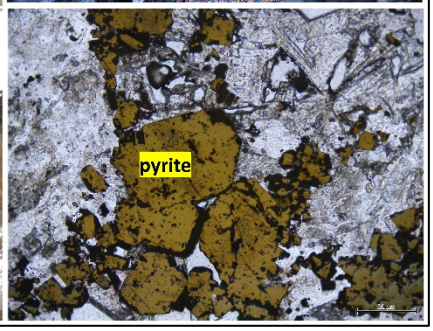

KM2-STH-G
Kanmantoo South Granite
Location: -35.1084542, 138.9971989

Extremely altered granite, hand sample no longer crystalline texture, individual grains indistinguishable. Largest grains are altered muscovite reaching 200um in length, can seen to exhibit twinning (top right image). Pleochroic biotite present homogenously distributed throughout as very small grains reaching 25um in length. Ground mass is heavily altered material, sericite in locations (not pictured) with majority being second order blue birefringent, undulatory extincting alteration material. Possibly berlin blue interface chlorite indicating iron rich environment.

Proportions:
Groundmass alteration 71%, Sericite alteration 20%, altered muscovite 5%, biotite 4%

Classification: Altered Granite

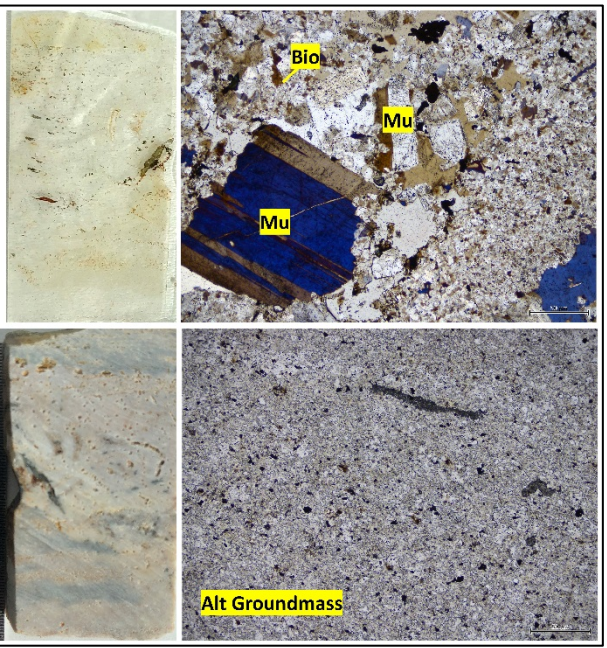

KM2-HWY-G
Kanmantoo Highway/Freeway Granite
Location: -35.086610, 138.95753

Hand sample porous with visible muscovite, tourmaline up to 2cm length with whole sample red/orange stained. Thin section with distinguishable tabluar tourmaline having strong blue green pleochroism. Regions of muscovite and chlorite surrounded by sericite groundmass. This altered groundmass makes most of the sample. Minor potassium feldspar.

Proportions:
Sericite alteration 60%, chlorite 20%, muscovite 10%, tourmaline 8%, potassium feldspar 2%.

Classification: Sericite altered granite

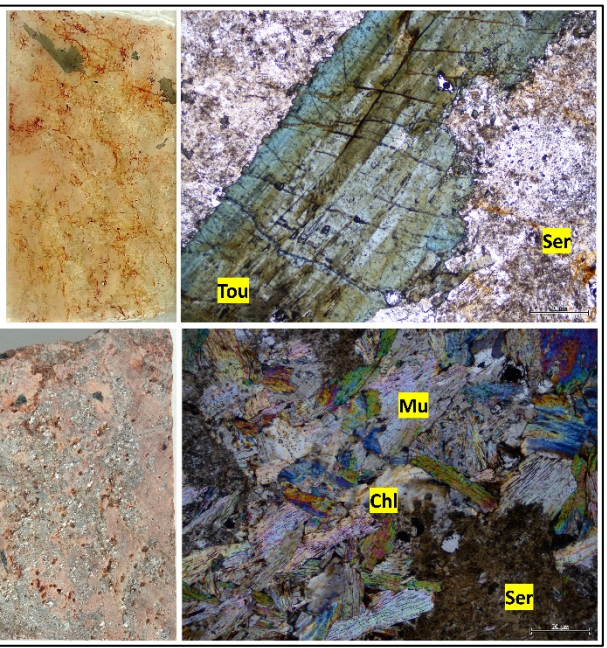

DAW-SYN
Dawesley Syenite
Location: -35.0451295, 138.9806177

Fabric visible within hand sample and thin section trending approximately 300^0 within these images, but not recognizable under microscope. Thin section exhibits largest grains of hornblende reaching 200um length. Hornblende surrounded with groundmass made of alkali feldspar (orthoclase), magnetite (opaques) and finer grained alteration material of which is likely the muscovite visible in hand sample. Orthoclase and magnetite both reaching 50um in length. Minor plagioclase present with distinctive zebra twinning (not pictured).

Proportions:
Orthoclase 70%, hornblende 18%, magnetite 8%, fine alteration (relic muscovite) 3%, plagioclase 1%.

Classification: Syenite

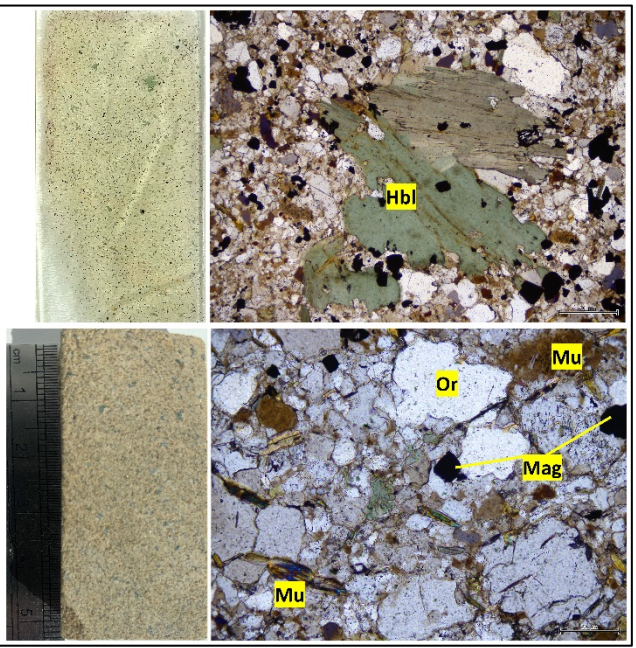

APPENDIX C: SEM-MLA EXTENDED METHODS

Appendix Table 4: Parameters of tungsten filament FEI Quanta600 scanning electron microscope with dual 30mm2 Bruker SDD detectors.

Location	The University of Adelaide, Adelaide Microscopy
Working Distance	10mm
Spot Size	7mm
Beam Energy	30kV
Magnification	250x
Samples Ran	KFP001, KP001, KP004, KP008, 2721785, 2721786, 2721787, 2721788, 2721789, 2721790, 2721791, 2721792, KM2-STH-G, KM2-HWY-G, DAW-SYN
MLA Key Minerals	Titanite, Monazite, Zircon

SEM Imagery from all 15 primary samples utilised throiughout this invesitgation

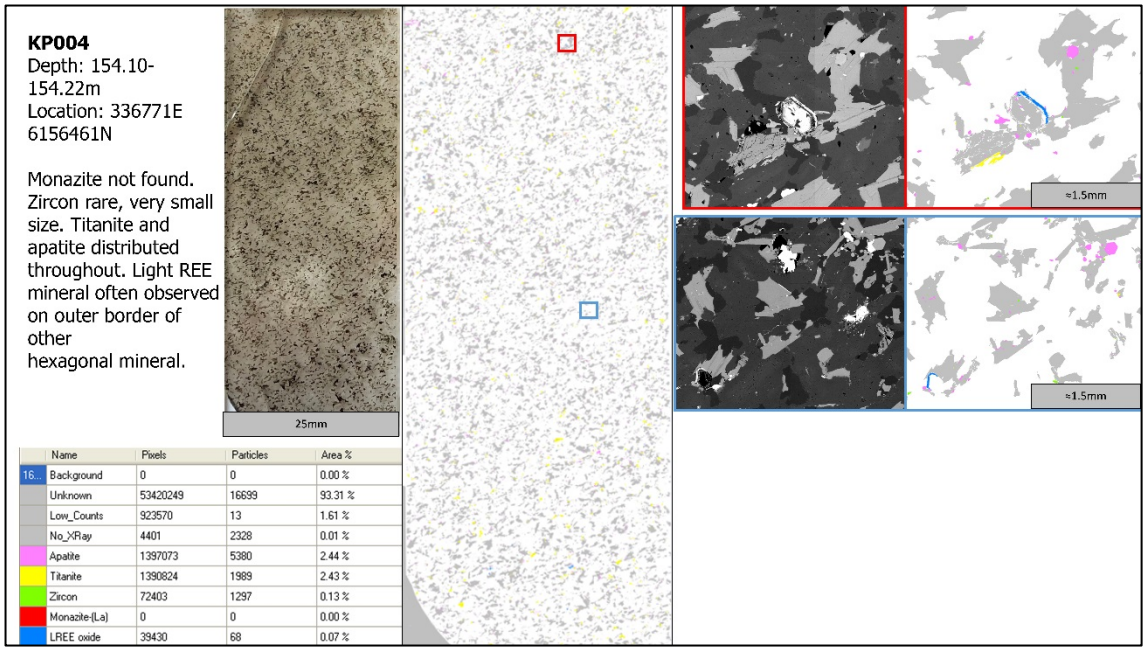

KP008
Depth: 224.4-224.55m
Location: 336771E 6156461N

Monazite not present. Apatite homogenously distributed throughout of variable size. Zircon sparse, largest displayed within inset images. Very small proportion of unknown light REE mineral.

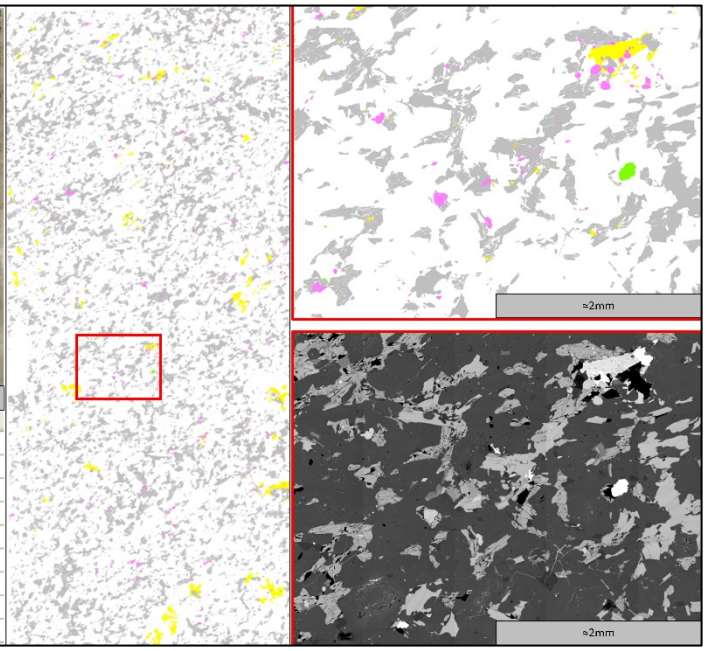

	Name	Pixels	Particles	Area %
16...	Background	0	0	0.00 %
	Unknown	27210269	8592	91.96 %
	Low_Counts	0	0	0.00 %
	No_XRay	4841	2866	0.02 %
	Apatite	898610	1854	3.04 %
	Titanite	1438779	728	4.86 %
	Zircon	33948	671	0.11 %
	Monazite-(La)	110	1	0.00 %
	LREE oxide	1222	8	0.00 %

KP001
Depth: 87.65-87.75m
Location: 336771E 6156461N

Monazite present, 35 individual grains of variable size (two largest pictured). Very low abundance of LREE mineral. Zircon rare, very small. Titanite present in only one location.

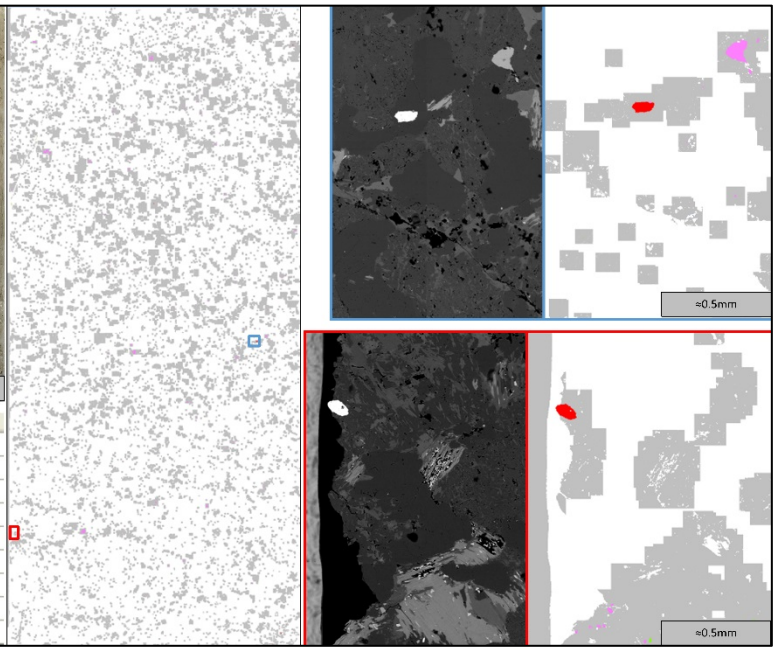

	Name	Pixels	Particles	Area %
16...	Background	0	0	0.00 %
	Unknown	62753680	6008	99.43 %
	Low_Counts	95348	5	0.15 %
	No_XRay	1587	1076	0.00 %
	Apatite	234341	1303	0.37 %
	Titanite	3762	99	0.01 %
	Zircon	13892	679	0.02 %
	Monazite-(La)	8214	35	0.01 %
	LREE oxide	662	21	0.00 %

KFP001
Depth: Surface grab
Location: 337297E 6157887N

Monazite not present. Many large titanite grains of which most display crystal habit (pictured). Apatite throughout however very small grains. Zircon sparse and very small, a cluster of larger grains is pictured.

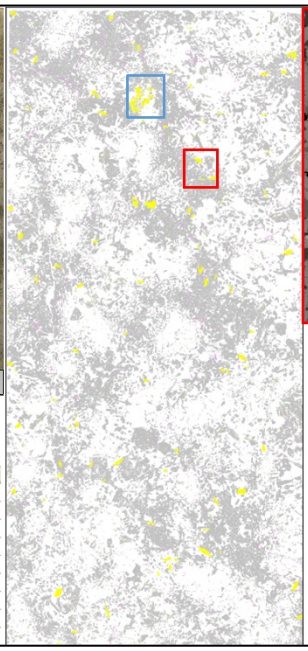

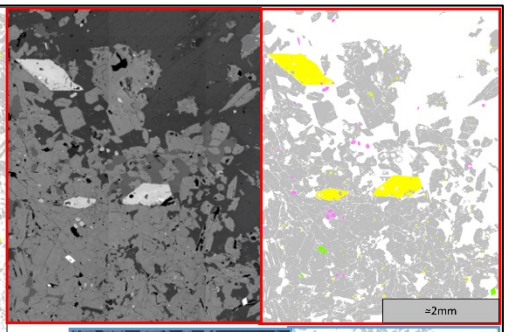

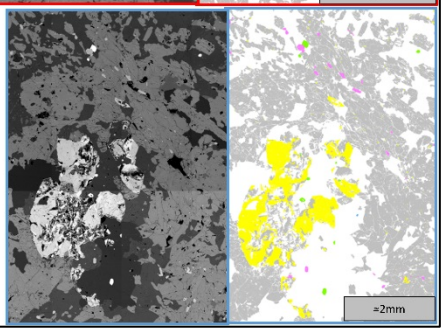

	Name	Pixels	Particles	Area %
16...	Background	0	0	0.00 %
	Unknown	93719636	26776	95.35 %
	Low_Counts	1071947	75	1.09 %
	No_XRay	21138	12939	0.02 %
	Apatite	1102710	2052	1.12 %
	Titanite	2334168	5901	2.37 %
	Zircon	39549	87	0.04 %
	Monazite-(La)	246	2	0.00 %
	LREE oxide	160	2	0.00 %

DAW-SYN
Lat: -35.0451295
Long: 138.9806177

Titanite most abundant and generally observed to be in small clusters. Monazite also present in clusters although rather sparse. Zircon homogenous throughout with no visible deterioration.

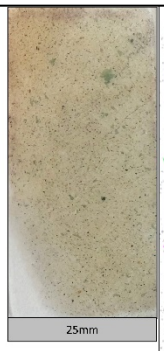

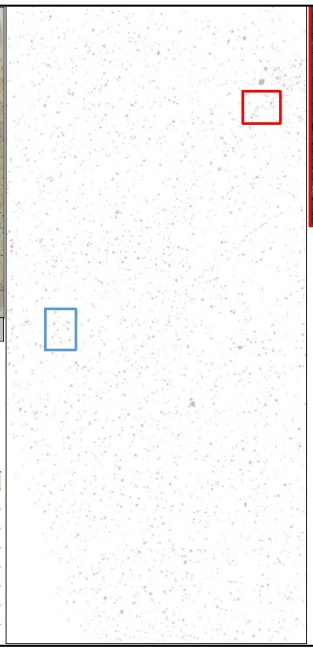

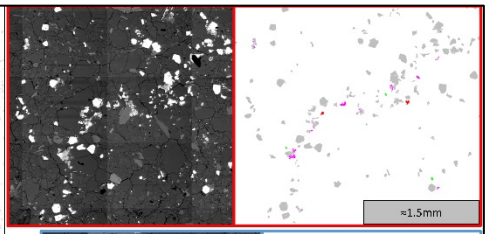

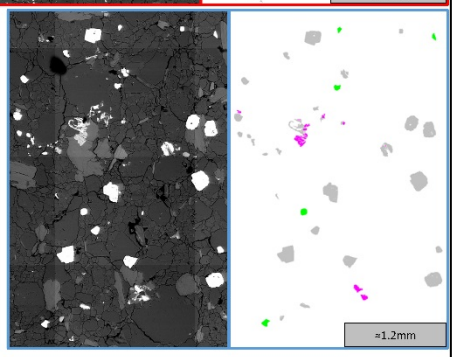

	Name	Pixels	Particles	Area %
16...	Background	0	0	0.00 %
	Unknown	4221885	6747	97.58 %
	Low_Counts	0	0	0.00 %
	No_XRay	1035	504	0.02 %
	Titanite	69189	628	1.60 %
	Monazite	1606	10	0.04 %
	Ag	474	3	0.01 %
	Zircon	32608	118	0.75 %

KM2-HWY-G
Lat: -35.086610
Long: 138.95753

Zircon found only in one location pictured in red. Only 8 monazite grains found, observed in close proximity to each other. Titanite is most abundant but still remains sparse. Majority of minerals present on the right half of the sample.

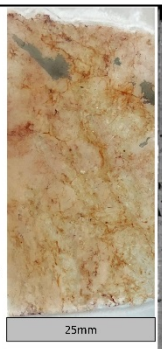

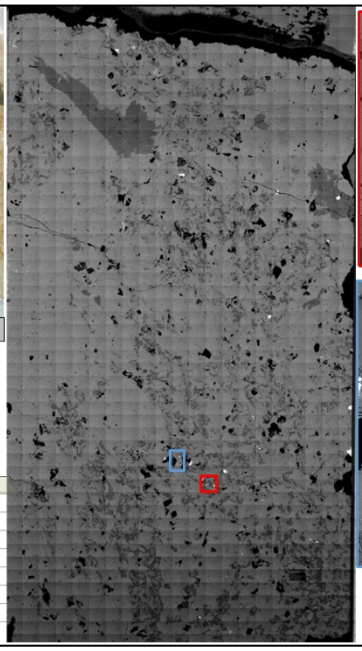

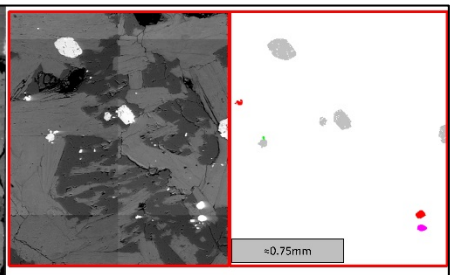

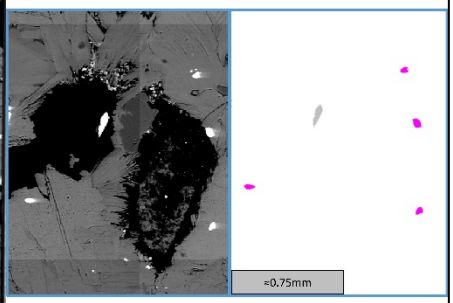

	Name	Pixels	Particles	Area %
16...	Background	0	0	0.00 %
	Unknown	9463338	545	99.90 %
	Low_Counts	0	0	0.00 %
	No_XRay	338	177	0.00 %
	Titanite	8192	47	0.09 %
	Monazite	1043	8	0.01 %
	Ag	0	0	0.00 %
	Zircon	29	1	0.00 %

KM2-STH-G
Lat: -35.1084542
Long: 138.9971989

Monazite most sparse mineral, largest grain pictured in red. Titanite homogenous throughout with good grain shape with minimal destruction. Zircon located in clusters of three or four grains and are smaller than titanite grains pictured in blue.

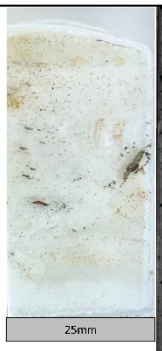

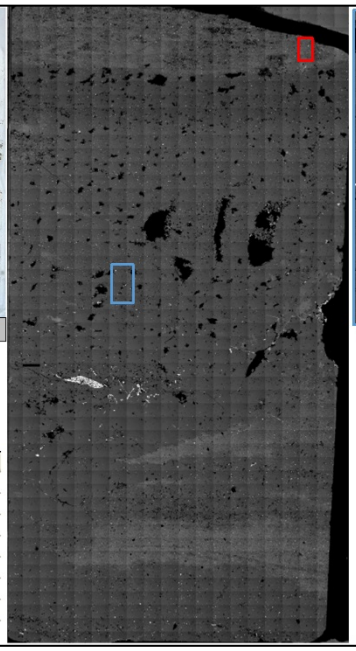

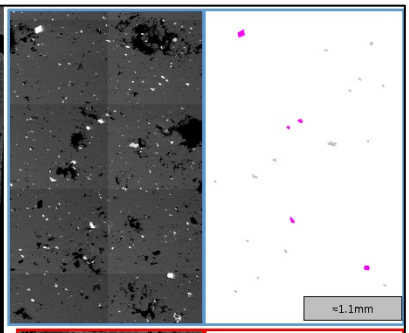

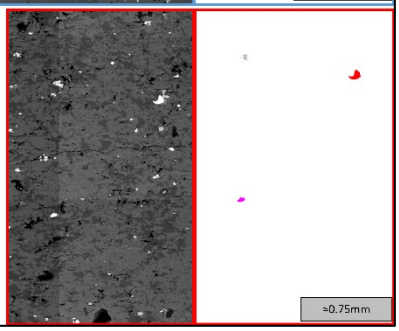

	Name	Pixels	Particles	Area %
16...	Background	0	0	0.00 %
	Unknown	505723	2251	96.79 %
	Low_Counts	0	0	0.00 %
	No_XRay	272	139	0.05 %
	Titanite	12519	58	2.40 %
	Monazite	942	6	0.18 %
	Ag	0	0	0.00 %
	Zircon	3048	23	0.58 %

2721785
Drill Hole: PADD 31
Depth: 132.75 - 133.00m

Obvious problem with SEM filament. Minerals only mapped in regions of lighter backscatter. Zircon and monazite not present. Titanite abundant throughout correctly mapped areas, it is assumed this same titanite abundance is present through the whole sample.

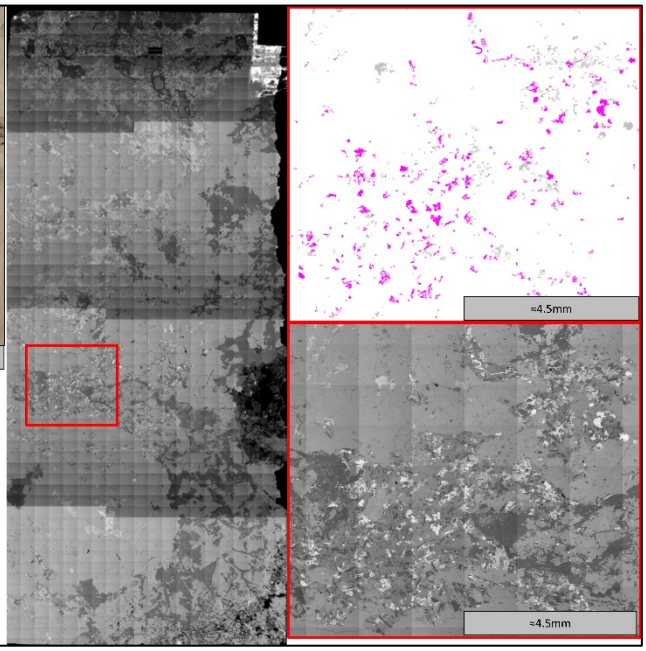

	Name	Pixels	Particles	Area %
16...	Background	0	0	0.00 %
	Unknown	3442731	7594	85.12 %
	Low_Counts	0	0	0.00 %
	No_XRay	5997	2976	0.15 %
	Titanite	594912	2241	14.71 %
	Monazite	0	0	0.00 %
	Ag	1061	9	0.03 %
	Zircon	0	0	0.00 %

2721786
Drill Hole: PADD 31
Depth: 132.00 – 132.75m

Monazite and zircon not present within sample. Titanite abundant throughout, present in all locations except within calcite (top left of sample). Titanite homogenously distributed but most abundant out of the calcite 'halo'.

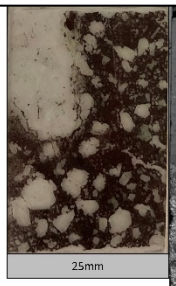

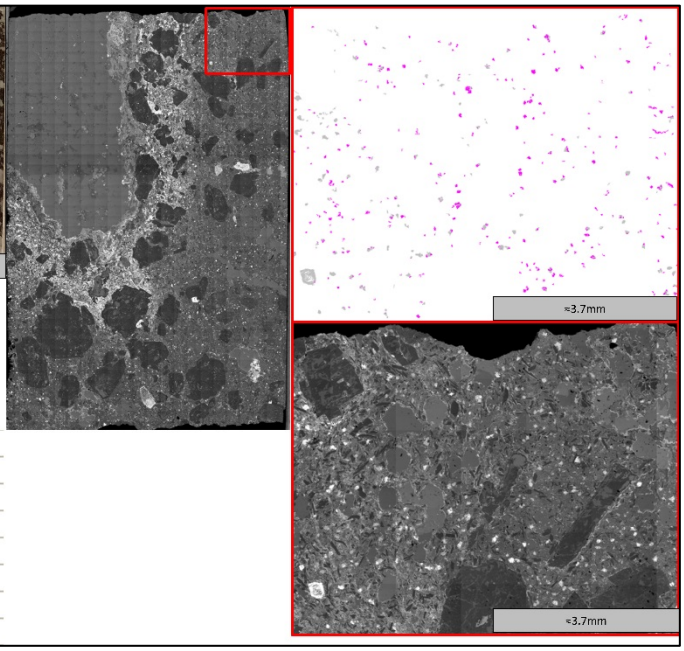

16...	Background	0	0	0.00 %
	Unknown	5563501	16430	88.63 %
	Low_Counts	252087	213	4.02 %
	No_XRay	16418	7492	0.26 %
	Titanite	445158	4843	7.09 %
	Monazite	0	0	0.00 %
	Ag	0	0	0.00 %
	Zircon	0	0	0.00 %

2721787
Drill Hole: PADD 31
Depth: 130.35 – 130.55m

Monazite and zircon not present. Titanite relatively not present. Grains are very small and likely not possibly for dating. Often found in close accusation to other 'bright' minerals of which are grey in top right image or white in bottom right image.

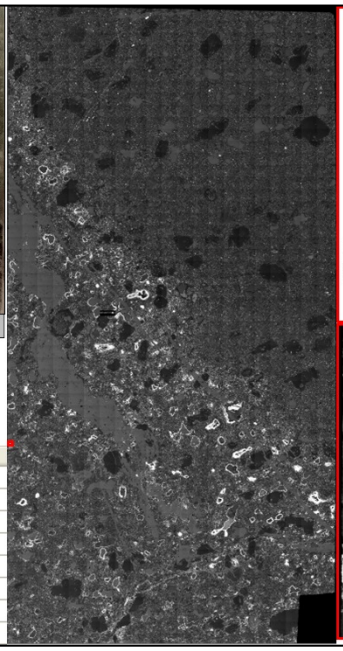

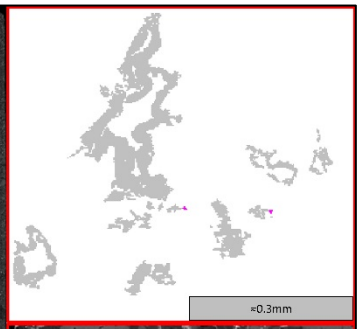

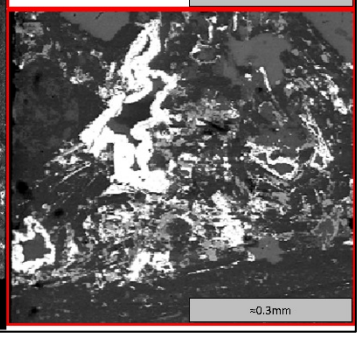

	Name	Pixels	Particles	Area %
16...	Background	0	0	0.00 %
	Unknown	6588320	18396	99.85 %
	Low_Counts	513	2	0.01 %
	No_XRay	8416	3747	0.13 %
	Titanite	1016	86	0.02 %
	Monazite	0	0	0.00 %
	Ag	4	1	0.00 %
	Zircon	0	0	0.00 %

2721788
Drill Hole: PADD 28
Depth: 155.65 – 155.90m

Monazite not present. Titanite found in clusters of small grains. Zircons homogenous throughout sample and are the largest size out of all three dating minerals. Largest zircons and titanite pictured.

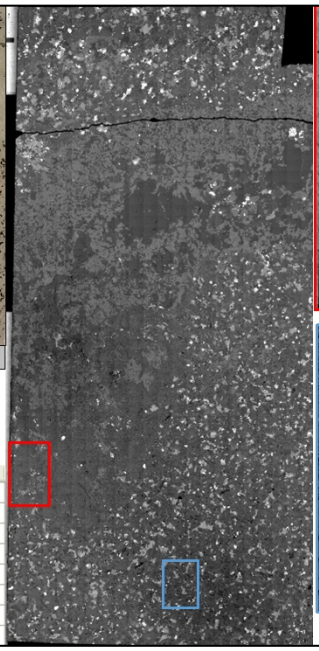

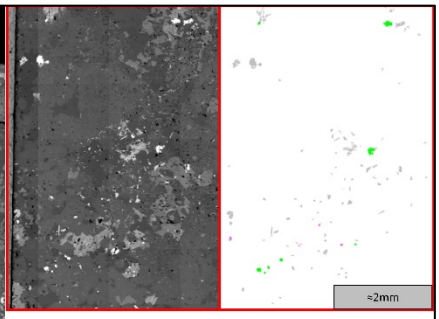

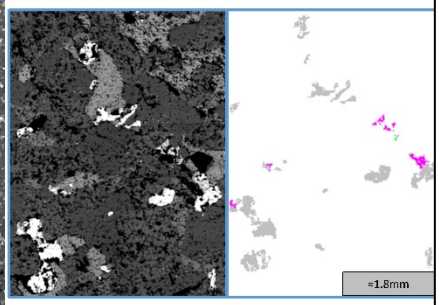

	Name	Pixels	Particles	Area %
16...	Background	0	0	0.00 %
	Unknown	5479997	7534	55.80 %
	Low_Counts	4252343	180	43.30 %
	No_XRay	2883	1393	0.03 %
	Titanite	54754	396	0.56 %
	Monazite	0	0	0.00 %
	Ag	2675	14	0.03 %
	Zircon	28224	67	0.29 %

2721789
Drill Hole: KMD-07-01
Depth: 336.40 – 336.55m

Thin section over polished when being created, sample too thin in top left section to produce backscatter. One zircon found by eye, pictured in blue. Titanite is the most abundant mineral, but sparse in sample. Most abundant cluster pictured in red.

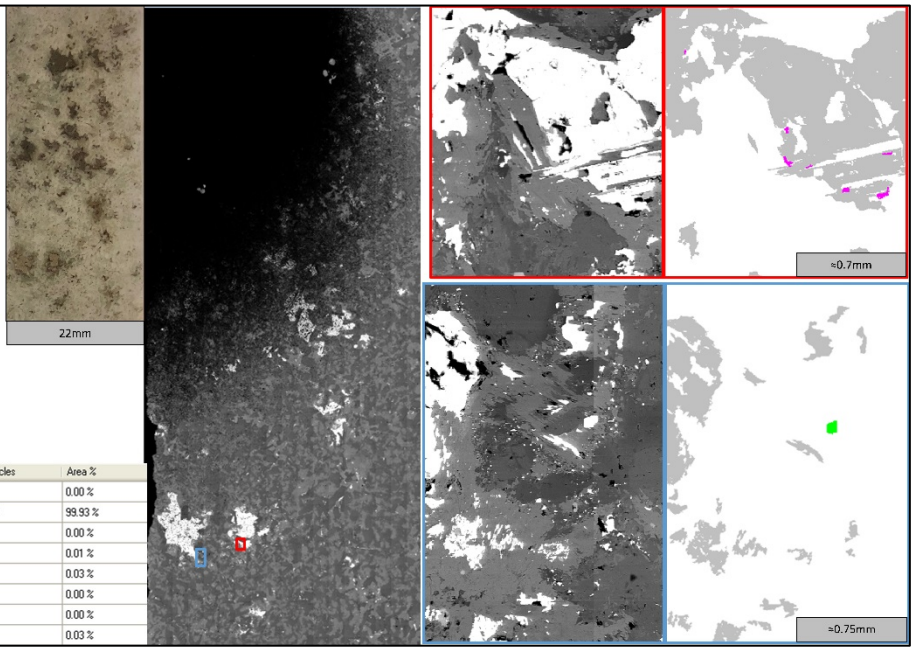

	Name	Pixels	Particles	Area %
16...	Background	0	0	0.00 %
	Unknown	4095453	3044	99.93 %
	Low_Counts	0	0	0.00 %
	No_XRay	605	286	0.01 %
	Titanite	1255	15	0.03 %
	Monazite	0	0	0.00 %
	Ag	0	0	0.00 %
	Zircon	1201	2	0.03 %

2721790
Drill Hole: KMD-07-01
Depth: 336.15 – 336.45m

Particles of Ag mineral are off the slide, possibly due to the resin. Monazite not present. Minimal zircon and titanite, most abundant clusters pictured in red and blue. Appears to have no spatial arrangement of these minerals within the sample.

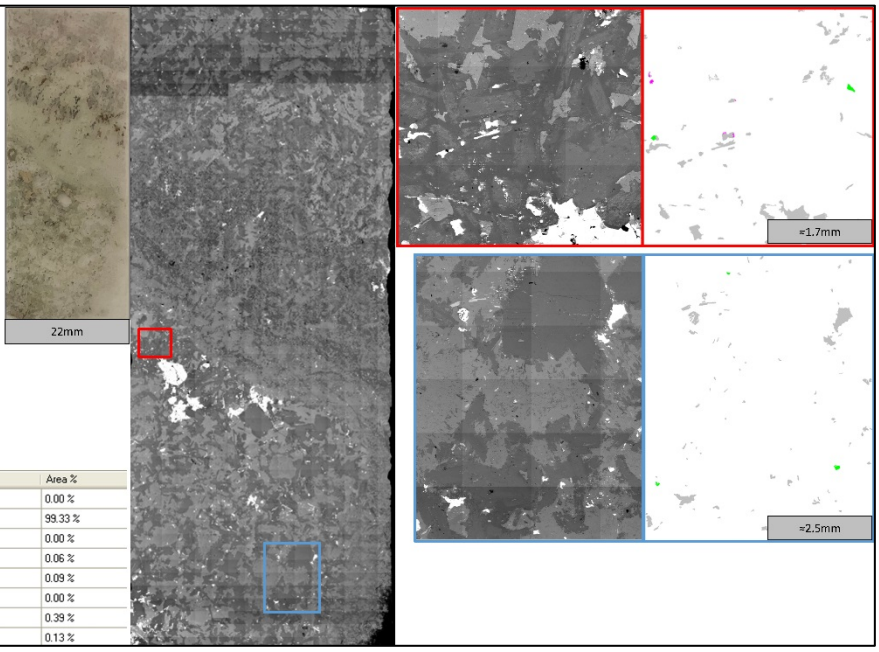

	Name	Pixels	Particles	Area %
16...	Background	0	0	0.00 %
	Unknown	3425576	5606	99.33 %
	Low_Counts	0	0	0.00 %
	No_XRay	1941	863	0.06 %
	Titanite	3108	49	0.09 %
	Monazite	0	0	0.00 %
	Ag	13316	33	0.39 %
	Zircon	4619	16	0.13 %

2721791
Drill Hole: S11
Depth: 580.90 – 580.11ft

Filament errors created brightness variations while scanning and thus some areas with assumed minerals have not been captured. One zircon and one monazite grain found within the sample (pictured in blue), other remaining mineral abundance is present off the sample, unsure if this is a SEM issue or not (pictured in red).

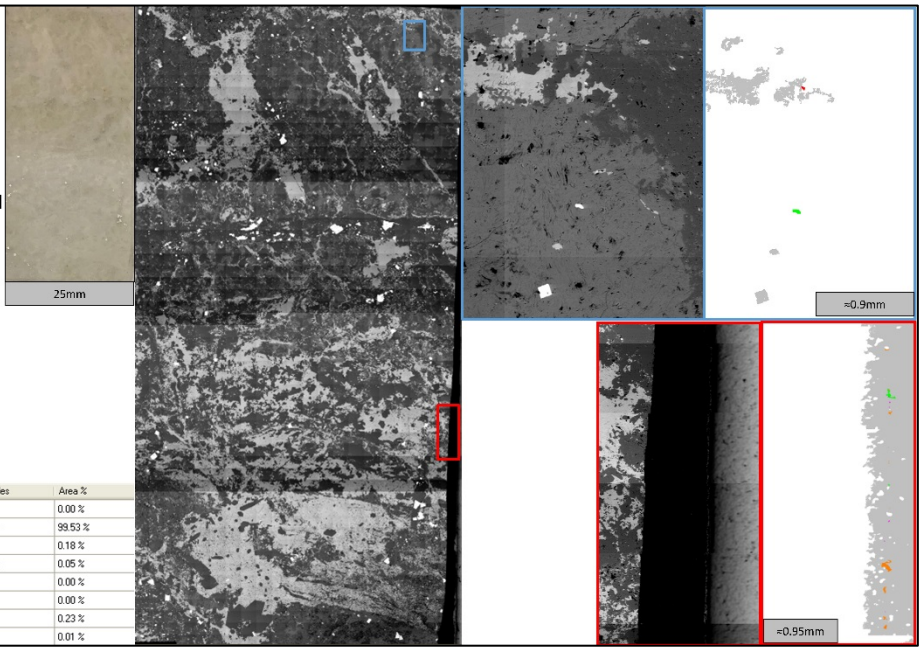

	Name	Pixels	Particles	Area %
16...	Background	0	0	0.00 %
	Unknown	39960743	26640	99.53 %
	Low_Counts	70462	27	0.18 %
	No_XRay	22067	11003	0.05 %
	Titanite	1265	26	0.00 %
	Monazite	391	16	0.00 %
	Ag	90613	21	0.23 %
	Zircon	4166	29	0.01 %

2721792
Drill Hole: S11
Depth: 582.00 – 582.20ft

Sample relatively barren of specific minerals, zircon most abundant.
Largest monazite grain pictured in blue with adjacent zircon.
Largest zircon pictured in red, however inclusions are present.

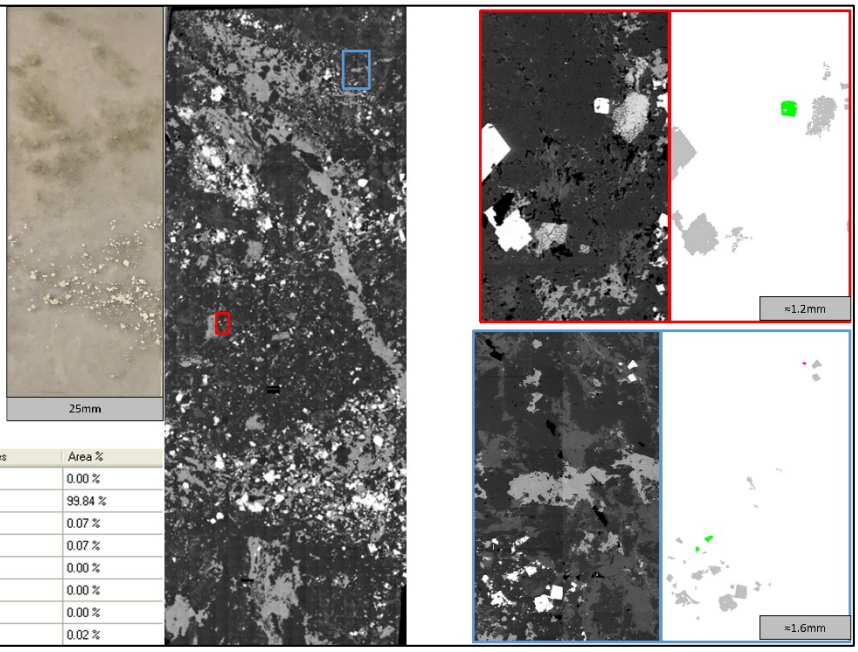

	Name	Pixels	Particles	Area %
16...	Background	0	0	0.00 %
	Unknown	18080054	22839	99.84 %
	Low_Counts	12767	14	0.07 %
	No_XRay	12472	5878	0.07 %
	Titanite	788	8	0.00 %
	Monazite	336	3	0.00 %
	Ag	0	0	0.00 %
	Zircon	3296	13	0.02 %

APPENDIX D: GEOCHRONOLOGY EXTENDED METHODS

Appendix Table 5: LA-ICP-MS Parameters and Extended Methods

Instrument	**Agilent 7900x with attached RESOlution LR 193 nm Excimer laser system**
Location	The University of Adelaide, Adelaide Microscopy
Fluence	Titanite 3.5 J/cm^2 Zircon 2.0 J/cm^2 Monazite 2.0 J/cm^2
Spot Size	Titanite 43 µm Zircon 19 µm Monazite 13 µm
Monazite Standards Concordant $^{206}Pb/^{238}U$ Age	Known: MAdel 513.9 ± 1.6 Ma (Payne, Hand, Barovich, & Wade, 2008) In House: AMBAT 520-525 Ma 222 450 Ma Calculated: Run 1: MAdel (primary) 515.5 ± 3.5 Ma (MSWD = 4.5) Run 1: AMBAT 519.1 ± 7.5 Ma (MSWD = 5.6) Run 1: 222 451.3 ± 3.6 Ma (MSWD = 0.0)
Zircon Standards Concordant $^{206}Pb/^{238}U$ Age	Published: GJ 600.7 ± 1.5 Ma (Jackson, Pearson, Griffin, & Belousova, 2004) Plesovice 337.13 ± 0.37 Ma (Slama et al., 2008) 91500 1065.4 ± 0.3 Ma (Wiedenbeck et al., 1995) Calculated: Run 1: GJ (primary) 602.3 ± 2.5 Ma (MSWD = 0.73) Run 2: GJ (primary) 602.6 ± 5.5 Ma (MSWD = 0.31) Run 1: Plesovice 340.4 ± 1.6 Ma (MSWD = 0.00059) Run 2: Plesovice 341.7 ± 3.6 Ma (MSWD = 0.00017) Run 1: 91500 1055.4 ± 6.2 Ma (MSWD = 4.0) Run 2: 91500 1064 ± 12 Ma (MSWD = 0.003)
Titanite Standards Concordant $^{206}Pb/^{238}U$ Age	Published: MKED 1521.02 ± 0.55 Ma (Spandler et al., 2016) In House: Mt Painter 442 Ma Calculated: Run 1: MKED (primary) 1518.8 ± 5.0 Ma (MSWD = 0.107) Run 2: MKED (primary) 1517.0 ± 3.8 Ma (MSWD = 6.5) Run 1: Mt Painter 439.2 ± 2.1 Ma (MSWD = 4.2) Run 2: Mt Painter 440.6 ± 4.6 Ma (MSWD = 3.1)
Samples Analysed	KP001: Monazite KP004: Titanite, Zircon KP008: Titanite, Zircon KFP001: Titanite, Zircon DAW-SYN: Zircon 2721785: Titanite 2721786: Titanite 2721788: Zircon

Geochronology plotting for all 15 primary samples with accosiated effective concordia plotting for multiple samples.

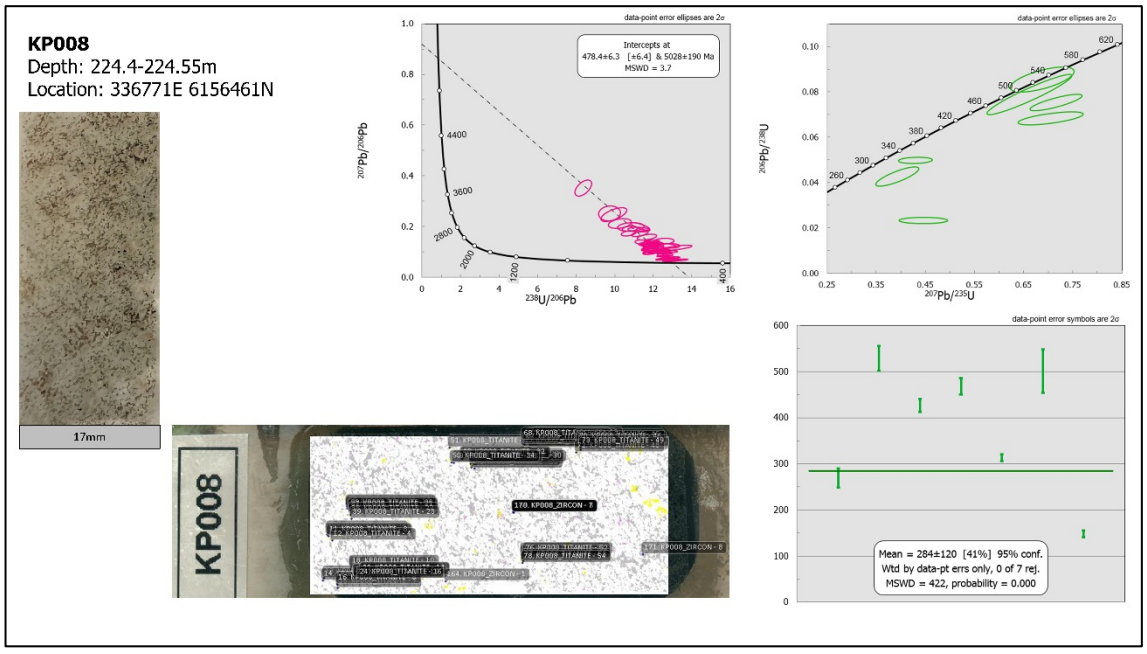

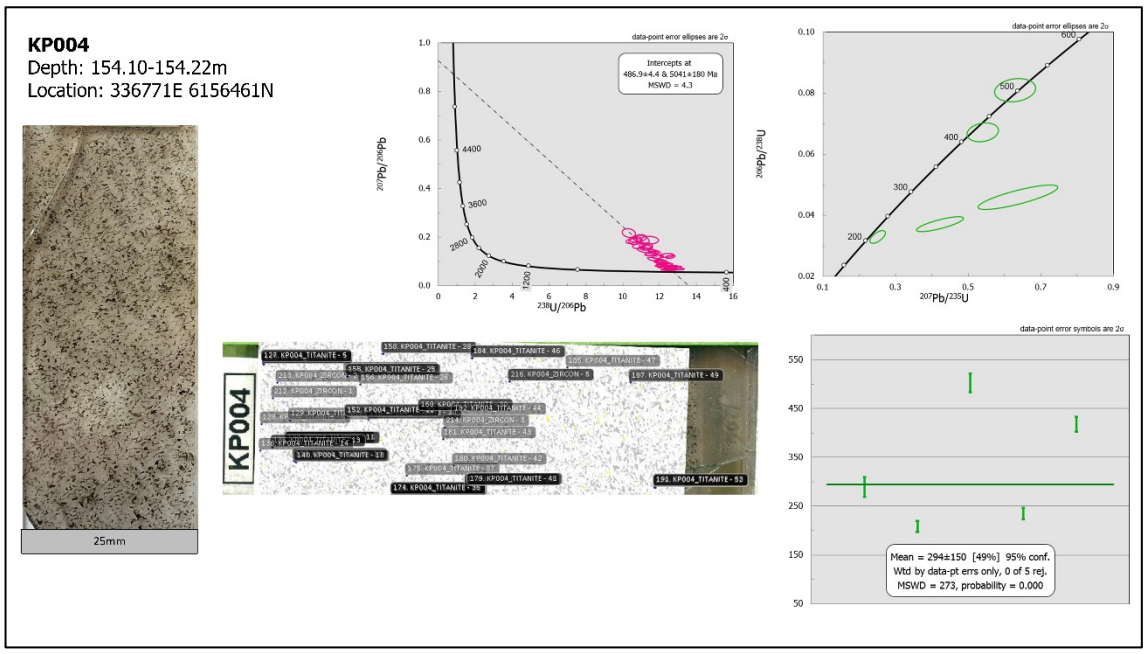

KP001
Depth: 87.65-87.75m
Location: 336771E 6156461N

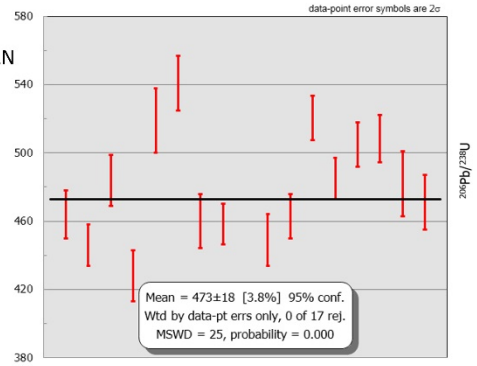

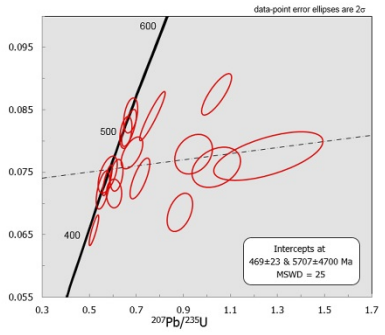

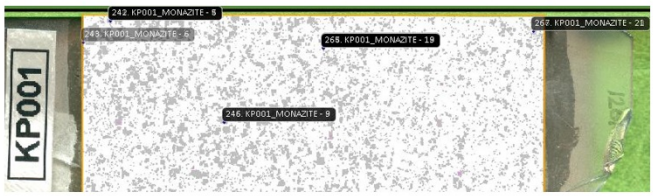

KFP001
Depth: Surface grab
Location: 337297E 6157887N

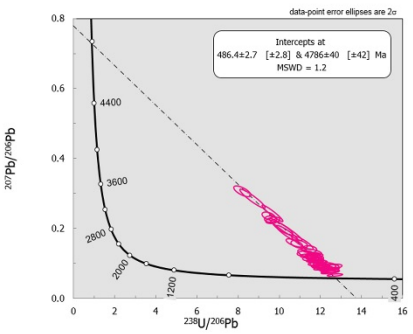

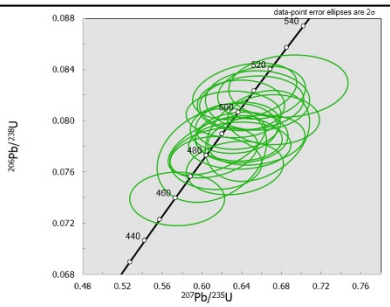

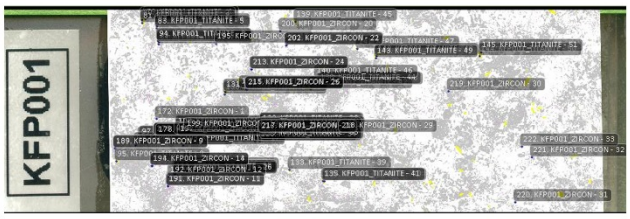

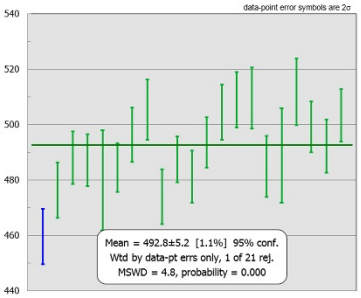

DAW-SYN
Lat: -35.0451295
Long: 138.9806177

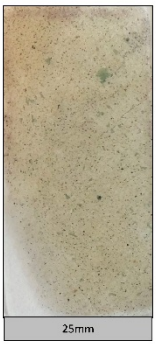

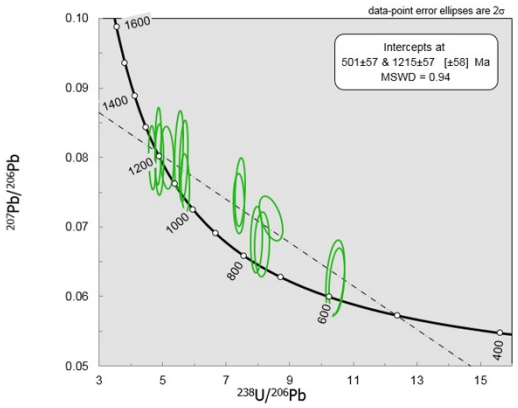

2721785
Drill Hole: PADD 31
Depth: 132.75 - 133.00m

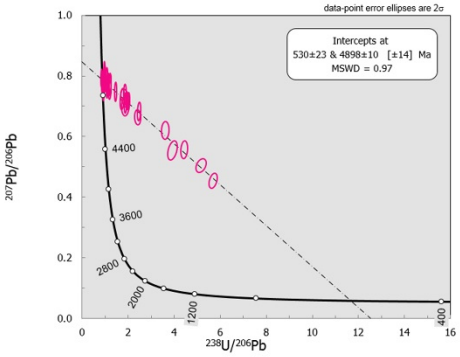

2721786
Drill Hole: PADD 31
Depth: 132.00 – 132.75m

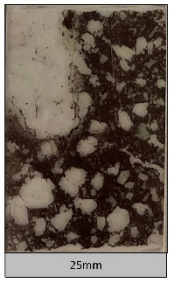

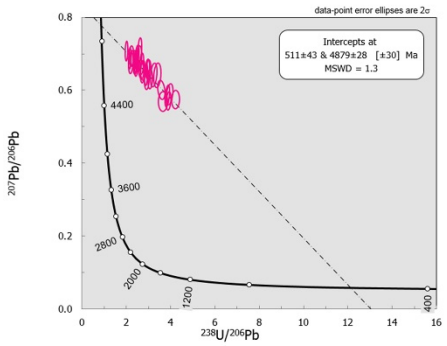

2721788
Drill Hole: PADD 28
Depth: 155.65 – 155.90m

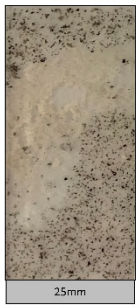

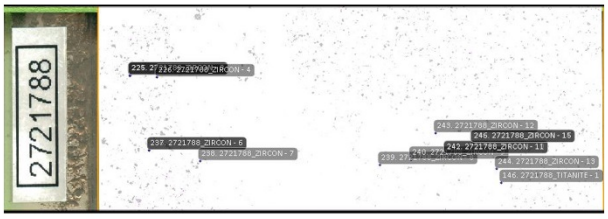

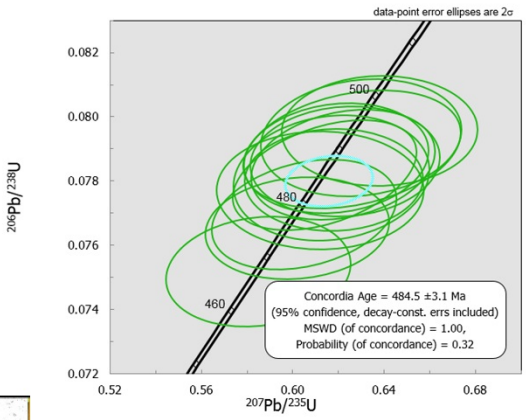

2721789
Drill Hole: KMD-07-01
Depth: 336.40 – 336.55m

Unable to date, Low abundance of minerals of which are all too small.

2721790
Drill Hole: KMD-07-01
Depth: 336.15 – 336.45m

Unable to date, Low abundance of minerals of which are all too small.

KM2-STH-G
Lat: -35.1084542
Long: 138.9971989

Unable to date, Low abundance of minerals of which are all too small.

2721791
Drill Hole: S11
Depth: 580.90 – 580.11ft

Dating will not be completed.
Very low count of all dating minerals and mineral size will likely result in inconclusive dating

KM2-HWY-G
Lat: -35.086610
Long: 138.95753

Unable to date, Low abundance of minerals of which are all too small.

2721787
Drill Hole: PADD 31
Depth: 130.35 – 130.55m

Unable to date.
Zircon and Monazite not present, titanite grains too small.

2721792
Drill Hole: S11
Depth: 582.00 – 582.20ft

Dating will not be completed.
Very low count of all dating minerals and mineral size will likely result in inconclusive dating.

Grain Selection:

Scanning electron microscope backscatter and mineral liberation imagery were utilised in the identification of dating minerals of zircon, monazite and titanite within each sample. Those samples with mineral grains large enough to test were done so ensuring the laser spot size could be fully encompassed within the grain and not overlaying any observable inclusions. Grains of titanite were the largest observed grains within all samples allowing for multiple spots to be taken from one single grain. A maximum of three spots were within each grain if available to do so, with zircon and monazite grains only every having one single spot taken per grain. Grain size posed a major problem throughout this investigation. Both zircon and monazite grains were often smaller than the ideal spot size and therefore should not be sampled due to a suite of likely errors. Therefore, the largest grains within a sample had spots placed first, followed by smaller grains until the spot size could no longer be easily encompassed within the grain. Spots were taken from all over a sample where possible. Following these parameters, multiple samples could not be dated due to the grains within being too small to analyse accurately (even with a reduced, less accurate spot size). A list of which samples were analysed is located above.

Data Processing and Reduction:

Data processing was completed using Iolite software (Paton et al., 2011) at Adelaide Microscopy, The University of Adelaide. Several known standards of which were either in house or published are listed above, and were used to correct instrument drift and down-hole element fractionation. An appropriate standard was run at minimum of every 20 spots and always after the final spot of a given series of the same mineral. During data reduction, a polynomial fit was used, most commonly spline 6, with Visual Age DRS reduction scheme. Bracketing was completed to capture the best uranium lead signal and to ensure the presence of inclusions within the key grain were minimised. It was found that due to the small size of many grains, namely zircon and monazite, the laser penetrated through the entire grain into the below mineral. This resulted in reduced signal of which bracketing was utilised to capture, but in some cases, the signal was too minimal and the spot was removed.

Common Lead:

Samples containing titanite of which was analysed all exhibited common lead. Variable concentrations of $^{207}Pb/^{235}U$ tracked back to the age of the earth. These samples were plotted using a Tera-Wasserburg (Tera & Wasserburg, 1972) to show both upper and lower intercepts of the trend, upper intercept representing the age of the Earth and lower intercept being the age of this sample.

For samples of which do not display a distinctive common lead trend, like that of KP001, but do show high variation between spots, another method was implemented. A proxy method using excel was used for sample KP001 in which the supplied Pb 206/204 value was converted to Pb 204/206 using a cut off value of 0.001. As Pb204 is non radiogenic and does not therefore form as a decay product of U235 or U238 it presence therefore suggests that Pb is common within the crystal lattice of the mineral and did not arise through radiogenic decay. The higher Pb 204/206 value, the more it will affect the spread of spot data, therefore spots with a Pb 204/206 value greater than 0.001 were classified as containing common lead and therefore removed from the data set leaving the remaining concordant data behind. However, this method is only a proxy

as the utilised equipment cannot distinguish between Pb204 and Hg204, therefore the value of Pb204 is not true and the abundance of Hg204 within is unknown.

Uranium Fractionation:

One sample, DAW-SYN, exhibited what can be assume to be uranium fractionation. Two intercepts are present on a Tera-Wasserburg plot of with the upper intercept is not representative of the age of the earth, like that for a common lead trend. The upper intercept represents the emplacement of the rock and the lower intercept represents the metamorphism age of the rock. For the DAW-SYN sample, it has been found that the upper intercept age is from that of the Grenvillean Orogen (1200-1000 Ma) and the lower intercept being the metamorphism associated with the Delamerian Orogeny. Further information on geochronology and recognising trends within data is located within Schoene (2014).

Appendix Table 6: Raw LA-ISP-MS data for all Monazite U-Pb Geochronology

Sample	Final 207_235	Final 207_235 Prop2SE	Final 206_238	Final 206_238 Prop2SE	Error Correlation
G_NIST610_1	0.673	0.020	0.084	0.002	0.432
G_NIST610_2	0.661	0.020	0.085	0.002	0.428
G_NIST610_3	0.688	0.026	0.089	0.003	0.778
G_NIST610_4	0.675	0.021	0.085	0.002	0.356
G_NIST610_5	0.654	0.020	0.083	0.002	0.511
G_NIST610_6	0.645	0.020	0.083	0.002	0.359
G_NIST610_7	28.490	0.830	0.228	0.006	0.947
G_NIST610_8	28.260	0.800	0.227	0.006	0.941
G_NIST610_9	28.480	0.810	0.229	0.006	0.862
G_NIST610_10	28.650	0.790	0.230	0.006	0.923
G_NIST610_11	28.390	0.810	0.228	0.006	0.852
G_NIST610_12	28.340	0.820	0.229	0.006	0.904
KFP001_1	0.578	0.034	0.075	0.002	0.550
KFP001_2	0.605	0.026	0.072	0.002	0.000
KFP001_3	0.943	0.066	0.078	0.003	0.263
KFP001_4	0.884	0.044	0.069	0.003	0.422
KFP001_5	0.769	0.044	0.084	0.003	0.939
KFP001_6	1.041	0.053	0.088	0.003	0.817
KFP001_7	0.716	0.034	0.074	0.003	0.747
KFP001_8	0.577	0.017	0.074	0.002	0.777
KFP001_9	0.520	0.016	0.066	0.002	0.869
KFP001_10	0.558	0.023	0.072	0.003	0.572
KFP001_11	0.617	0.022	0.075	0.002	0.324
KFP001_12	0.676	0.025	0.084	0.002	0.387
KFP001_13	0.681	0.037	0.078	0.002	0.581
KFP001_14	0.656	0.021	0.081	0.002	0.368
KFP001_15	0.669	0.025	0.082	0.002	0.684
KFP001_16	1.260	0.190	0.078	0.003	0.605
KFP001_17	1.039	0.084	0.076	0.003	0.314
KFP001_18	0.674	0.020	0.085	0.002	0.343
KFP001_19	0.647	0.019	0.083	0.002	0.524
KFP001_20	0.647	0.021	0.082	0.002	0.514
KFP001_21	0.661	0.021	0.084	0.002	0.292
KFP001_22	0.667	0.021	0.084	0.002	0.533
KFP001_23	0.647	0.019	0.082	0.002	0.455
KFP001_24	0.660	0.020	0.084	0.002	0.380
KFP001_25	0.659	0.020	0.084	0.002	0.495
KFP001_26	0.657	0.020	0.084	0.002	0.407
KFP001_27	0.560	0.017	0.073	0.002	0.442
KFP001_28	0.567	0.017	0.072	0.002	0.351
KFP001_29	0.560	0.017	0.072	0.002	0.371
KFP001_30	0.554	0.017	0.072	0.002	0.027
KFP001_31	0.552	0.017	0.072	0.002	0.295
KFP001_32	0.566	0.017	0.072	0.002	0.350

Appendix Table 7: Raw LA-ISP-MS data for all Zircon U-Pb Geochronology

Sample	Run Number	Final 207_235	Final 207_235 Prop2SE	Final 206_238	Final 206_238 Prop2SE	Error Correlation
DAW_SYN_2	1	1.939	0.110	0.177	0.004	0.000
DAW_SYN_3	1	2.029	0.110	0.182	0.004	0.003
DAW_SYN_4	1	2.249	0.130	0.205	0.005	0.403
DAW_SYN_5	1	2.318	0.130	0.206	0.004	0.182
DAW_SYN_6	1	2.363	0.130	0.214	0.004	0.530
DAW_SYN_7	1	1.843	0.095	0.175	0.003	0.498
DAW_SYN_8	1	1.168	0.074	0.119	0.004	0.865
DAW_SYN_9	1	1.391	0.073	0.135	0.002	0.104
DAW_SYN_10	1	2.148	0.130	0.195	0.007	0.655
DAW_SYN_11	1	0.818	0.049	0.095	0.002	0.000
DAW_SYN_12	1	0.850	0.086	0.083	0.003	0.561
DAW_SYN_13	1	0.990	0.110	0.091	0.004	0.074
DAW_SYN_14	1	1.180	0.069	0.126	0.002	0.223
DAW_SYN_15	1	1.146	0.068	0.123	0.003	0.322
DAW_SYN_16	1	1.000	0.110	0.097	0.005	0.275
DAW_SYN_17	1	1.369	0.072	0.135	0.003	0.422
DAW_SYN_19	1	0.829	0.056	0.096	0.002	0.000
G_NIST610_1	1	26.660	1.400	0.211	0.006	0.943
G_NIST610_2	1	26.620	1.400	0.211	0.006	0.859
G_NIST610_3	1	26.480	1.400	0.211	0.006	0.907
G_NIST610_4	1	26.430	1.400	0.208	0.005	0.891
G_NIST610_5	1	26.410	1.400	0.211	0.005	0.968
G_NIST610_6	1	26.380	1.400	0.211	0.005	0.875
G_NIST610_7	1	26.480	1.400	0.211	0.005	0.932
G_NIST610_8	1	26.530	1.400	0.211	0.005	0.894
G_NIST610_9	1	27.190	1.400	0.215	0.005	0.949
G_NIST610_10	1	27.740	1.500	0.221	0.006	0.974
G_NIST610_11	1	27.270	1.400	0.212	0.005	0.959
G_NIST610_12	1	27.260	1.400	0.212	0.005	0.646
KP008_1	1	0.393	0.036	0.043	0.003	0.815
KP008_2	1	0.688	0.053	0.086	0.005	0.645
KP008_3	1	0.705	0.054	0.068	0.002	0.653
KP008_4	1	0.716	0.043	0.075	0.003	0.820
KP008_5	1	0.430	0.028	0.050	0.001	0.158
KP008_6	1	0.662	0.071	0.079	0.007	0.941
KP008_7	1	0.446	0.041	0.023	0.001	0.000
X2721788_1	1	0.605	0.033	0.077	0.001	0.288
X2721788_2	1	0.630	0.036	0.079	0.002	0.138
X2721788_3	1	0.585	0.033	0.075	0.001	0.144
X2721788_4	1	0.612	0.037	0.078	0.002	0.000
X2721788_5	1	0.602	0.033	0.077	0.001	0.120
X2721788_6	1	0.614	0.033	0.078	0.001	0.413
X2721788_7	1	0.619	0.033	0.079	0.001	0.137
X2721788_8	1	0.622	0.033	0.079	0.001	0.241
X2721788_9	1	0.617	0.035	0.078	0.002	0.132
X2721788_10	1	0.623	0.034	0.079	0.001	0.076
X2721788_11	1	0.618	0.032	0.078	0.001	0.030
X2721788_12	1	0.626	0.039	0.079	0.002	0.282
X2721788_13	1	0.638	0.035	0.080	0.001	0.022
Z_GJ1_1	1	0.844	0.049	0.098	0.002	0.000
Z_GJ1_2	1	0.852	0.050	0.099	0.002	0.000
Z_GJ1_3	1	0.789	0.047	0.098	0.002	0.000
Z_GJ1_4	1	0.828	0.048	0.097	0.002	0.000
Z_GJ1_5	1	0.787	0.048	0.098	0.002	0.088
Z_GJ1_6	1	0.812	0.050	0.099	0.002	0.062
Z_GJ1_7	1	0.819	0.047	0.099	0.002	0.092
Z_GJ1_8	1	0.790	0.047	0.097	0.002	0.144
Z_GJ1_9	1	0.804	0.046	0.099	0.002	0.143
Z_GJ1_10	1	0.817	0.048	0.098	0.002	0.000
Z_GJ1_11	1	0.824	0.049	0.097	0.002	0.112
Z_GJ1_12	1	0.807	0.049	0.099	0.002	0.111
Z_GJ1_13	1	0.789	0.046	0.097	0.002	0.000
Z_GJ1_14	1	0.824	0.048	0.097	0.002	0.125
Z_GJ1_15	1	0.797	0.049	0.098	0.002	0.000

Z_GJ1_16	1	0.819	0.051	0.099	0.002	0.210
Z_GJ1_17	1	0.853	0.050	0.099	0.002	0.067
Z_GJ1_18	1	0.819	0.047	0.098	0.002	0.010
Z_Plesovice_1	1	0.406	0.022	0.054	0.001	0.301
Z_Plesovice_2	1	0.401	0.022	0.054	0.001	0.151
Z_Plesovice_3	1	0.402	0.022	0.054	0.001	0.027
Z_Plesovice_4	1	0.396	0.022	0.054	0.001	0.031
Z_Plesovice_5	1	0.395	0.022	0.055	0.001	0.060
Z_Plesovice_6	1	0.393	0.022	0.055	0.001	0.001
Z_Plesovice_7	1	0.390	0.022	0.054	0.001	0.122
Z_Plesovice_8	1	0.393	0.022	0.054	0.001	0.091
Z_Plesovice_9	1	0.388	0.021	0.054	0.001	0.315
Z_Plesovice_10	1	0.398	0.022	0.054	0.001	0.000
Z_Plesovice_11	1	0.403	0.022	0.055	0.001	0.013
Z_Plesovice_12	1	0.411	0.023	0.055	0.001	0.000
Z_91500_1	1	1.862	0.120	0.179	0.004	0.162
Z_91500_2	1	1.842	0.120	0.175	0.004	0.157
Z_91500_3	1	1.861	0.120	0.175	0.005	0.000
Z_91500_4	1	1.878	0.130	0.176	0.004	0.000
Z_91500_5	1	1.875	0.120	0.179	0.004	0.109
Z_91500_6	1	1.891	0.120	0.178	0.005	0.000
Z_91500_7	1	1.849	0.130	0.182	0.005	0.000
Z_91500_8	1	1.888	0.120	0.178	0.004	0.191
Z_91500_9	1	1.828	0.110	0.175	0.004	0.082
Z_91500_10	1	1.823	0.120	0.176	0.004	0.088
Z_91500_11	1	1.799	0.120	0.179	0.004	0.218
Z_91500_12	1	1.919	0.130	0.177	0.005	0.244
KFP001_1	1	0.575	0.039	0.074	0.002	0.000
KFP001_2	1	0.614	0.038	0.077	0.002	0.000
KFP001_3	1	0.640	0.038	0.079	0.002	0.061
KFP001_4	1	0.655	0.040	0.079	0.002	0.186
KFP001_5	1	0.610	0.045	0.077	0.003	0.274
KFP001_6	1	0.638	0.042	0.078	0.002	0.031
KFP001_7	1	0.672	0.038	0.080	0.002	0.000
KFP001_8	1	0.656	0.043	0.082	0.002	0.000
KFP001_9	1	0.633	0.040	0.076	0.002	0.159
KFP001_10	1	0.637	0.036	0.079	0.001	0.000
KFP001_11	1	0.612	0.036	0.078	0.002	0.320
KFP001_12	1	0.636	0.035	0.080	0.002	0.114
KFP001_13	1	0.650	0.043	0.081	0.002	0.127
KFP001_14	1	0.660	0.036	0.082	0.002	0.176
KFP001_15	1	0.643	0.043	0.082	0.002	0.310
KFP001_16	1	0.615	0.040	0.078	0.002	0.546
KFP001_17	1	0.656	0.043	0.079	0.003	0.304
KFP001_18	1	0.687	0.049	0.083	0.002	0.107
KFP001_19	1	0.632	0.039	0.081	0.002	0.000
KFP001_20	1	0.632	0.036	0.079	0.002	0.056
KFP001_21	1	0.639	0.036	0.081	0.002	0.008
G_NIST610_1	2	25.440	1.500	0.211	0.008	0.967
G_NIST610_2	2	25.540	1.500	0.211	0.007	0.959
G_NIST610_3	2	27.990	1.700	0.212	0.008	0.940
G_NIST610_4	2	28.000	1.700	0.213	0.008	0.953
KP004_1	2	0.637	0.090	0.046	0.003	0.815
KP004_2	2	0.251	0.018	0.033	0.002	0.630
KP004_3	2	0.629	0.046	0.081	0.003	0.171
KP004_4	2	0.422	0.053	0.037	0.002	0.788
KP004_5	2	0.540	0.036	0.067	0.003	0.206
Z_GJ1_1	2	0.804	0.053	0.097	0.003	0.000
Z_GJ1_2	2	0.804	0.055	0.097	0.003	0.005
Z_GJ1_3	2	0.851	0.059	0.100	0.003	0.186
Z_GJ1_4	2	0.812	0.054	0.097	0.003	0.066
Z_GJ1_5	2	0.818	0.055	0.098	0.003	0.000
Z_GJ1_6	2	0.830	0.058	0.098	0.003	0.061
Z_GJ1_7	2	0.816	0.054	0.098	0.003	0.176
Z_GJ1_8	2	0.798	0.055	0.099	0.003	0.115
Z_Plesovice_1	2	0.384	0.025	0.054	0.002	0.074
Z_Plesovice_2	2	0.401	0.025	0.054	0.002	0.000
Z_Plesovice_3	2	0.386	0.024	0.055	0.002	0.190
Z_Plesovice_4	2	0.404	0.026	0.054	0.002	0.000

Z_Plesovice_5	2	0.413	0.027	0.054	0.002	0.064
Z_Plesovice_6	2	0.422	0.028	0.054	0.002	0.008
Z_91500_1	2	1.777	0.120	0.175	0.006	0.075
Z_91500_2	2	1.830	0.140	0.181	0.006	0.165
Z_91500_3	2	1.768	0.130	0.179	0.006	0.159
Z_91500_4	2	1.868	0.140	0.178	0.006	0.198
Z_91500_5	2	2.011	0.150	0.183	0.006	0.147
Z_91500_6	2	1.898	0.140	0.182	0.006	0.000

Appendix Table 8: Raw LA-ISP-MS data for all Titanite U-Pb Geochronology

Sample	Run Number	Final 207_235	Final 207_235 Prop2SE	Final 206_238	Final 206_238 Prop2SE	Error Correlation
G_NIST610_1	1	31.420	0.900	0.249	0.006	0.791
G_NIST610_2	1	31.290	0.900	0.246	0.006	0.901
G_NIST610_3	1	30.850	0.890	0.248	0.006	0.907
G_NIST610_4	1	30.920	0.890	0.248	0.006	0.898
G_NIST610_5	1	30.670	0.890	0.243	0.006	0.861
G_NIST610_6	1	30.660	0.880	0.244	0.006	0.864
G_NIST610_7	1	30.330	0.880	0.243	0.006	0.932
G_NIST610_8	1	30.200	0.870	0.243	0.006	0.894
G_NIST610_9	1	30.340	0.880	0.243	0.006	0.836
G_NIST610_10	1	30.400	0.880	0.245	0.006	0.753
G_NIST610_11	1	30.380	0.880	0.244	0.006	0.387
G_NIST610_12	1	30.470	0.880	0.242	0.006	0.763
KFP001_1	1	0.934	0.034	0.080	0.002	0.187
KFP001_2	1	1.690	0.120	0.087	0.002	0.487
KFP001_3	1	1.077	0.042	0.084	0.002	0.404
KFP001_4	1	1.530	0.170	0.088	0.003	0.834
KFP001_5	1	0.930	0.031	0.081	0.002	0.234
KFP001_6	1	3.272	0.130	0.104	0.003	0.590
KFP001_7	1	1.950	0.160	0.091	0.003	0.667
KFP001_8	1	3.410	0.200	0.105	0.003	0.796
KFP001_9	1	0.871	0.035	0.080	0.002	0.119
KFP001_10	1	5.140	0.390	0.122	0.005	0.921
KFP001_11	1	1.074	0.056	0.083	0.002	0.520
KFP001_12	1	0.724	0.024	0.079	0.002	0.181
KFP001_13	1	1.014	0.058	0.081	0.002	0.327
KFP001_14	1	1.277	0.061	0.085	0.002	0.353
KFP001_15	1	4.530	0.600	0.115	0.007	0.977
KFP001_16	1	1.464	0.064	0.086	0.002	0.109
KFP001_17	1	1.027	0.074	0.083	0.002	0.474
KFP001_18	1	1.466	0.068	0.088	0.002	0.559
KFP001_19	1	0.859	0.046	0.080	0.002	0.315
KFP001_20	1	1.400	0.110	0.085	0.003	0.731
KFP001_21	1	0.827	0.031	0.081	0.002	0.016
KFP001_22	1	3.175	0.120	0.103	0.003	0.476
KFP001_23	1	1.247	0.067	0.085	0.002	0.692
KFP001_24	1	0.991	0.054	0.079	0.002	0.043
KFP001_25	1	3.460	0.420	0.103	0.004	0.978
KFP001_26	1	1.970	0.270	0.090	0.003	0.926
KFP001_27	1	1.366	0.076	0.087	0.003	0.436
KFP001_28	1	1.178	0.059	0.084	0.002	0.098
KFP001_29	1	1.053	0.036	0.084	0.002	0.111
KFP001_30	1	0.911	0.042	0.081	0.002	0.280
KFP001_31	1	1.579	0.074	0.089	0.002	0.445
KFP001_32	1	2.030	0.170	0.093	0.003	0.862
KFP001_33	1	1.381	0.072	0.086	0.002	0.419
KFP001_34	1	1.180	0.054	0.085	0.003	0.059
KFP001_35	1	0.981	0.037	0.083	0.002	0.067
KFP001_36	1	1.092	0.076	0.083	0.002	0.665
KFP001_37	1	2.720	0.310	0.098	0.004	0.928
KFP001_38	1	1.438	0.072	0.085	0.002	0.345
KFP001_39	1	1.053	0.093	0.081	0.003	0.772
KFP001_40	1	2.470	0.340	0.096	0.004	0.956
KFP001_41	1	2.620	0.510	0.097	0.006	0.981
KFP001_42	1	1.290	0.094	0.085	0.002	0.726

KFP001_43	1	0.918	0.034	0.080	0.002	0.270
KFP001_44	1	1.580	0.110	0.086	0.003	0.848
KFP001_45	1	1.003	0.061	0.082	0.002	0.664
KP008_1	1	1.676	0.094	0.088	0.002	0.561
KP008_2	1	1.272	0.053	0.085	0.002	0.436
KP008_3	1	0.775	0.027	0.079	0.002	0.344
KP008_4	1	1.320	0.063	0.085	0.002	0.526
KP008_5	1	5.810	0.360	0.120	0.005	0.041
KP008_6	1	3.420	0.230	0.100	0.006	0.009
KP008_7	1	2.520	0.210	0.092	0.005	0.506
KP008_8	1	2.850	0.210	0.097	0.005	0.350
KP008_9	1	2.098	0.092	0.089	0.003	0.000
KP008_10	1	1.857	0.099	0.086	0.003	0.149
KP008_11	1	3.570	0.360	0.103	0.005	0.394
KP008_12	1	1.067	0.044	0.079	0.002	0.469
KP008_13	1	1.318	0.062	0.084	0.002	0.214
KP008_14	1	1.576	0.110	0.080	0.003	0.374
KP008_15	1	0.927	0.033	0.080	0.002	0.142
KP008_16	1	1.147	0.055	0.084	0.002	0.270
KP008_17	1	0.788	0.026	0.080	0.002	0.000
KP008_18	1	1.556	0.072	0.086	0.003	0.510
KP008_19	1	1.136	0.042	0.083	0.002	0.342
KP008_20	1	0.780	0.028	0.080	0.002	0.413
KP008_21	1	0.709	0.023	0.075	0.002	0.000
KP008_22	1	1.157	0.050	0.082	0.002	0.204
KP008_23	1	1.430	0.110	0.085	0.002	0.913
KP008_24	1	1.115	0.041	0.085	0.002	0.116
KP008_25	1	1.442	0.061	0.084	0.002	0.243
KP008_26	1	1.253	0.048	0.084	0.002	0.061
KP008_27	1	1.501	0.061	0.085	0.002	0.288
KP008_28	1	1.395	0.062	0.084	0.002	0.418
KP008_29	1	1.185	0.065	0.080	0.002	0.681
KP008_30	1	2.451	0.120	0.093	0.003	0.386
KP008_31	1	1.571	0.067	0.084	0.002	0.523
KP008_32	1	2.440	0.220	0.088	0.003	0.909
KP008_33	1	1.599	0.072	0.084	0.002	0.290
KP008_34	1	2.300	0.140	0.089	0.004	0.771
KP008_35	1	2.227	0.097	0.093	0.003	0.290
KP008_36	1	0.803	0.028	0.078	0.002	0.221
KP008_37	1	0.690	0.022	0.078	0.002	0.520
KP008_38	1	0.814	0.027	0.077	0.002	0.337
KP008_39	1	1.629	0.073	0.084	0.002	0.471
KP008_40	1	0.722	0.028	0.077	0.002	0.000
KP008_41	1	1.355	0.098	0.079	0.003	0.713
KP008_42	1	1.506	0.093	0.083	0.003	0.561
KP008_43	1	1.408	0.073	0.083	0.002	0.487
KP008_44	1	1.161	0.046	0.081	0.002	0.000
KP008_45	1	1.218	0.060	0.076	0.004	0.000
KP008_46	1	1.329	0.086	0.078	0.003	0.560
KP008_47	1	1.101	0.052	0.079	0.003	0.756
KP008_48	1	1.506	0.076	0.083	0.002	0.614
KP008_49	1	0.974	0.055	0.079	0.002	0.563
MtPainter_1	1	0.550	0.021	0.070	0.002	0.000
MtPainter_2	1	0.552	0.022	0.071	0.002	0.000
MtPainter_3	1	0.566	0.020	0.072	0.002	0.067
MtPainter_4	1	0.553	0.019	0.070	0.002	0.184
MtPainter_5	1	0.550	0.019	0.071	0.002	0.015
MtPainter_6	1	0.529	0.019	0.071	0.002	0.000
MtPainter_8	1	0.537	0.019	0.069	0.002	0.111
MtPainter_9	1	0.551	0.021	0.071	0.002	0.176
MtPainter_10	1	0.545	0.020	0.070	0.002	0.192
MtPainter_11	1	0.539	0.019	0.071	0.002	0.000
MtPainter_12	1	0.543	0.019	0.070	0.002	0.030
MtPainter_13	1	0.555	0.021	0.070	0.002	0.227
MtPainter_14	1	0.555	0.021	0.070	0.002	0.141
MtPainter_15	1	0.560	0.021	0.070	0.002	0.000
MtPainter_16	1	0.527	0.021	0.069	0.002	0.118
MtPainter_17	1	0.529	0.020	0.070	0.002	0.000
MtPainter_18	1	0.530	0.019	0.070	0.002	0.081

T_MKED1_1	1	3.457	0.100	0.263	0.006	0.319
T_MKED1_2	1	3.472	0.100	0.268	0.006	0.281
T_MKED1_3	1	3.504	0.100	0.265	0.006	0.139
T_MKED1_4	1	3.406	0.100	0.267	0.006	0.166
T_MKED1_5	1	3.428	0.100	0.263	0.006	0.072
T_MKED1_6	1	3.448	0.100	0.266	0.006	0.111
T_MKED1_7	1	3.434	0.100	0.263	0.006	0.207
T_MKED1_8	1	3.452	0.100	0.266	0.006	0.268
T_MKED1_9	1	3.522	0.100	0.269	0.006	0.246
T_MKED1_10	1	3.419	0.100	0.263	0.006	0.021
T_MKED1_11	1	3.613	0.110	0.272	0.007	0.290
T_MKED1_12	1	3.498	0.110	0.265	0.006	0.208
T_MKED1_13	1	3.469	0.110	0.266	0.006	0.299
T_MKED1_14	1	3.484	0.110	0.266	0.006	0.199
T_MKED1_15	1	3.448	0.100	0.265	0.006	0.278
T_MKED1_16	1	3.461	0.110	0.265	0.006	0.200
T_MKED1_17	1	3.438	0.100	0.264	0.006	0.378
T_MKED1_18	1	3.463	0.100	0.266	0.006	0.153
G_NIST610_1	2	30.490	0.990	0.248	0.004	0.860
G_NIST610_2	2	30.480	0.990	0.246	0.004	0.909
G_NIST610_3	2	30.540	0.990	0.248	0.004	0.926
G_NIST610_4	2	30.520	0.990	0.246	0.004	0.891
G_NIST610_5	2	30.590	0.990	0.246	0.004	0.846
G_NIST610_6	2	30.670	1.000	0.246	0.004	0.897
G_NIST610_7	2	30.870	1.000	0.246	0.004	0.815
G_NIST610_8	2	31.040	1.000	0.248	0.004	0.893
G_NIST610_9	2	30.720	1.000	0.246	0.004	0.901
G_NIST610_10	2	30.680	1.000	0.245	0.004	0.859
G_NIST610_11	2	30.200	0.990	0.243	0.004	0.860
G_NIST610_12	2	30.200	0.990	0.243	0.004	0.877
G_NIST610_13	2	30.210	0.990	0.244	0.004	0.835
G_NIST610_14	2	30.190	0.990	0.243	0.004	0.820
G_NIST610_15	2	30.320	0.990	0.247	0.004	0.452
G_NIST610_16	2	30.330	0.990	0.245	0.004	0.761
KP004_1	2	0.721	0.030	0.081	0.001	0.787
KP004_2	2	0.714	0.026	0.077	0.001	0.217
KP004_3	2	2.360	0.210	0.090	0.002	0.625
KP004_4	2	2.072	0.110	0.092	0.002	0.156
KP004_5	2	0.819	0.034	0.077	0.001	0.333
KP004_6	2	0.823	0.031	0.080	0.001	0.444
KP004_7	2	0.765	0.027	0.080	0.001	0.420
KP004_8	2	0.715	0.025	0.080	0.001	0.150
KP004_9	2	0.779	0.027	0.080	0.001	0.031
KP004_10	2	0.747	0.029	0.079	0.001	0.327
KP004_11	2	1.385	0.072	0.081	0.002	0.319
KP004_12	2	1.912	0.098	0.089	0.002	0.379
KP004_13	2	2.425	0.130	0.093	0.002	0.403
KP004_14	2	1.649	0.100	0.086	0.002	0.788
KP004_15	2	1.363	0.063	0.084	0.002	0.145
KP004_16	2	1.903	0.110	0.088	0.002	0.352
KP004_17	2	2.900	0.230	0.097	0.003	0.506
KP004_18	2	1.032	0.043	0.082	0.002	0.000
KP004_19	2	1.173	0.048	0.084	0.002	0.196
KP004_20	2	1.379	0.072	0.084	0.002	0.383
KP004_21	2	1.581	0.085	0.087	0.002	0.153
KP004_22	2	1.555	0.067	0.087	0.002	0.101
KP004_23	2	1.135	0.076	0.083	0.002	0.488
KP004_24	2	1.770	0.170	0.089	0.003	0.782
KP004_25	2	1.026	0.039	0.081	0.001	0.129
KP004_26	2	0.771	0.031	0.080	0.001	0.302
KP004_27	2	0.694	0.024	0.079	0.001	0.151
KP004_28	2	0.760	0.027	0.080	0.001	0.033
KP004_29	2	1.299	0.048	0.079	0.001	0.000
KP004_30	2	0.753	0.027	0.079	0.001	0.000
KP004_31	2	2.250	0.170	0.087	0.003	0.499
KP004_32	2	0.943	0.040	0.083	0.002	0.290
KP004_33	2	0.885	0.036	0.083	0.001	0.294
KP004_34	2	1.277	0.096	0.086	0.002	0.762
KP004_35	2	2.416	0.110	0.096	0.002	0.156

KP004_36	2	0.962	0.040	0.083	0.002	0.370
KP004_37	2	1.149	0.050	0.083	0.002	0.226
KP004_38	2	0.955	0.043	0.081	0.001	0.440
KP004_39	2	2.470	0.150	0.092	0.002	0.287
KP004_40	2	0.855	0.031	0.079	0.001	0.051
KP004_41	2	2.370	0.150	0.094	0.002	0.296
KP004_42	2	2.010	0.130	0.089	0.002	0.339
KP004_43	2	0.970	0.037	0.081	0.002	0.181
MtPainter_1	2	0.537	0.021	0.070	0.001	0.105
MtPainter_2	2	0.530	0.020	0.070	0.001	0.098
MtPainter_3	2	0.543	0.022	0.070	0.001	0.169
MtPainter_4	2	0.536	0.021	0.070	0.001	0.000
MtPainter_5	2	0.543	0.022	0.071	0.001	0.000
MtPainter_7	2	0.566	0.023	0.070	0.001	0.227
MtPainter_9	2	0.540	0.023	0.070	0.001	0.196
MtPainter_11	2	0.559	0.021	0.071	0.001	0.010
MtPainter_12	2	0.553	0.021	0.071	0.001	0.035
MtPainter_13	2	0.546	0.022	0.071	0.001	0.000
MtPainter_14	2	0.559	0.021	0.070	0.001	0.016
MtPainter_15	2	0.567	0.023	0.071	0.001	0.134
MtPainter_16	2	0.549	0.021	0.070	0.001	0.115
MtPainter_17	2	0.538	0.021	0.071	0.001	0.134
MtPainter_18	2	0.544	0.023	0.070	0.001	0.078
MtPainter_19	2	0.546	0.021	0.071	0.001	0.101
MtPainter_20	2	0.553	0.023	0.071	0.001	0.374
MtPainter_23	2	0.549	0.021	0.072	0.001	0.204
T_MKED1_1	2	3.455	0.120	0.264	0.004	0.330
T_MKED1_2	2	3.456	0.110	0.266	0.004	0.080
T_MKED1_3	2	3.467	0.110	0.267	0.004	0.336
T_MKED1_4	2	3.419	0.110	0.261	0.004	0.312
T_MKED1_5	2	3.502	0.120	0.268	0.004	0.347
T_MKED1_6	2	3.503	0.120	0.269	0.004	0.056
T_MKED1_7	2	3.501	0.120	0.266	0.004	0.019
T_MKED1_8	2	3.439	0.120	0.266	0.004	0.168
T_MKED1_9	2	3.420	0.110	0.263	0.004	0.149
T_MKED1_10	2	3.433	0.110	0.264	0.004	0.037
T_MKED1_11	2	3.473	0.120	0.266	0.004	0.160
T_MKED1_12	2	3.481	0.120	0.264	0.004	0.549
T_MKED1_13	2	3.469	0.120	0.263	0.004	0.248
T_MKED1_14	2	3.444	0.120	0.266	0.004	0.060
T_MKED1_15	2	3.427	0.110	0.265	0.004	0.048
T_MKED1_16	2	3.478	0.120	0.266	0.004	0.362
T_MKED1_17	2	3.658	0.150	0.267	0.004	0.907
T_MKED1_18	2	3.560	0.120	0.267	0.004	0.512
T_MKED1_19	2	3.430	0.110	0.267	0.004	0.284
T_MKED1_20	2	3.423	0.110	0.266	0.004	0.183
T_MKED1_21	2	3.515	0.120	0.265	0.004	0.269
T_MKED1_22	2	3.509	0.120	0.268	0.004	0.214
T_MKED1_23	2	3.431	0.120	0.264	0.004	0.000
T_MKED1_24	2	3.444	0.120	0.263	0.004	0.288
X2721785_1	2	70.800	3.000	0.687	0.020	0.593
X2721785_2	2	48.940	1.800	0.495	0.012	0.500
X2721785_3	2	122.300	5.100	1.140	0.036	0.598
X2721785_4	2	51.800	2.100	0.528	0.016	0.449
X2721785_5	2	37.960	1.500	0.404	0.011	0.432
X2721785_6	2	10.990	0.470	0.176	0.004	0.172
X2721785_7	2	50.700	2.400	0.512	0.015	0.732
X2721785_8	2	37.900	2.000	0.414	0.017	0.825
X2721785_9	2	95.000	3.700	0.903	0.028	0.454
X2721785_10	2	113.300	4.400	1.038	0.028	0.561
X2721785_11	2	117.200	4.500	1.044	0.029	0.508
X2721785_12	2	110.600	4.300	1.067	0.034	0.503
X2721785_13	2	114.700	5.100	1.063	0.042	0.690
X2721785_14	2	113.500	5.200	1.056	0.039	0.660
X2721785_15	2	112.300	4.700	1.047	0.035	0.604
X2721785_16	2	86.800	3.400	0.819	0.024	0.449
X2721785_17	2	54.800	2.400	0.538	0.015	0.547
X2721785_18	2	53.700	5.500	0.536	0.045	0.953
X2721785_19	2	13.430	0.540	0.194	0.007	0.528

X2721785_20	2	17.320	0.820	0.225	0.006	0.425
X2721785_21	2	87.500	4.100	0.816	0.028	0.708
X2721785_22	2	57.000	2.700	0.571	0.023	0.599
X2721785_23	2	112.200	5.200	1.021	0.038	0.584
X2721785_24	2	108.100	4.800	1.000	0.034	0.589
X2721785_25	2	113.900	5.400	1.048	0.035	0.588
X2721785_26	2	130.600	5.000	1.194	0.034	0.620
X2721785_27	2	112.900	5.200	1.075	0.042	0.686
X2721785_28	2	101.200	4.400	0.927	0.032	0.586
X2721785_29	2	109.500	5.000	1.015	0.041	0.660
X2721785_30	2	86.100	3.600	0.829	0.029	0.636
X2721785_31	2	112.400	4.100	1.048	0.026	0.478
X2721785_32	2	85.600	3.500	0.816	0.028	0.752
X2721785_33	2	51.300	4.100	0.531	0.039	0.889
X2721785_34	2	120.400	5.100	1.121	0.034	0.453
X2721785_35	2	19.400	0.970	0.254	0.011	0.478
X2721785_36	2	23.700	1.200	0.277	0.010	0.644
X2721785_37	2	94.400	4.100	0.887	0.032	0.535
X2721786_1	2	23.100	1.400	0.279	0.011	0.820
X2721786_2	2	42.300	2.100	0.454	0.019	0.695
X2721786_3	2	38.600	1.700	0.416	0.013	0.579
X2721786_4	2	32.650	1.400	0.364	0.012	0.516
X2721786_5	2	30.680	1.200	0.338	0.008	0.502
X2721786_6	2	38.300	1.400	0.401	0.012	0.421
X2721786_7	2	20.520	0.830	0.253	0.007	0.369
X2721786_8	2	36.900	1.800	0.390	0.016	0.585
X2721786_9	2	27.230	1.300	0.308	0.012	0.550
X2721786_10	2	20.100	0.770	0.255	0.006	0.342
X2721786_11	2	30.530	1.200	0.345	0.008	0.356
X2721786_12	2	34.510	1.300	0.372	0.010	0.443
X2721786_13	2	21.500	1.300	0.274	0.013	0.767
X2721786_14	2	38.390	1.400	0.410	0.009	0.359
X2721786_15	2	37.500	1.500	0.383	0.011	0.419
X2721786_16	2	43.900	1.700	0.463	0.011	0.452
X2721786_17	2	48.650	1.800	0.499	0.013	0.545
X2721786_18	2	41.800	1.800	0.441	0.014	0.802
X2721786_19	2	38.500	1.600	0.418	0.013	0.782
X2721786_20	2	37.590	1.400	0.408	0.011	0.381
X2721786_21	2	32.700	1.500	0.364	0.012	0.763
X2721786_22	2	34.000	1.800	0.375	0.014	0.801
X2721786_23	2	28.340	1.200	0.326	0.009	0.566
X2721786_24	2	29.990	1.300	0.331	0.010	0.639
X2721786_25	2	18.740	0.910	0.236	0.008	0.680
X2721786_26	2	39.500	1.700	0.419	0.012	0.689
X2721786_27	2	25.980	1.300	0.294	0.011	0.578
X2721786_28	2	43.000	2.100	0.450	0.017	0.738
X2721786_29	2	29.620	1.200	0.342	0.009	0.571
X2721786_30	2	20.970	0.790	0.260	0.006	0.101

APPENDIX E: TRACE ELEMENT ANALYSIS EXTENDED METHODS

Appendix Table 9: Monazite trace element analysis parameters

Instrument	Agilent 7900x with attached RESOlution LR 193 nm Excimer laser system
Location	The University of Adelaide, Adelaide Microscopy
Fluence	Monazite 2.0 J/cm^2
Spot Size	Monazite 13 µm
Monazite Standards	NIST 610
Iolite	DRS: Trace_Element_IS Default Index Content in Sample: 20% Ce

Appendix Table 10: Trace element spot analysis parameters utilised for quantitative pyrite ablation sections

Instrument	Agilent 7900x with attached RESOlution LR 193 nm Excimer laser system
Location	The University of Adelaide, Adelaide Microscopy
Fluence	Pyrite 4.0 J/cm^2
Spot Size	Pyrite 30 µm
Energy	35%
Rate	5 Hz
Pyrite Standards: Spot size: 70 µm Energy: 35% Rate: 10 Hz Fluence: 4.0 J/cm^2	Primary: STDGL3 Secondary: GSD-1G
Iolite	DRS: Trace_Element_IS Default Index Content in Sample: 46.5%

Appendix Table 11: Trace element mapping parameters utilised for semi-quantitative pyrite grain mapping

Instrument	Agilent 7900x with attached RESOlution LR 193 nm Excimer laser system
Location	The University of Adelaide, Adelaide Microscopy
Fluence	Pyrite 4.0 J/cm^2
Spot Size	Pyrite 15 µm
Speed	15 µm/s ablation 30 µm/s pre-ablation
Energy	35%
Rate	10 Hz
Pyrite Standards: Spot size: 70 µm Energy: 35% Rate: 10 Hz Fluence: 4.0 J/cm^2	Primary: STDGL3 Secondary: GSD-1G

Pyrite trace element quantitative plotting from ablation transects from multiple pyrite grains from within two samples.

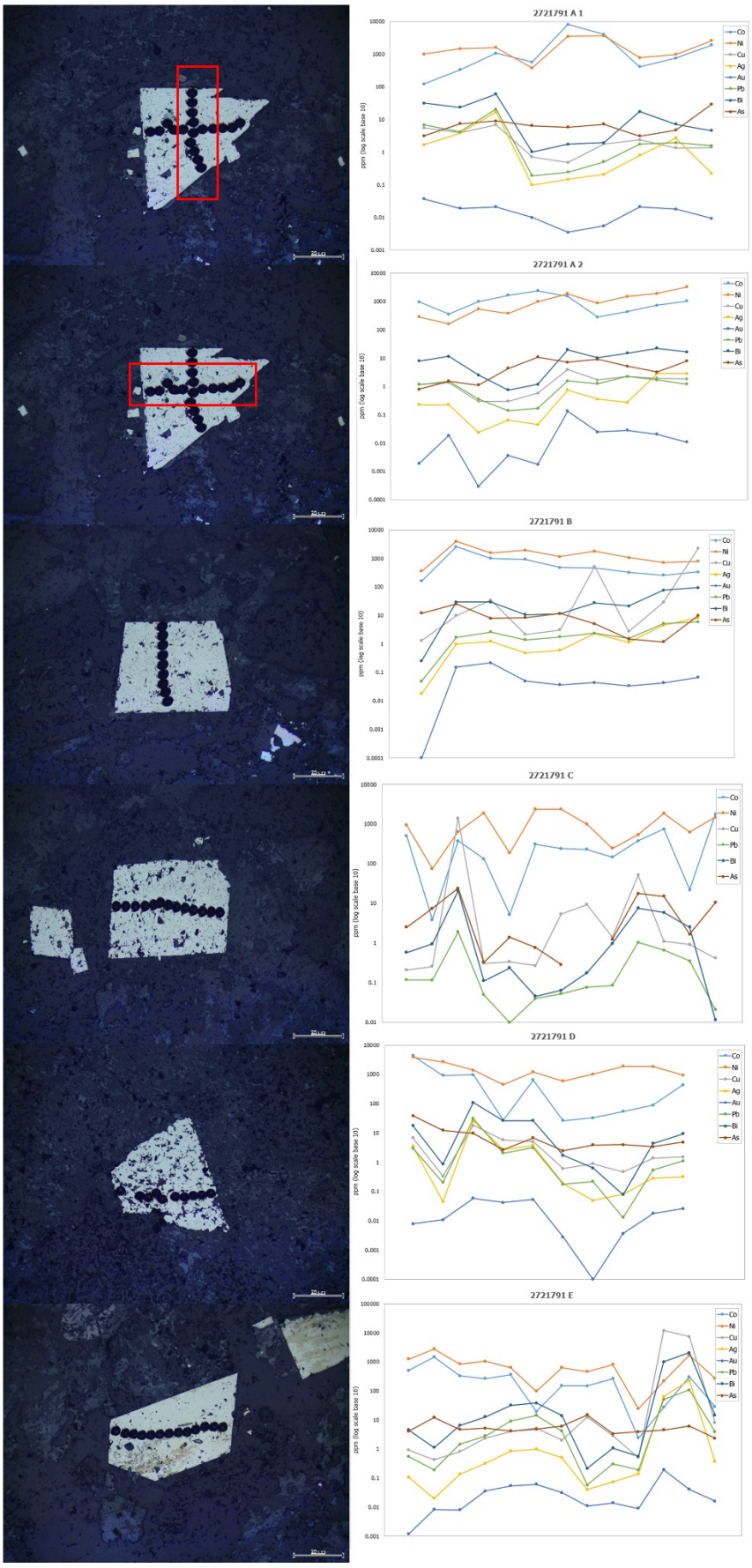
2721791 A 1
2721791 A 2
2721791 B
2721791 C
2721791 D
2721791 E
Co
Ni
Cu
Ag
Au
Pb
Bi
As
ppm (log scale base 10)

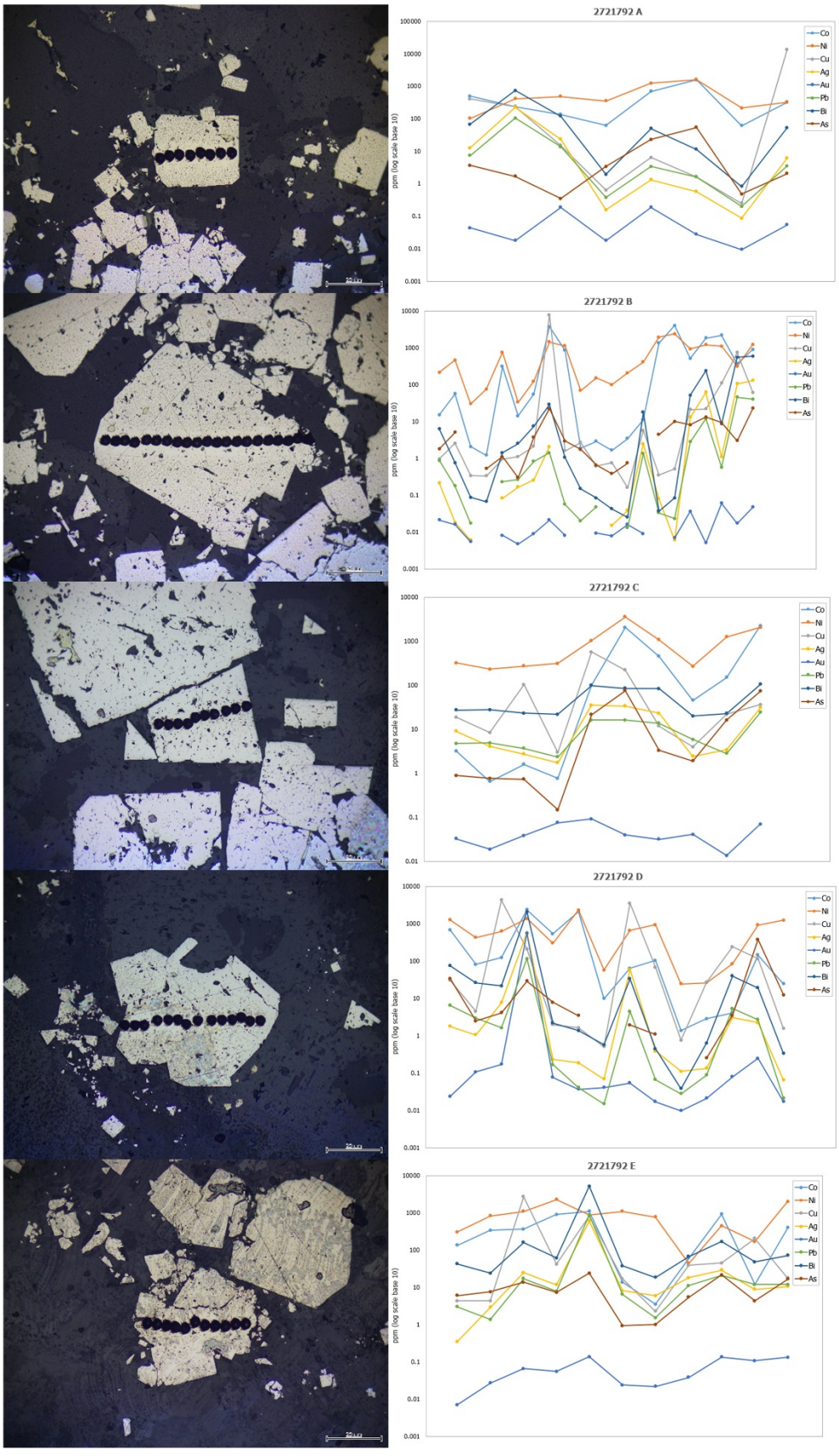
2721792 A
2721792 B
2721792 C
2721792 D
2721792 E
ppm (log scale base 10)
Co
Ni
Cu
Ag
Au
Pb
Bi
As

Sample 2721791-1
As, Sb, Se, Te not displayed due to no visible abundance
Diagram units counts per area.

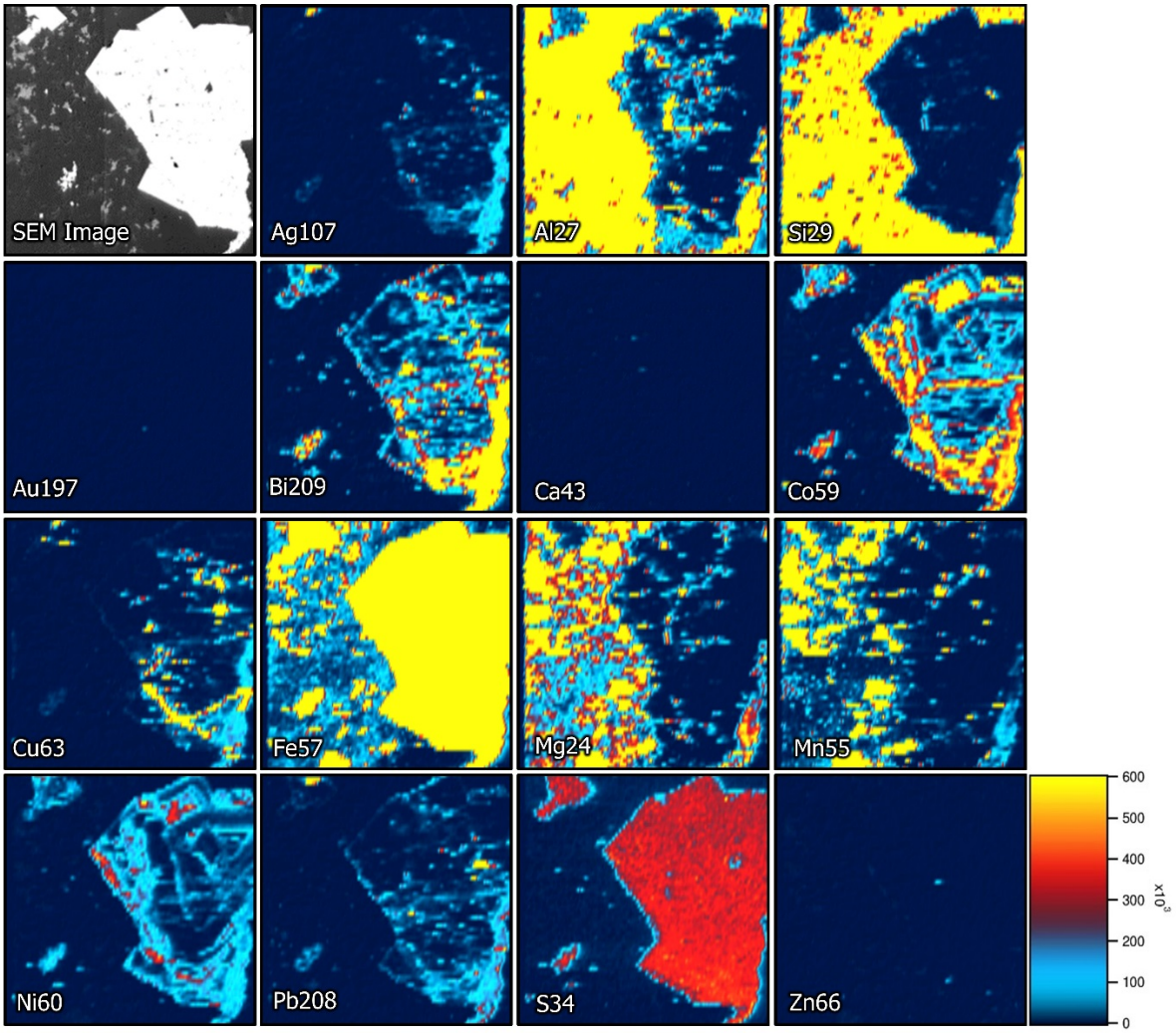

Sample 2721791-2
As, Sb, Se, Te not displayed due to no visible abundance
Diagram units counts per area.

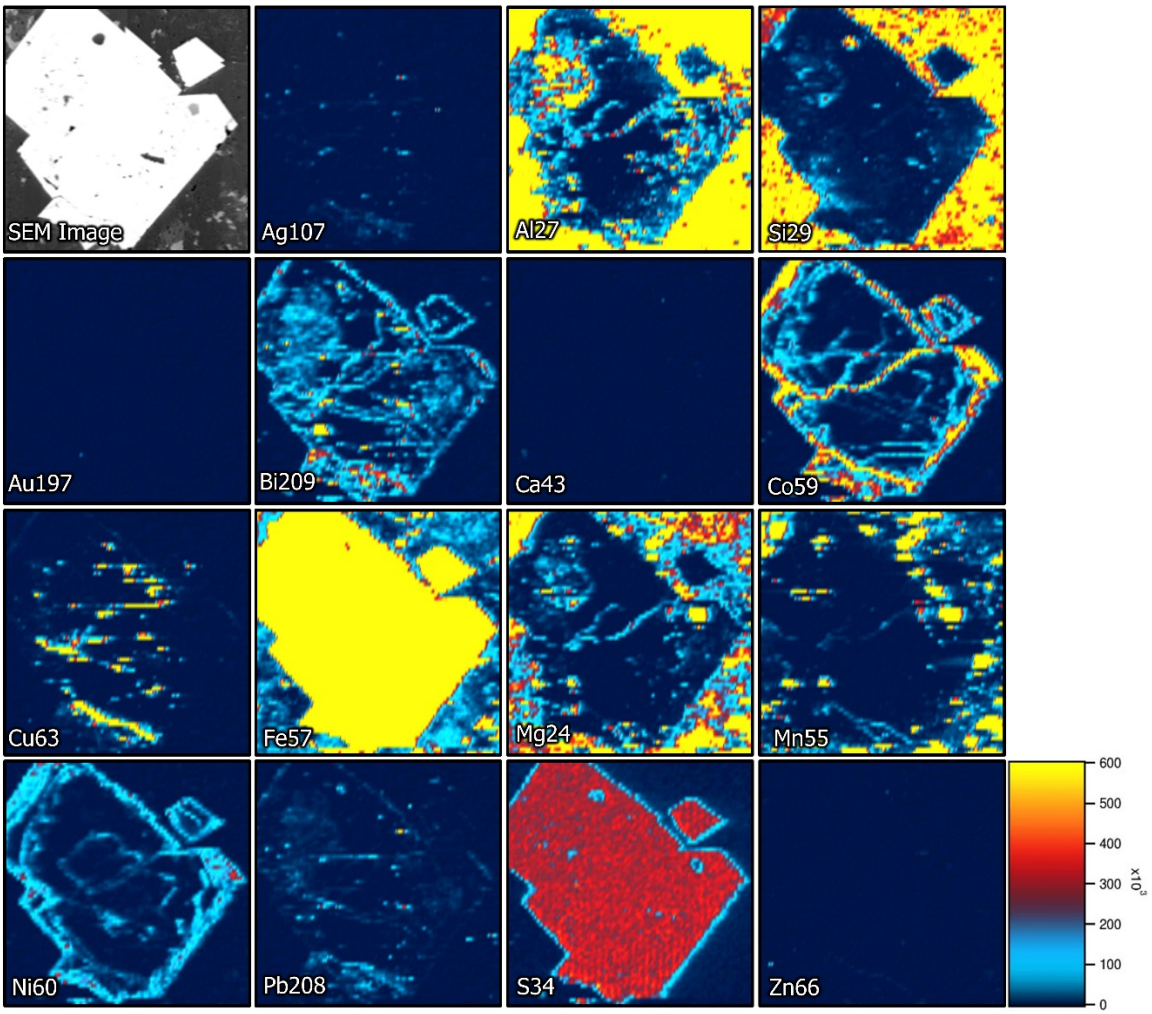

Sample 2721791-2
As, Sb, Se, Te not displayed due to no visible abundance
Diagram units ppm.

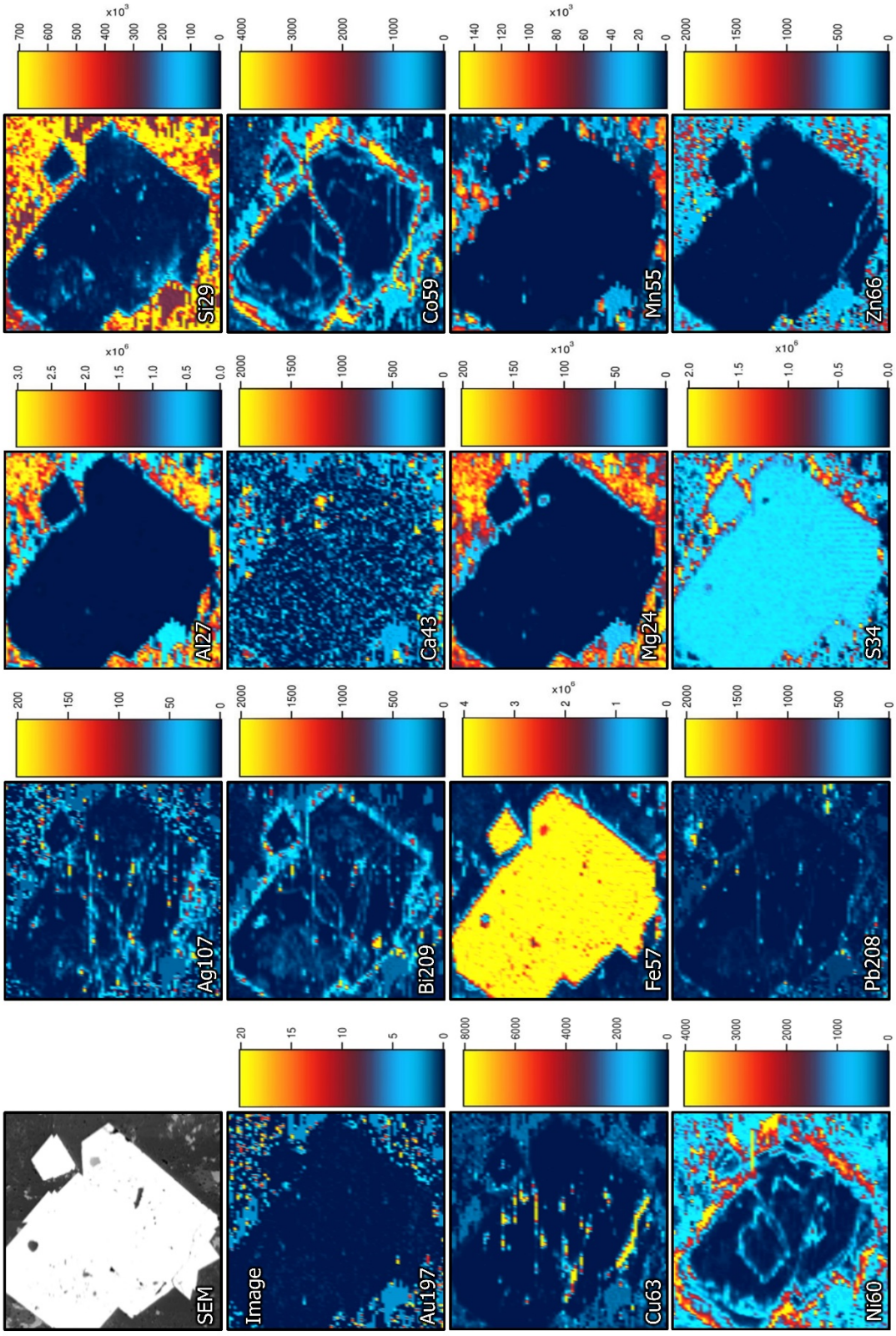

Sample 2721792-1
Ca, Sb, Se, Te not displayed due to no visible abundance
Diagram units counts per area.

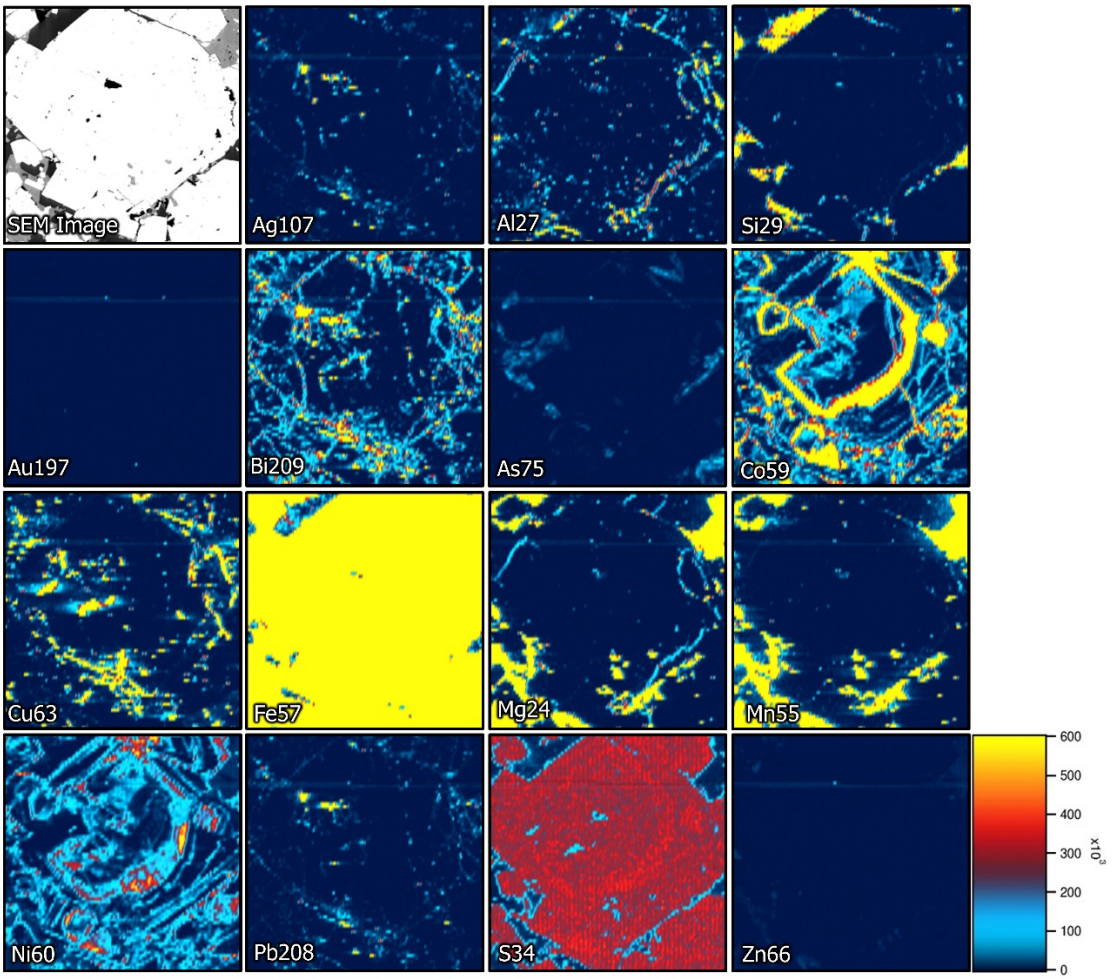

Sample 2721792-2
Ca Sb, Se, Te not displayed due to no visible abundance
Diagram units counts per area.

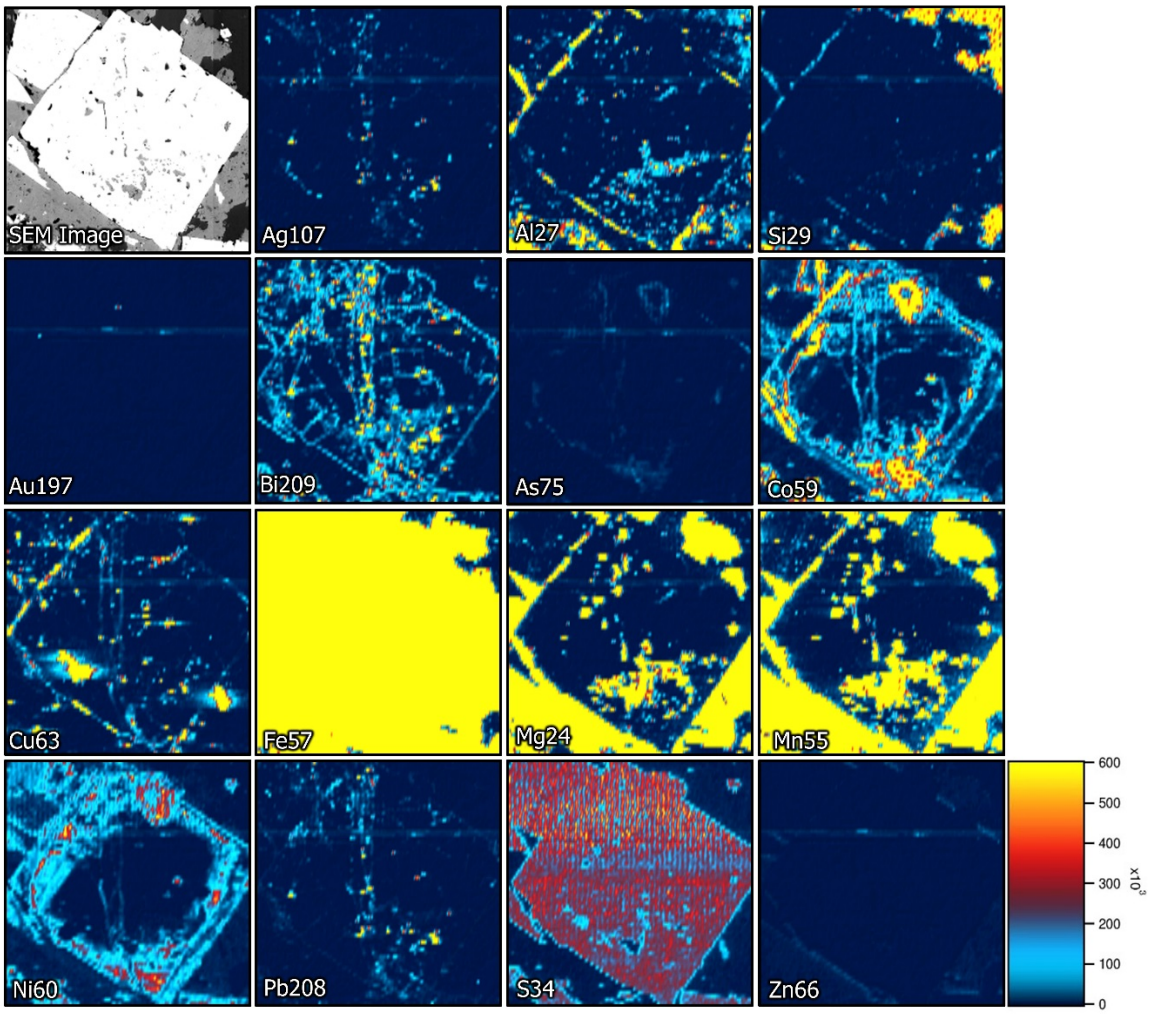

Sample 2721792-3
Ca, Sb, Se, Te not displayed due to no visible abundance
Diagram units counts per area.

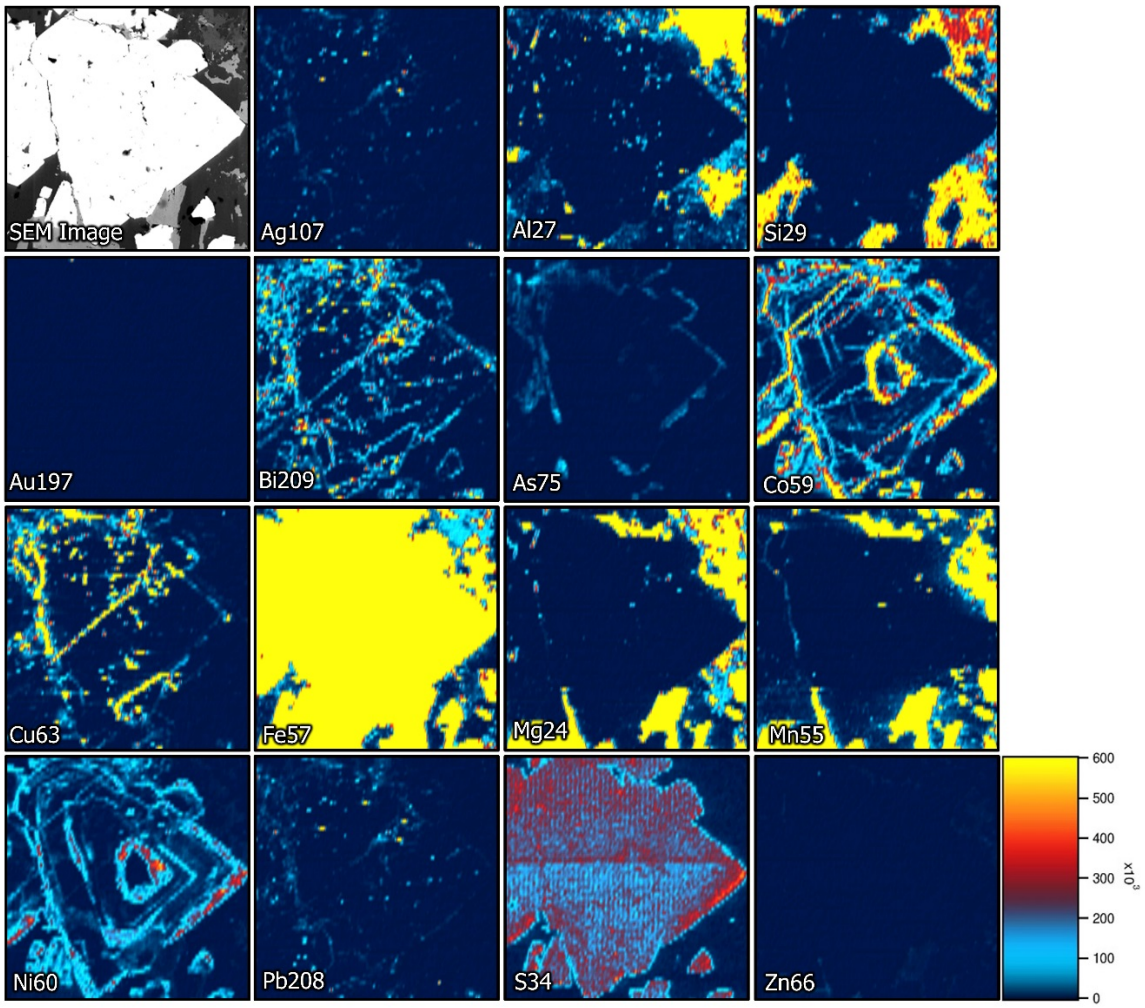

Appendix Table 12: Raw Trace Element data for quantitative pyrite ablation sections. Ablation number 1 representing diagram location A, increasing in ablation number to diagram location B.

Sample/Standard	Co (ppm)	Ni (ppm)	Cu (ppm)	As (ppm)	Au (ppm)	Pb (ppm)	Bi (ppm)
GSD-1G	43.960	64.300	45.900	37.700	5.550	56.800	40.300
GSD-1G	43.600	63.500	46.300	38.400	5.540	56.700	39.400
GSD-1G	44.580	64.400	45.800	37.000	5.350	57.400	40.070
GSD-1G	45.400	66.900	53.500	37.800	5.640	57.900	41.830
GSD-1G	46.090	68.700	56.900	37.800	5.390	57.600	42.300
GSD-1G	45.800	67.100	50.100	36.700	5.470	58.000	41.990
GSD-1G	44.280	64.800	47.500	36.800	5.220	58.000	41.470
GSD-1G	46.110	67.400	53.600	40.000	5.630	59.700	43.430
GSD-1G	45.770	65.000	52.300	39.900	5.570	60.300	43.320
GSD-1G	47.030	69.000	50.900	40.000	5.450	59.000	43.800
GSD-1G	46.560	68.900	50.700	38.000	5.290	58.900	42.860
GSD-1G	46.290	67.900	48.300	39.000	5.280	58.000	42.300
GSD-1G	45.500	65.900	45.200	36.600	5.050	57.300	42.520
GSD-1G	44.340	63.000	50.200	36.100	4.860	57.400	41.500
GSD-1G	43.800	64.100	51.500	36.000	4.740	58.200	40.200
2721791 A1	124.000	1001.000	5.550	3.140	0.037	6.740	31.800
2721791 A1	333.000	1470.000	3.850	7.380	0.019	4.180	23.600
2721791 A1	1070.000	1603.000	6.900	8.900	0.021	20.900	60.000
2721791 A1	577.000	374.000	0.720	6.460	0.010	0.190	1.010
2721791 A1	8070.000	3510.000	0.480	5.840	0.004	0.240	1.750
2721791 A1	4070.000	3630.000	1.760	7.100	0.006	0.500	1.920
2721791 A1	409.000	780.000	2.400	3.120	0.021	1.730	17.300
2721791 A1	760.000	980.000	1.350	4.690	0.018	1.920	7.200
2721791 A1	1900.000	2590.000	1.380	29.500	0.009	1.560	4.520
2721791 A1	978.000	290.000	1.190	0.810	0.002	1.170	7.900
2721791 A2	357.000	163.000	1.390	1.540	0.019	1.520	11.700
2721791 A2	989.000	552.000	0.300	1.120	0.000	0.364	2.570
2721791 A2	1660.000	384.000	0.300	4.380	0.004	0.143	0.750
2721791 A2	2390.000	992.000	0.590	10.900	0.002	0.171	1.210
2721791 A2	1560.000	1880.000	4.000	7.260	0.135	1.590	19.800
2721791 A2	282.000	883.000	1.720	9.100	0.025	1.270	10.300
2721791 A2	442.000	1500.000	2.270	5.280	0.029	2.250	15.200
2721791 A2	740.000	1910.000	1.990	3.220	0.021	1.710	22.500
2721791 A2	1030.000	3300.000	1.850	8.000	0.011	1.230	16.700
2721791 B	160.000	356.000	1.320	12.000	0.000	0.050	0.254
2721791 B	2560.000	4010.000	9.800	25.000	0.153	1.710	29.600
2721791 B	1016.000	1578.000	35.000	7.900	0.220	2.620	29.800
2721791 B	936.000	1970.000	2.150	8.500	0.050	1.400	10.700
2721791 B	487.000	1167.000	3.080	11.800	0.037	1.790	11.600
2721791 B	475.000	1820.000	520.000	5.070	0.044	2.390	27.700
2721791 B	321.000	1075.000	2.780	1.480	0.034	1.560	21.400
2721791 B	262.000	719.000	29.000	1.200	0.043	5.230	77.400
2721791 B	335.000	803.000	2240.000	9.900	0.067	6.000	94.000
2721791 C	512.000	945.000	0.210	2.540	0.008	0.120	0.580
2721791 C	3.910	76.000	0.260	7.490	0.005	0.117	0.950
2721791 C	382.000	653.000	1410.000	24.300	0.115	1.940	21.000
2721791 C	133.400	1900.000	0.310	0.330	0.006	0.050	0.112
2721791 C	5.250	188.000	0.340	1.400	0.000	0.010	0.238
2721791 C	312.000	2380.000	0.270	0.770	0.004	0.040	0.046
2721791 C	243.000	2400.000	5.400	0.290	0.003	0.053	0.065
2721791 C	232.000	998.000	9.400	-0.001	0.020	0.077	0.179
2721791 C	149.000	245.000	1.420	1.260	0.007	0.086	0.980
2721791 C	381.000	547.000	52.000	17.900	0.035	1.040	7.700
2721791 C	756.000	1880.000	1.110	15.200	0.001	0.666	5.960
2721791 C	22.000	630.000	0.930	1.680	0.000	0.356	2.540
2721791 C	1800.000	1509.000	0.420	10.600	0.003	0.021	0.012
2721791 D	4430.000	3930.000	6.900	39.200	0.008	3.000	17.900
2721791 D	929.000	2740.000	0.340	12.400	0.011	0.206	0.860
2721791 D	990.000	1420.000	18.300	9.800	0.059	31.000	110.000
2721791 D	27.200	451.000	5.850	2.690	0.042	2.090	26.800
2721791 D	643.000	1220.000	5.100	6.910	0.054	3.140	26.600
2721791 D	26.600	597.000	0.620	2.500	0.003	0.178	1.750
2721791 D	32.900	1023.000	0.900	3.900	0.000	0.220	0.640
2721791 D	55.000	1890.000	0.470	4.000	0.004	0.013	0.078

2721791 D	90.000	1870.000	1.390	3.420	0.018	0.541	4.400
2721791 D	447.000	940.000	1.540	4.900	0.026	1.110	9.400
2721791 E	521.000	1270.000	0.930	4.100	0.001	0.550	4.560
2721791 E	1500.000	2800.000	0.430	12.300	0.008	0.192	1.120
2721791 E	335.000	846.000	0.820	4.800	0.008	1.470	6.550
2721791 E	265.000	1069.000	2.350	5.300	0.036	2.830	12.900
2721791 E	365.000	644.000	4.090	4.240	0.055	9.110	32.500
2721791 E	19.600	98.000	5.230	4.840	0.062	14.600	38.400
2721791 E	154.000	638.000	2.010	6.200	0.032	4.200	14.100
2721791 E	151.000	466.000	12.600	15.000	0.011	0.058	0.214
2721791 E	265.000	810.000	2.900	3.400	0.014	0.310	1.090
2721791 E	2.400	24.300	0.510	3.980	0.009	0.191	0.560
2721791 E	27.400	221.000	12100.000	4.600	0.194	51.000	1010.000
2721791 E	307.000	1700.000	7500.000	6.220	0.041	108.000	2100.000
2721791 E	29.400	273.000	8.200	2.350	0.016	3.990	14.800
2721792 A	494.000	104.000	410.000	3.700	0.044	7.400	68.000
2721792 A	237.000	415.000	240.000	1.690	0.018	105.000	740.000
2721792 A	135.000	485.000	15.100	0.350	0.187	13.600	121.300
2721792 A	63.000	356.000	0.630	3.400	0.018	0.380	1.960
2721792 A	700.000	1250.000	6.470	23.300	0.190	3.420	50.700
2721792 A	1600.000	1610.000	1.610	54.600	0.028	1.610	11.500
2721792 A	60.800	214.100	0.250	0.480	0.010	0.200	0.820
2721792 A	325.000	319.000	13600.000	2.080	0.055	3.510	53.100
2721792 B	15.200	216.000	0.960	1.800	0.021	0.860	6.200
2721792 B	56.600	468.000	2.570	5.100	0.016	0.176	0.760
2721792 B	2.070	29.800	0.340		0.005	0.017	0.087
2721792 B	1.210	76.100	0.330	0.520	-0.001	-0.014	0.067
2721792 B	309.000	759.000	0.940	1.100	0.008	0.230	1.410
2721792 B	14.100	33.300	1.100	0.300	0.005	0.267	2.510
2721792 B	55.000	124.000	2.120	3.700	0.009	0.820	7.400
2721792 B	3800.000	1454.000	7900.000	22.300	0.021	1.410	29.000
2721792 B	861.000	1131.000	1.590	2.950	0.008	0.056	1.060
2721792 B	1.880	69.900	2.700	1.750	-0.001	0.020	0.150
2721792 B	2.890	151.000	0.610	0.660	0.009	0.048	0.084
2721792 B	1.660	100.000	0.750	0.380	0.008	-0.005	0.042
2721792 B	3.460	207.000	0.160	0.740	0.016	0.013	0.025
2721792 B	11.030	415.000	5.760		0.009	1.360	17.790
2721792 B	1359.000	1932.000	0.350	4.400	-0.001	0.033	0.037
2721792 B	4060.000	2390.000	0.510	10.000	0.007	0.023	0.083
2721792 B	519.000	940.000	21.000	8.100	0.036	2.800	52.000
2721792 B	1840.000	1213.000	22.100	13.100	0.005	12.000	241.000
2721792 B	2210.000	1120.000	109.000	9.400	0.060	0.570	8.500
2721792 B	369.000	318.000	740.000	3.000	0.017	45.300	557.000
2721792 B	904.000	1230.000	61.000	22.900	0.047	40.300	594.000
2721792 C	3.250	328.000	19.000	0.900	0.033	4.800	27.700
2721792 C	0.660	235.000	8.500	0.770	0.019	4.920	28.100
2721792 C	1.610	277.000	104.000	0.740	0.039	3.740	23.600
2721792 C	0.770	318.000	3.000	0.150	0.076	2.390	22.100
2721792 C	101.700	1050.000	580.000	21.800	0.093	16.300	100.000
2721792 C	2100.000	3620.000	224.000	76.400	0.040	16.400	86.000
2721792 C	463.000	1100.000	12.000	3.360	0.032	13.800	85.000
2721792 C	45.700	272.000	4.010	1.930	0.041	5.880	20.200
2721792 C	153.000	1270.000	22.200	16.500	0.014	2.860	23.000
2721792 C	2290.000	2090.000	37.000	74.100	0.071	24.500	107.000
2721792 D	677.000	1253.000	30.300	33.300	0.024	6.470	75.100
2721792 D	82.100	426.000	4.500	2.500	0.108	2.930	26.000
2721792 D	124.000	630.000	4300.000	4.100	0.172	1.640	21.600
2721792 D	2370.000	1372.000	210.000	29.300	560.000	115.000	2100.000
2721792 D	540.000	302.000	1.980	7.800	0.077	0.168	2.190
2721792 D	2147.000	2316.000	1.640	3.440	0.037	0.041	1.370
2721792 D	9.770	57.600	0.510		0.041	0.015	0.571
2721792 D	64.000	664.000	3520.000	1.960	0.054	4.490	33.600
2721792 D	104.000	930.000	69.000	1.100	0.017	0.067	0.449
2721792 D	1.370	24.300	0.760		0.010	0.028	0.038
2721792 D	2.870	26.100	27.000	0.250	0.021	0.089	0.640
2721792 D	4.080	84.500	240.000	3.500	0.079	5.300	40.000
2721792 D	146.000	916.000	115.000	376.000	0.249	2.710	19.000
2721792 D	24.600	1250.000	1.540	12.300	0.017	0.021	0.334
2721792 E	134.000	307.000	4.300	6.000	0.007	2.980	42.600

2721792 E	342.000	823.000	4.320	7.600	0.027	1.370	24.000
2721792 E	364.000	1103.000	2710.000	13.600	0.066	17.100	161.600
2721792 E	910.000	2300.000	42.000	7.300	0.055	7.900	62.000
2721792 E	1100.000	880.000	810.000	24.200	0.137	880.000	5200.000
2721792 E	13.800	1093.000	16.800	0.930	0.024	6.510	37.800
2721792 E	3.510	776.000	2.270	1.000	0.022	1.510	18.600
2721792 E	61.000	44.400	39.000	5.400	0.038	11.200	67.700
2721792 E	915.000	454.000	45.200	21.700	0.134	20.700	168.100
2721792 E	12.000	171.000	205.000	4.300	0.107	12.000	48.100
2721792 E	396.000	2036.000	17.800	16.500	0.132	11.900	72.400
STD-GL3	74.900	241.000	357.000	351.000	20.000	62.900	19.500
STD-GL4	77.900	244.000	365.000	362.000	19.900	61.000	19.600
STD-GL5	76.100	243.000	363.000	355.000	19.560	59.000	19.360
STD-GL6	74.200	243.000	360.000	356.000	19.300	59.200	19.080
STD-GL7	74.400	242.000	361.000	350.000	19.800	61.500	19.360
STD-GL8	78.800	244.000	361.000	367.000	20.700	60.900	19.710
STD-GL9	74.500	239.000	362.000	352.000	18.890	60.000	18.640
STD-GL10	76.800	247.000	360.000	359.000	20.700	62.600	20.300
STD-GL11	77.300	251.000	364.000	358.000	20.300	63.900	19.800
STD-GL12	75.800	235.000	358.000	353.000	19.700	58.900	19.200
STD-GL13	76.200	246.000	362.000	363.000	19.500	61.300	19.600
STD-GL14	74.400	241.000	360.000	352.000	19.400	57.800	18.900
STD-GL15	77.100	250.000	365.000	351.000	19.430	62.200	20.100
STD-GL16	76.000	237.000	357.000	361.000	20.500	62.600	19.210

Appendix Table 13: Raw monazite trace element data utilised in comparison between Kimpton (2019) Kanmantoo hydrothermal monazites

Sample	Sm	Gd	Lu	Eu	Th	U	Y2O3 wt%	LREE (apfu)	HREE (apfu)
KP001_1	10098.005	5611.392	6.361	409.919	55863.965	893.573	0.638	0.820	0.004
KP001_2	7864.316	4275.584	5.617	549.481	58982.370	1053.257	0.440	0.820	0.003
KP001_3	10563.415	6711.160	17.323	816.484	48698.313	1998.811	1.103	0.790	0.007
KP001_4	10380.382	7592.954	52.181	615.464	72919.117	3824.351	2.199	0.773	0.011
KP001_5	9869.117	6603.337	25.361	435.437	65435.240	5131.941	1.331	0.778	0.008
KP001_6	8958.929	5907.226	29.972	380.373	88281.422	3367.773	1.111	0.725	0.007
KP001_7	9319.535	5611.763	15.157	415.872	63883.910	3394.616	0.784	0.798	0.005
KP001_8	8816.142	5691.052	28.641	372.830	76445.235	8305.734	1.237	0.767	0.007
KP001_9	8891.143	5806.922	38.412	318.364	77162.017	11851.092	1.577	0.760	0.008
KP001_10	7560.522	4294.895	12.836	486.841	87146.202	1848.913	0.692	0.810	0.004
KP001_11	7571.310	4676.589	23.388	338.207	115201.402	5265.107	1.031	0.760	0.006
KP001_12	7513.630	4234.025	11.675	480.619	75598.902	2069.535	0.714	0.815	0.004
KP001_13	7721.743	4385.950	8.401	439.830	74622.924	1512.226	0.635	0.819	0.004
KP001_14	7790.568	4671.951	10.013	409.483	86030.811	2640.668	0.659	0.807	0.004
KP001_15	9734.881	5973.272	11.975	488.653	53395.505	1664.474	0.963	0.817	0.006
KP001_16	12989.575	7708.702	2.236	2108.234	11082.974	193.266	0.716	0.879	0.006

Appendix Table 14: Kanappa drilling project geochemistry data utilised within fertility studies

Sample	SiO2 (wt%)	Sr (ppm)	Y (ppm)	V (ppm)	Sc (ppm)
KNP199	62.7	626.0	14.7	98.0	8.0
KNP200	64.0	635.0	15.3	97.0	8.5
KNP201	59.1	689.0	15.8	113.0	8.8
KNP202	65.7	572.0	18.5	91.0	8.2
KNP203	61.0	693.0	15.5	100.0	8.4
KNP204	59.7	720.0	17.6	95.0	8.8
KNP205	63.0	695.0	12.3	87.0	6.5
KNP206	58.3	860.0	17.7	110.0	8.4
KNP207	56.5	855.0	19.9	123.0	10.1
KNP208	56.9	923.0	19.1	118.0	9.3
KNP209	63.2	595.0	18.2	83.0	8.7
KNP211	63.9	156.5	14.1	91.0	12.7
KNP212	67.2	60.6	15.7	81.0	12.3
KNP213	63.4	69.3	15.8	101.0	14.1
KNP214	59.6	618.0	17.7	112.0	9.6
KNP215	58.9	739.0	17.5	122.0	8.8
KNP216	60.6	574.0	18.1	97.0	7.7
KNP432	36.7	724.0	17.7	35.0	5.7
KNP433	69.3	500.0	24.3	53.0	7.1
KNP434	68.5	531.0	18.9	46.0	6.0
KNP435	68.2	494.0	18.0	42.0	5.8
KNP436	68.6	537.0	19.6	43.0	6.3
KNP461	57.1	1090.0	151.0	18.8	13.2
KNP462	55.5	1005.0	151.0	20.6	13.3
KNP463	60.2	733.0	125.0	18.5	11.1
KNP464	59.9	689.0	136.0	22.0	12.3
KNP465	58.5	694.0	125.0	21.2	11.8
KNP467	58.4	364.0	106.0	13.2	10.2